

Development of phenazine- and phenazinone-based photosensitizers for
singlet oxygen generation

(一重項酸素生成能力を有するフェナジンおよびフェナジノン系
光増感色素の開発)

March, 2024

Kazuki Ohira

Applied Chemistry Program,
Graduate School of Advanced Science and Engineering,
Hiroshima University

Contents

Chapter 1	General introduction	1
Chapter 2	Phenazine-based photosensitizers for singlet oxygen generation	14
Chapter 3	Development of phenazine-2,3-diol-based photosensitizers: effect of formyl groups on singlet oxygen generation	42
Chapter 4	Development of phenazine-2,3-diol-based photosensitizers: effect of substitution of the cyano group for the nitro group on singlet oxygen generation	70
Chapter 5	Development of water-soluble phenazine-2,3-diol-based photosensitizers for singlet oxygen generation	100
Chapter 6	Synthesis and optical properties of phenazinone-based photosensitizers for singlet oxygen generation	123
Summary		147
List of publication		149
Acknowledgments		151

Chapter 1

General introduction

Photosensitization is a process by which a photochemical or photophysical alternation occurs in one molecular entity as a result of initial photoabsorption by another molecular entity called a photosensitizer (PS).¹ The beginning of photosensitization traces back to 1873 when Hermann Wilhelm Vogel discovered that the yellow corallin dye in the photographic emulsions increased the range of color sensitivity (Fig. 1a).² This discovery enabled the addition of sensitivity to visible light (400–700 nm), bringing color photography closer to commercial viability (Fig. 1b and c). Meanwhile, even to this day, photosensitization continues to attract considerable attention from researchers due to the growing applications such as photocatalysis,³ dye-sensitized solar cell (DSSC),⁴ perovskite solar cell (PSC),⁵ and photodynamic therapy (PDT) for cancer treatment.

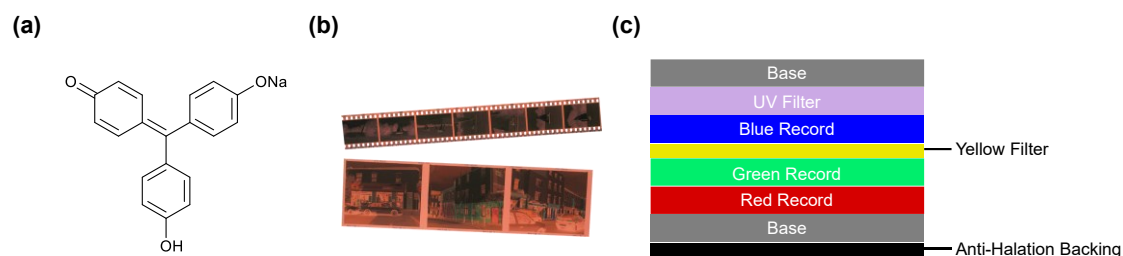


Fig. 1 (a) Chemical structure of corallin dye. (b) Picture of color negative film. (c) Illustration of layers of color negative film. Each layer consists of light sensitive emulsions.

PDT using PSs with the ability to produce singlet oxygen ($^1\text{O}_2$) and low-power laser light has attracted much attention as a treatment for cancer in an early stage with less stress on bodies. In other words, PDT is a treatment method in which the reactive $^1\text{O}_2$ destroys cancer cells. In 1931, Kautsky and de Bruijn⁶ proposed that the quenching of triplet excited states ($^3\text{PS}^*$) produced $^1\text{O}_2$ as a reactive

intermediate in photosensitized-oxygenation, and in 1964, this became generally accepted when Foote et al.⁷ demonstrated that the oxygenation of several compounds by chemically generated and by radio-frequency generated $^1\text{O}_2$, was consistent with the oxygenation by photosensitized $^1\text{O}_2$. The mechanism of $^1\text{O}_2$ generation by PS is shown in Fig. 2. PSs are excited to the singlet excited states ($^1\text{PS}^*$) by photoirradiation, undergo intersystem crossing (ISC) to be the triplet excited states ($^3\text{PS}^*$), and generate reactive $^1\text{O}_2$ via energy transfer from $^3\text{PS}^*$ to ground-state triplet oxygen ($^3\text{O}_2$) (Type II mechanism). Therefore, $^1\text{O}_2$ -generating PSs for PDT require the following properties: (1) strong absorption of light in the phototherapeutic window (650–900 nm), which can penetrate deep into living tissues, (2) high triplet quantum yield (Φ_T) originating from efficient ISC from $^1\text{PS}^*$ to $^3\text{PS}^*$, (3) high $^1\text{O}_2$ generation quantum yield (Φ_Δ) due to efficient energy transfer from $^3\text{PS}^*$ to $^3\text{O}_2$, (4) good solubility in water, (5) specific accumulation in tumor tissues (high affinity for tumor), (6) no induction of skin inflammation and rashes by photosensitivity of PSs, (7) low toxicity without light irradiation. On the other hand, superoxide ($\text{O}_2^{\cdot-}$) is generated via Type I mechanism involving electron transfer from radical anion of PS ($\text{PS}^{\cdot-}$), which is formed by electron transfer between $^3\text{PS}^*$ and surrounding electron donors including solvent and substrate, to $^3\text{O}_2$. Similar to $^1\text{O}_2$, $\text{O}_2^{\cdot-}$ is a reactive oxygen species (ROS), but considered to show less anticancer activity than $^1\text{O}_2$.

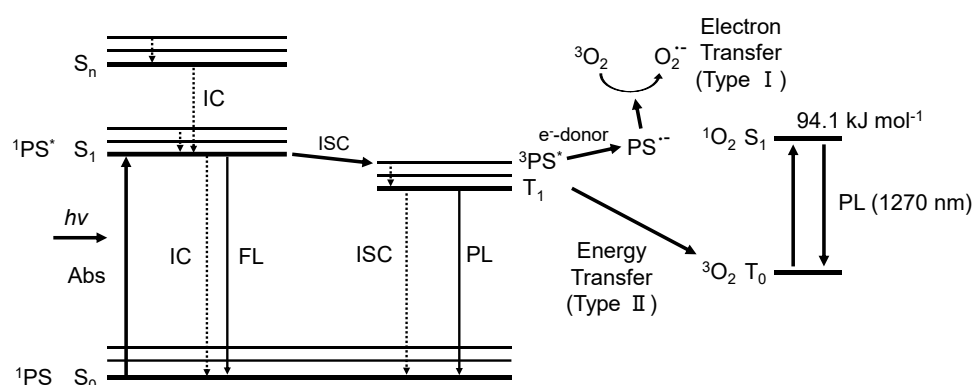


Fig. 2 Energy state diagram for quenching of excited $^3\text{PS}^*$ by ground-state oxygen ($^3\text{O}_2$). Here, Abs represents photoabsorption, FL represents fluorescence, PL represents phosphorescence, IC represents internal conversion, and ISC represents intersystem crossing.

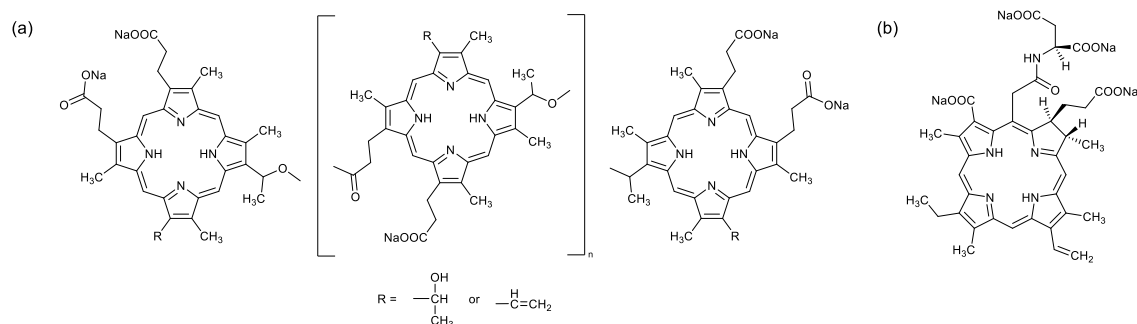


Fig. 3 Chemical structures of porphyrin-based PSs: (a) Porfimer sodium and (b) Talaporfin sodium.

Porphyrin dyes⁸ have a strong Soret absorption band at 400–450 nm ($\epsilon = 10^6 \text{ M}^{-1} \text{ cm}^{-1}$) and a weak Q absorption band at 500–700 nm ($\epsilon = 10^4 \text{ M}^{-1} \text{ cm}^{-1}$), and therefore, have been expected as excellent PDT dyes with the photosensitizing ability in the phototherapeutic window since the early days. Currently, in Japan, porfimer sodium (photofrin) and talaporfin sodium (Laserphyrin) are approved by the Ministry of Health, Labor and Welfare and practically used for PDT, as porphyrin-based PSs (Fig. 3).

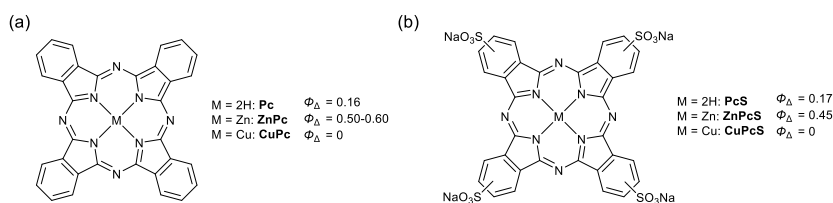


Fig. 4 Chemical structures of phthalocyanine-based PSs: (a) metal phthalocyanines and (b) water-soluble phthalocyanines.

Phthalocyanine dyes⁹ have a weak Soret absorption band at 300–400 nm and a strong Q absorption band above 650 nm ($\epsilon = \sim 10^5 \text{ M}^{-1} \text{ cm}^{-1}$). Porphyrin dyes show high light collection efficiency in the Soret absorption bands, whereas phthalocyanine dyes show high light collection efficiency in the Q absorption bands. Therefore, phthalocyanine dyes are expected to be second-generation PSs for PDT with excellent photosensitizing abilities in the phototherapeutic window. To render phthalocyanine dyes water-soluble, the introduction of sulfonic acid, sulfonate, carboxylic acid, and carboxylate into

the phthalocyanine skeleton is an effective way. Phthalocyanine dyes with diamagnetic metal ions such as Zn^{2+} and Al^{3+} as the central metal exhibit high Φ_{Δ} values, whereas those with paramagnetic metal ions including Co^{2+} and Cu^{2+} show significantly low Φ_{Δ} values, compared to the metal-free phthalocyanine (Fig. 4). This is due to the long-lived triplet states of phthalocyanine-based PSs with a diamagnetic metal ($\tau_{\text{T}} = 10^2 \mu\text{s}$).

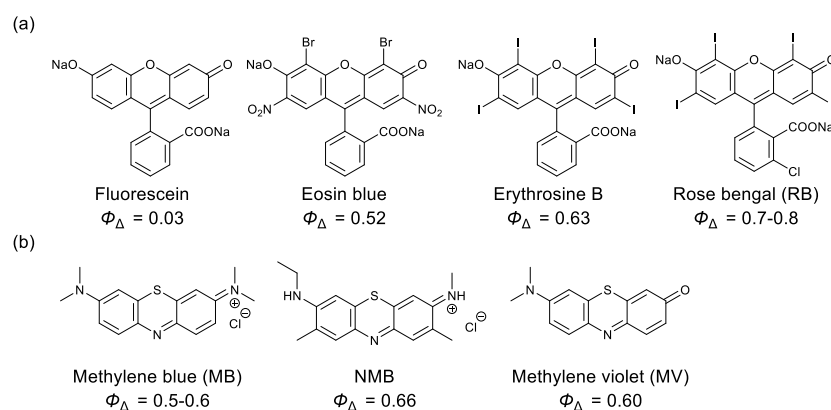


Fig. 5 Chemical structures of (a) xanthene- and (b) phenothiazinium-based PSs.

Xanthene dyes¹⁰ and phenothiazinium dyes¹¹ show photoabsorption maximum wavelengths at ca. 550–650 nm ($\epsilon = 10^5 \text{ M}^{-1} \text{ cm}^{-1}$). These xanthene and phenothiazinium dyes have excited triplet energy levels (energy difference between $^1\text{O}_2$ ($^1\Delta_{\text{g}}$) and $^3\text{O}_2$ ($^3\Sigma_{\text{g}}^-$) (94.1 kJ mol^{-1})), and thereby, show high Φ_{Δ} values due to the efficient energy transfer between PS^* and $^3\text{O}_2$. Many studies on the photochemical and electrochemical properties of xanthene and phenothiazinium dyes have revealed that the introduction of bromine and iodine atoms into the xanthene skeleton bathochromically shifts the photoabsorption maximum wavelength, and the heavy atom effect of halogen atoms improves the Φ_{T} and Φ_{Δ} values. Therefore, tetraiodide-substituted rose bengal (**RB**) and erythrosine B are efficient photosensitizing dyes (Fig. 5). The Φ_{Δ} values of rose bengal (**RB**) and methylene blue (**MB**) are ca. 0.7–0.8 and 0.5–0.6, respectively, and they are used as standard photosensitizing dyes for xanthene and phenothiazinium dyes.¹⁶ Most xanthene and phenothiazinium dyes have high Φ_{Δ} values but cannot

absorb light above 650 nm. Thus, the improvement of photoabsorption in the phototherapeutic window is required for use in PDT.

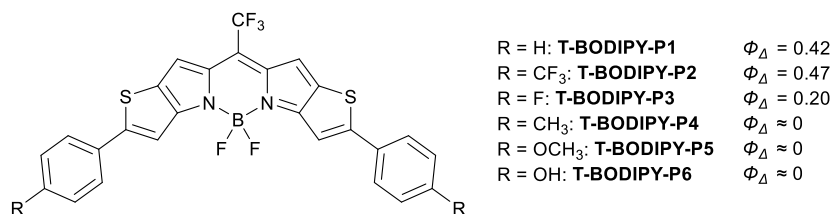


Fig. 6 Chemical structures of thienopyrrole-fused BODIPY-based PSs.

Boron-dipyrromethene (BODIPY)¹² dyes show excellent photostability, strong photoabsorption in red and near-infrared regions, and highly fluorescent properties. Most BODIPY dyes have photoabsorption maxima around 500–550 nm ($\epsilon = 10^5 \text{ M}^{-1} \text{ cm}^{-1}$) and are unavailable in the phototherapeutic window (650–900 nm). Thus, the effects of substituents on the photoabsorption maximum wavelengths of BODIPY dyes have been investigated. As shown in Fig. 6, a thienopyrrole-fused BODIPY dye, **T-BODIPY-P1** (R = H), without any heavy atom substitution shows a high ϵ (120,000 $\text{M}^{-1} \text{ cm}^{-1}$) around 690 nm, a moderate Φ_{fl} value (0.22), and relatively high Φ_{Δ} value (0.42). Thus, these thienopyrrole-fused BODIPY dyes with high brightness ($\text{BT} = \epsilon \times \Phi_{\text{fl}}$) and high phototoxicity ($\text{PP} = \epsilon \times \Phi_{\Delta}$) have attracted much interest in achieving both fluorescence imaging of cancer cells and PDT.

For PSs, halogen atoms such as iodide and bromide atoms are often introduced into the chromophores to promote ISC based on heavy atom effect,¹³ but it raised concerns about dark cytotoxicity.¹⁴ To overcome the drawbacks, halogen-atom-free PSs such as a family of heteroanthracenes have been extensively studied.¹⁵

For the detection and quantification of $^1\text{O}_2$, photodetection and scavenger methods are well-established. In 1976, Krasnovsky was the first to report the direct photodetection of phosphorescence at 1270 nm of photosensitized- $^1\text{O}_2$ in CCl_4 solutions (Fig. 2).¹⁷ Later in 1979, Khan and Kasha reported a direct observation of photosensitized phosphorescence in liquid solutions including water at room temperature.¹⁸ However, due to the weak phosphorescence, this method requires a specialized and sensitive spectrophotometer to detect near-infrared phosphorescence. On the other hand, the scavenger methods are generally used as an indirect spectroscopic method for the $^1\text{O}_2$ detection. In the methods, $^1\text{O}_2$ generation can be indirectly estimated from changes in photoabsorption and fluorescence spectra of scavengers such as 1,3-diphenylisobenzofuran (DPBF),¹⁹ 1,5-dihydroxynaphthalene (DHN),²⁰ 9,10-anthracenediyl-bis(methylene)dimalonic acid (ABDA),²¹ and singlet oxygen sensor green (SOSG)²² (Fig. 7a–c). In addition, the estimation of 4-oxo-TEMPO radicals formed via the reaction of 4-oxo-TEMP, a spin trapping agent, with $^1\text{O}_2$ by electron paramagnetic resonance (EPR) spectroscopy enables to indirectly detect and quantify photosensitized $^1\text{O}_2$ (Fig. 7d).

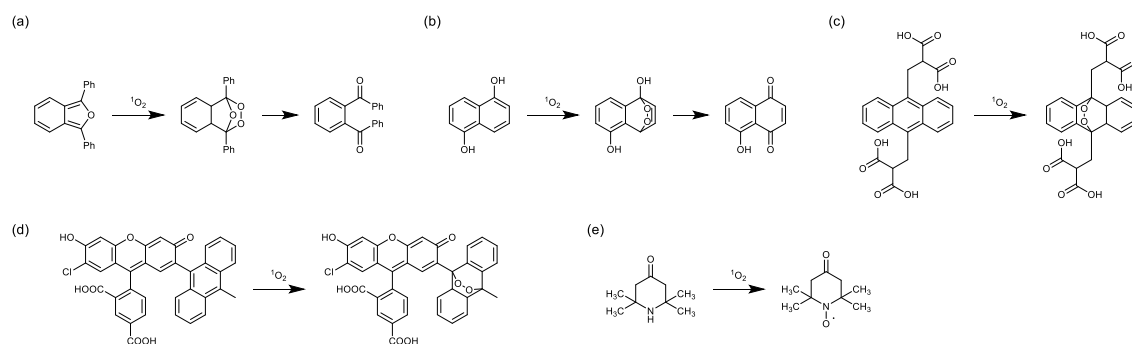


Fig. 7 (a)–(d) Reaction of $^1\text{O}_2$ scavengers (a: DPBF, b: DHN, c: ABDA, and d: SOSG) and (e) reaction of a spin trapping agent (4-oxo-TEMP) with $^1\text{O}_2$.

As a desirable heteroanthracene-based chromophore for $^1\text{O}_2$ generation, we focused on phenazine, an anthracene analogue with two nitrogen atoms at the 9, 10-positions (Fig. 8). In 1968, T.G. Pavlopoulos reported the phosphorescence property of phenazine,²³ but to the best of our knowledge, there are few

reports on the evaluation of $^1\text{O}_2$ generation ability for phenazine derivatives. Therefore, in this thesis, the author reports the preparation and photophysical properties of phenazine-based PSs. Furthermore, in order to further development, $^1\text{O}_2$ generation properties of phenazinone-based PSs incorporating a carbonyl group into the chromophore were investigated.

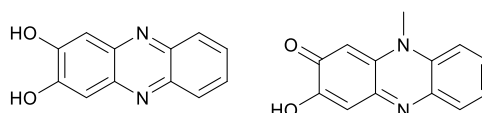


Fig. 8 Chemical structures of phenazine-2,3-diol and phenazinone.

In Chapter 2, phenazine-based PSs **KI-1** which is conjugated with two hydroxy groups and two thiophenes and its derivatives **KI-2–5** have been developed (Fig. 9). It was found that the introduction of a nitro group could extend the photoabsorption edge up to the NIR region (700–800 nm) but inhibited the photosensitized $^1\text{O}_2$ generation due to the fast nonradiative decay of $^1\text{PS}^*$. On the other hand, a superior photosensitizing ability was achieved by the modification with formyl groups, according to El-Sayed's rule.

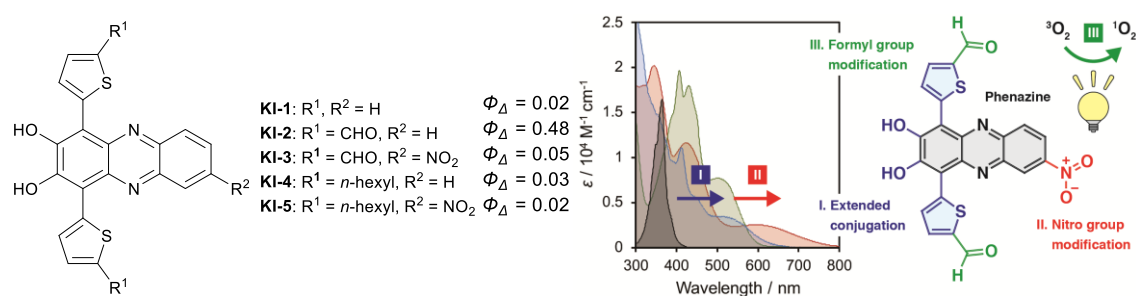


Fig. 9 Chemical structures of **KI-1–5**.

In Chapter 3, in order to gain insight into the enhancement of ISC and $^1\text{O}_2$ generation by formyl groups, phenazine-based PSs **KO-0–3** with zero to three formyl groups have been developed (Fig. 10). It was found that the Φ_{Δ} values of **KO-0–3** increase in the order of **KO-0** (0.036) < **KO-1** (0.22) < **KO-2** (0.33) < **KO-3** (0.41) with increasing number of formyl groups. This result indicates that formyl

groups facilitate ISC from $^1\text{PS}^*$ to $^3\text{PS}^*$ according to El-Sayed's rule. On the basis of the estimation of the Φ_{Δ} values, time-dependent density functional theory (TD-DFT) calculation, and spin-orbit coupling (SOC) matrix elements calculations, the $^1\text{O}_2$ generation properties of **KO-0-3** are discussed.

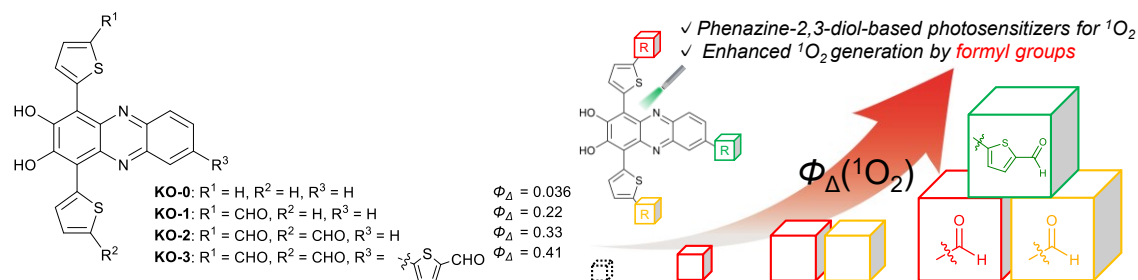


Fig. 10 Chemical structures of **KO-0-3**.

In Chapter 4, cyano-substituted phenazine-based PSs **YC-1** and **YC-2** have been developed (Fig. 11). As described above (Chapter 2), the introduction of a nitro group could extend the photoabsorption edge up to the NIR region (700–800 nm) but inhibited the photosensitized $^1\text{O}_2$ generation due to the fast nonradiative decay of $^1\text{PS}^*$. Therefore, **YC-2** with a cyano group in place of the nitro group of **KI-3** and its derivative **YC-1** were synthesized, and the substituent effect on the optical and $^1\text{O}_2$ generation properties was investigated. It was found that the substitution of the cyano group for the nitro group in phenazine-based chromophore reduces the rapid nonradiative decay of $^1\text{PS}^*$ and the ΔE_{ST} values, leading to the efficient ISC for $^1\text{O}_2$ generation. Furthermore, based on the photoabsorption spectral and ^1H NMR measurements, **YC-1** and **YC-2** exist in an equilibrium between the diol form and the phenoxide form in the THF solution.

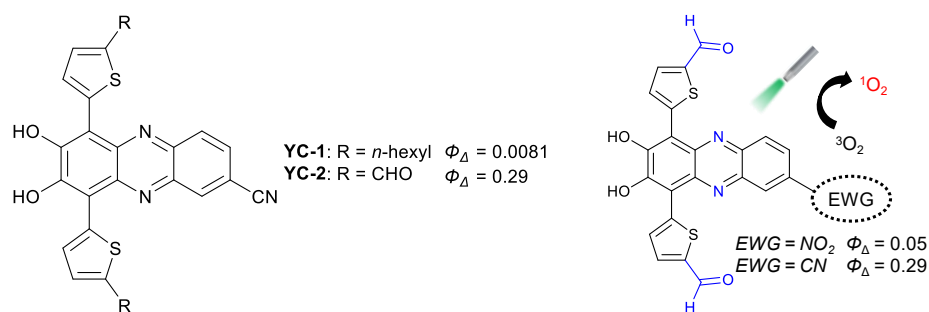


Fig. 11 Chemical structures of **YC-1** and **YC-2**.

In Chapter 5, water-soluble phenazine-based PSs **KY-1Na** and **KY-2Na** have been developed (Fig. 12). For use in water purification systems and photodynamic therapy (PDT) for cancer treatment, the PSs are required to possess high solubility in water as well as efficient ISC. Thus, in order to attain the solubility of phenazine-based PSs in water, we have developed **KY-1Na** and **KY-2Na** bearing one and two carboxylic acid sodium salts, respectively, as the water-soluble derivatives of **KO-2** exhibiting a moderate Φ_{Δ} value (0.17) in DMSO. It was found that the logarithms ($\log P_{o/w}$) of the 1-octanol/water partition coefficient ($P_{o/w}$) for **KY-1Na** and **KY-2Na** were determined to be -0.9 , indicating that both the PSs were more hydrophilic than RoseBengal (-0.6) and have hydrophilicity equivalent to **MB** (-0.9). The estimated Φ_{Δ} of **KY-1Na** and **KY-2Na** in water were 0.06 and 0.19, respectively. Based on the estimation of the Φ_{Δ} and photocytotoxicity toward murine colon carcinoma cells (Coron 26), the $^1\text{O}_2$ generation properties and photodynamic activities of these PSs are discussed.

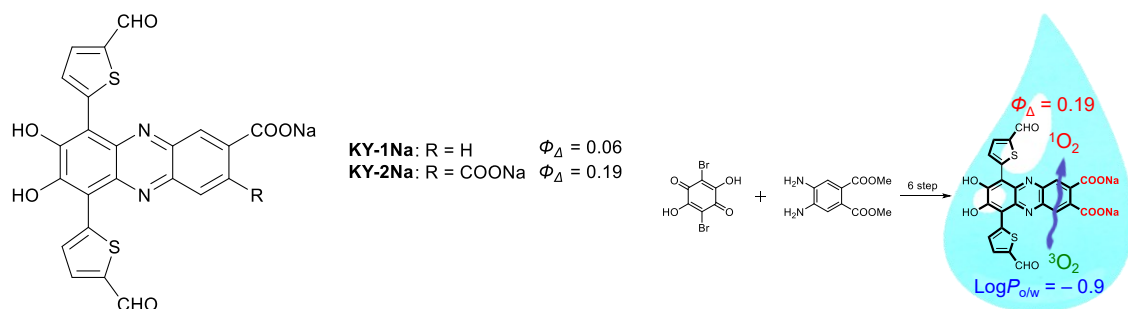


Fig. 12 Chemical structures of **KY-1Na** and **KY-2Na**.

In Chapter 6, phenazinone-based PSs **PZ1–3** have been developed (Fig. 13). The El-Sayed rule states that the rate of ISC is relatively large if the radiationless transition involves a change of orbital type, such as $^1(n\pi^*)$ to $^3(\pi\pi^*)$ and $^1(\pi\pi^*)$ to $^3(n\pi^*)$ transitions. Indeed, in Chapter 1–5, it was indicated that formyl substituents allow ISC based on the El-Sayed rule, leading to the efficient $^1\text{O}_2$ generation of phenazine-based PSs. Thus, based on our continuous work, we have designed **PZ1–3** incorporating a carbonyl group into the chromophore in expectation of more efficient ISC and $^1\text{O}_2$ generation. It was found that **PZ1** exhibited a high $^1\text{O}_2$ generation ability ($\Phi_{\Delta} = 0.86$), which is a superior

photosensitizing ability to **PZ2** ($\Phi_{\Delta} = 0.54$) and **PZ3** ($\Phi_{\Delta} = 0.069$) with a flexible substituent.

Therefore, the phenazinone-based PSs with improved Φ_{Δ} promise future practical applications.

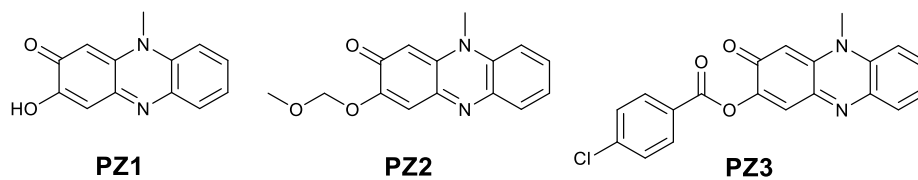


Fig. 13 Chemical structures of **PZ1–3**.

Reference

1. IUPAC. Compendium of Chemical Terminology, 2nd ed. (the "Gold Book"). Compiled by A. D. McNaught and A. Wilkinson. Blackwell Scientific Publications, Oxford (1997). Online version (2019-) created by S. J. Chalk. ISBN 0-9678550-9-8. <https://doi.org/10.1351/goldbook.P04652>
2. (a) H. W. Vogel, *Berichte*, **1983**, 6, 1302; (b) T. Tani, *KYORITSU SHUPPAN CO., LTD.*, **2020**, 1, Dye sensitization : from color film to perovskite solar cell.
3. (a) A. Fujishima and K. Honda, *Nature*, **1972**, 238, 37; (b) P. Bellotti, T. Rogge, F. Paulus, R. Laskar, N. Rendel, J. Ma, K. N. Houk, and F. Clorius, *J. Am. Chem. Soc.*, **2022**, 144, 15662–15671; (c) R. Matsuura, C. W. Lo, S. Wada, J. Somei, H. Ochiai, T. Murakami, N. Saito, T. Ogawa, A. Shinjo, Y. Benno, M. Nakagawa, M. Takei, and Y. Aida, *Viruses*, **2021**, 13, 942.
4. (a) B. O'Regan and M. Grätzel, *Nature*, **1991**, 353, 737; (b) Y. Kurumisawa, T. Higashino, S. Nimura, Y. Tsuji, H. Iiyama, and H. Imahori, *J. Am. Chem. Soc.*, **2019**, 141, 9910–9919; (c) Y. Ooyama, K. Yamaji, and J. Ohshita, *Mater. Chem. Front.*, **2017**, 1, 2243–2255.
5. (a) A. Kojima, K. Teshima, Y. Shirai, and T. Miyasaka, *J. Am. Chem. Soc.*, **2009**, 131, 6050–6051; (b) M.M. Lee, J. Teuscher, T. Miyasaka, T. N. Murakami, and H. J. Snaith, *Science*, **2012**, 338, 643–647; (c) J. Burschka, N. Pellet, S. J. Moon, R. H. Baker, P. Gao, M. K. Nazeeruddin, and M. Grätzel, *Nature*, **2013**, 499, 316–320; (d) S. Hu, P. Zhao, K. Nakano, R. D. J. Oliver, J. Pascual, J. A. Smith, T. Yamada, M. A. Truong, R. Murdey, N. Shioya, T. Hasegawa, M. Ehara, M. B. Johnston, K. Tajima, Y. Kanemitsu, H. J. Snaith, and A. Wakamiya, *Adv. Mater.*, **2023**, 35, 2208320.
6. (a) H. Kautsky and H. de Bruijn, *Naturwissenschaften*, **1931**, 19, 1043; (b) S. Nonell and C. Flors, *the Royal Society of Chemistry*, **2016**, Singlet Oxygen: Applications in Biosciences and Nanosciences.
7. (a) C. S. Foote and S. J. Wexler, *J. Am. Chem. Soc.*, **1964**, 86, 3879; (b) E. J. Corey and W. C.

- Taylor, *J. Am. Chem. Soc.*, **1964**, 86, 3881.
8. (a) M. Ethirajan, Y. Chen, P. Joshi, and R. K. Pandey, *Chem. Soc. Rev.*, **2011**, 40, 340–362; (b) M. C. DeRosa and R. J. Crutchley, *Coord. Chem. Rev.*, **2002**, 233–234, 351–371.
 9. B. Barut, C. Ö. Yalçın and Ü. Demirbaş, *J. Photochem. Photobiol. A Chem.*, **2021**, 405, 112946.
 10. T. M. Ebaston, F. Nakonechny, E. Talalai, G. Gellerman and L. Patsenker, *Dyes Pigm.*, **2021**, 184, 108854.
 11. (a) K. Piwovar, A. Blacha-Grzechnik and J. Zak, *J. Electrochem. Soc.*, **2019**, 166, G163–G169; (b) F. Ronzani, A. Trivella, E. Arzoumanian, S. Blanc, M. Sarakha, C. Richard, E. Oliveros and S. Lacombe, *Photochem. Photobiol. Sci.*, **2013**, 12, 2160–2169.
 12. (a) L. Wang, J. Bai, and Y. Qian, *New J. Chem.*, **2019**, 43, 16829–16834; (b) H. Wang, C. Li, Q. Wu, H. Wen, T. Sun, and Z. Xie, *J. Mater. Chem. B*, **2022**, 10, 4967–4973; (c) M. Liu, C. Wang, and Y. Qian, *New J. Chem.*, **2021**, 45, 18082–18089; (d) J. Chen, Y. Cui, K. Song, T. Liu, L. Zhou, B. Bao, R. Wang, and L. Wang, *Biomater. Sci.*, **2021**, 9, 2115–2123; (e) I. J. Gomez, M. Russo, O. A. Arcidiacono, E. M. Sanchez-Carnerero, P. Klan, and L. Zajickova, *Mater. Chem. Front.*, **2022**, 6, 1719–1726.
 13. (a) Y. Ooyama, T. Enoki and J. Ohshita, *RSC Adv.*, **2016**, 6, 5428–5435; (b) A. Mohan, E. Sebastian, M. Gudem and M. Hariharan, *J. Phys. Chem. B*, **2020**, 124, 6867–6874.
 14. O. J. Stacey and S. J. A. Pope, *RSC Adv.*, **2013**, 3, 25550–25564.
 15. (a) J. Miao, Y. Huo, G. Yao, Y. Feng, J. Weng, W. Zhao and W. Guo, *Angew. Chem. Int. Ed.*, **2022**, 61, e202201815; (b) L. A. Ortiz-Rodriguez, S. J. Hoehn, A. Loreda, L. Wang, H. Xiao and C. E. Crespo-Hernández, *J. Am. Chem. Soc.*, **2021**, 143, 2676–2681.
 16. L. Huang, X. Cui, B. Therrien and J. Zhao, *Chem. Eur. J.*, **2013**, 19, 17472–17482.
 17. (a) A. A. Krasnovsky Jr., *Biofizika*, **1976**, 21, 748; (b) A. A. Krasnovsky Jr., *Photochem. Photobiol.*, **1979**, 29, 29.

18. A. U. Khan and M. Kasha, *Proc. Natl. Acad. Sci. U. S. A.*, **1979**, *76*, 6047.
19. K. Gollnick and A. Griesbeck, *Tetrahedron*, **1985**, *41*, 2057–2068.
20. S. Takizawa, R. Aboshi, and S. Murata, *Photochem. Photobiol. Sci.*, **2011**, *10*, 895–903.
21. (a) D. Steinebrunner, G. Schnurpfeil, H. H. Doeblner, J. A. T. Burgos, D. Wöhrle and A. Wittstock, *Photochem. Photobiol. Sci.*, **2021**, *20*, 547–558; (b) T. Entradas, S. Waldron and M. Volk, *J. Photochem. Photobiol. B: Biol.*, **2020**, *204*, 111787.
22. (a) C. Flors, M. J. Fryer, J. Waring, B. Reeder, U. Bechtold, P. M. Mullineaux, S. Nonell, M. T. Wilson, and N. R. Baker, *J. Exp. Bot.*, **2006**, *57*, 1725–1734; (b) S. Kim, M. Fujitsuka, and T. Majima, *J. Phys. Chem. B*, **2013**, *117*, 13985–13992.
23. T. G. Pavlopoulos, *J. Chem. Phys.*, **1969**, *51*, 2936.

Chapter 2

Phenazine-based photosensitizers for singlet oxygen generation

Introduction

Singlet oxygen ($^1\text{O}_2$) can be generated from ground-state oxygen in the air by light irradiation of a photosensitizer. Upon light irradiation, a photosensitizer is excited to an excited singlet state (S_1), and then, undergoes intersystem crossing (ISC) to be an excited triplet state (T_1), and generates $^1\text{O}_2$ via energy transfer from the T_1 to ground-state oxygen. The strong oxidizing ability, green atom-economic feature, and remote controllability of $^1\text{O}_2$ are highly useful for intriguing applications,¹ such as selective oxidation in organic synthesis,² photocatalytic degradation of organic molecules and germs in water purification,³ and tumor cell killing in photodynamic therapy (PDT).⁴ Therefore, to date, various kinds of organic photosensitizer possessing the ability to produce $^1\text{O}_2$ have been developed.⁵ A family with tetrapyrrole structures such as porphyrins, chlorins, and phthalocyanines are undoubtedly one of the most studied photosensitizers because of their high quantum yields ($\Phi_{\Delta\text{S}}$) of $^1\text{O}_2$ generation, and some of them are commercially available as PDT agents.⁶ As represented by rose bengal (RB) and methylene blue, which are usually used as a standard to determine $\Phi_{\Delta\text{S}}$ for new photosensitizers, xanthene and phenothiazine-based photosensitizers are even equal to the tetrapyrrole family and have been extensively studied.^{1, 5(b)} Because xanthene and phenothiazine share a common structure, where either or both of the two central carbon atoms of anthracene are replaced by heteroatoms, heterocyclic anthracene analogues (heteroanthracenes) have promise as next-generation photosensitizers. Here we focus on the phenazine structure, an anthracene analogue with two nitrogen atoms at the 9,10-positions (Fig. 1). Despite the considerable potential of phenazines as photosensitizers, new phenazine derivatives and their photosensitizing abilities have been rarely

investigated.⁷ In this study, we extended the conjugation of the phenazine structure, further modified the new structure with different functional groups, and evaluated the photophysical properties and photosensitized $^1\text{O}_2$ generation to establish synthetic guidelines for new phenazine-based and also other photosensitizers with the excellent ability to produce $^1\text{O}_2$.

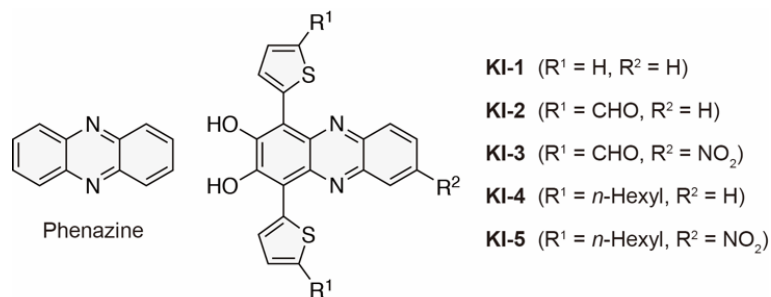


Fig. 1 Chemical structures of phenazine and phenazine-based photosensitizers **KI-1**, **KI-2**, **KI-3**, **KI-4**, and **KI-5** with different functional groups.

Experimental

Materials

All solvents and reagents were used as received, unless otherwise noted. Rose bengal (RB) was purchased from Sigma Aldrich and recrystallized from MeOH twice. 1,3-Diphenylisobenzofuran (DPBF) was purchased from Tokyo Chemical Industry and recrystallized from a mixture of CH₂Cl₂ and MeOH. 2,2,6,6-Tetramethyl-4-piperidone (4-oxo-TEMP) was purchased from FUJIFILM Wako Pure Chemical and purified by sublimation twice.

General

¹H NMR and ¹³C NMR spectra were recorded using Varian-400 (400 MHz) and Varian-500 (500 MHz) FT NMR spectrometers. FT-IR spectra were recorded on a Perkin Elmer Spectrum One NTS using the ATR method. High-resolution mass spectral data were acquired using a Thermo Fisher Scientific LTQ Orbitrap XL. Photoabsorption spectra were recorded using Shimadzu UV-3150 and UV-3600-plus spectrophotometers. Fluorescence spectra were measured using a Hitachi F-4500 spectrophotometer. The fluorescence quantum yields (Φ_{fs}) were determined with a Hamamatsu C9920-01 instrument equipped with CCD by use of a calibrated integrating sphere system. Irradiance of monochromatic and continuous lights for photosensitizing reactions was adjusted using a Newport 1918-C optical power meter.

Evaluation of ¹O₂ quantum yield

Quantum yields ($\Phi_{\Delta\text{S}}$) for singlet oxygen (¹O₂) generation by phenazine photosensitizers **KI-1**, **KI-2**, **KI-3**, **KI-4**, **KI-5**, and **KI-6** were evaluated by monitoring the changes in the photoabsorption spectra of 1,3-diphenylisobenzofuran (DPBF), a known ¹O₂ scavenger, in tetrahydrofuran (THF) upon photoirradiation. DPBF can trap the generated ¹O₂ through oxidation. THF was bubbled with air for 15 min, prior to preparing the solutions. The absorbance of DPBF was adjusted to *ca.* 1.0 in the air-saturated THF solutions. The concentration of the phenazine photosensitizers and rose bengal (RB)

was adjusted so that the absorbance at the irradiation wavelength (509 nm) was *ca.* 0.03. The THF solutions containing DPBF and **KI-1**, **KI-2**, **KI-3**, **KI-4**, **KI-5**, **KI-6**, or RB were irradiated with monochromatic light (509 nm, 300 $\mu\text{W cm}^{-2}$) that was obtained by passage of xenon light (HAL-320, Asahi Spectra) through a monochromator (CMS-100, Asahi Spectra). Except for the nonirradiated solutions, each spectrum was recorded immediately after photoirradiation for 1 min. The procedure was promptly repeated until the total photoirradiation time reached 10 min. The changes in optical density (ΔOD) of DPBF were plotted against photoirradiation time to obtain the slopes (m_s), which are required for estimation of $\Phi_{\Delta\text{S}}$. The Φ_{Δ} values of the phenazine photosensitizers were determined by the relative method using RB ($\Phi_{\Delta} = 0.80$ in MeOH) as a standard according to the following eqn (1):

$$\Phi_{\Delta\text{sam}} = \Phi_{\Delta\text{ref}} \times [(m_{\text{sam}}/m_{\text{ref}}) \times (L_{\text{ref}}/L_{\text{sam}})] \quad (1)$$

where $\Phi_{\Delta\text{sam}}$ and $\Phi_{\Delta\text{ref}}$ are $^1\text{O}_2$ quantum yields of phenazine photosensitizer and RB, respectively, m_{sam} and m_{ref} are slopes in the plots of ΔOD at the photoabsorption maximum wavelength of DPBF (413 nm) against photoirradiation time, and L_{sam} and L_{ref} are light harvesting efficiencies, which are given by $L = 1 - 10^{-A}$ (“ A ” is the absorbance at the photoirradiation wavelength).

Photosensitizing ability

The photosensitizing abilities of phenazine derivatives upon exposure to continuous visible light (>510 nm, 30 mW cm^{-2}) were evaluated in THF solutions containing **KI-1**, **KI-2**, **KI-3**, **KI-4**, **KI-5**, or **KI-6** (5 μM) and DPBF as a $^1\text{O}_2$ scavenger (50 μM). THF was bubbled with air for 15 min, prior to preparing the solutions. The continuous light was obtained by passage of xenon light (HAL-302, Asahi Spectra) through a 510 nm long path filter. Except for the nonirradiated solutions, each spectrum was recorded immediately after photoirradiation for 0.5 or 1 min. The procedure was promptly repeated until the total irradiation time reached 5 or 10 min. Then, $\ln(C_t/C_0)$ was plotted against photoirradiation time, where C_t is the concentration of DPBF at the reaction time (t) and C_0 is the initial concentration

of DPBF before photoirradiation. C_t was calculated based on Lambert–Beer law ($A_{\text{DPBF}} = \epsilon cl$) using the maximum absorbance at 413 nm. Because the $\ln(C_t/C_0)$ plots showed linear decreases with increasing photoirradiation time, the slopes were used to estimate the first-order rate constants (k_{obs}) of the DPBF oxidation by $^1\text{O}_2$ generated using the phenazine photosensitizers. The k_{obs} value for RB was also obtained in a similar way.

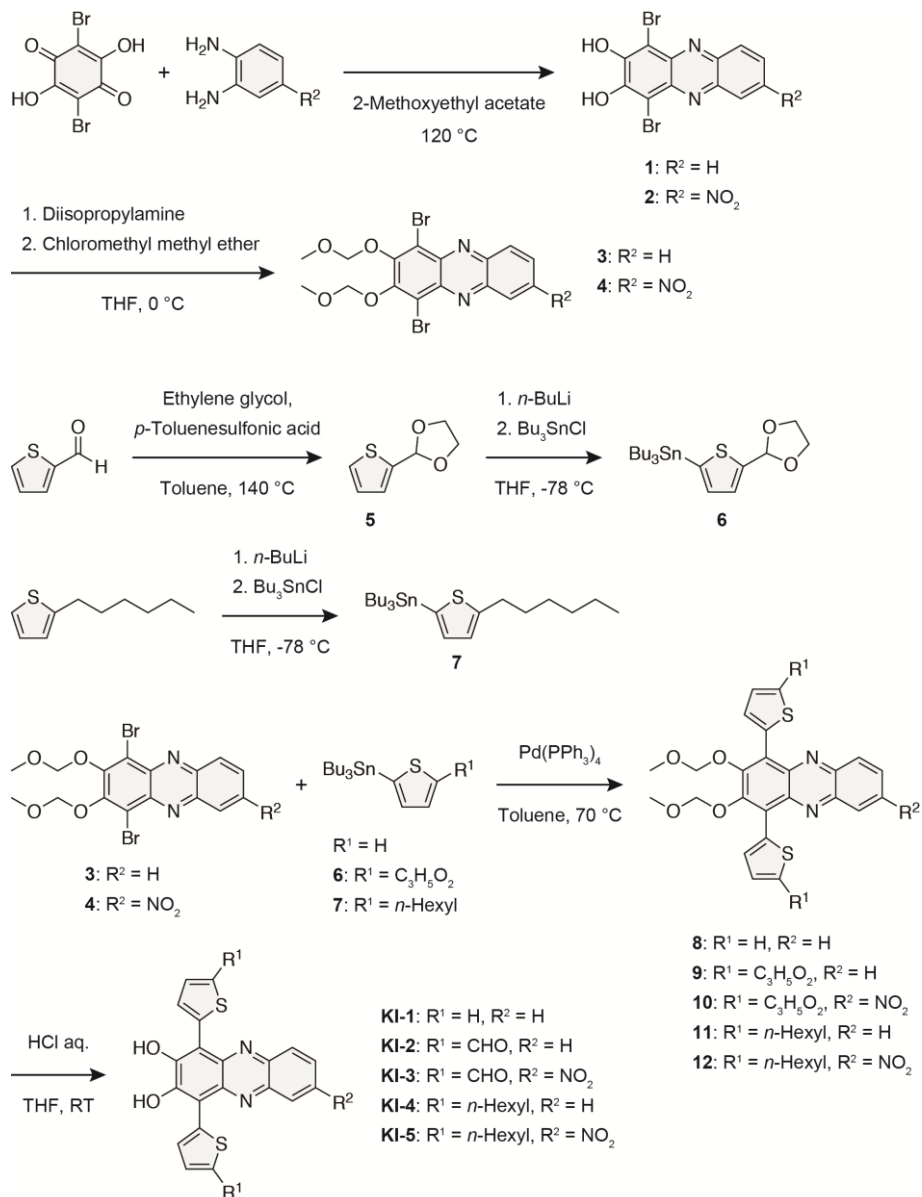
EPR measurements

Air-saturated THF solutions containing **KI-2**, **KI-3**, or RB as a photosensitizer (5 μM) and 2,2,6,6-tetramethyl-4-piperidone (4-oxo-TEMP) as a spin-trapping agent (50 mM) were prepared. THF was bubbled with air for 15 min, prior to preparing the solutions. Their electron paramagnetic resonance (EPR) spectra before and after exposure to continuous visible light (>510 nm, 30 mW cm^{-2}) for 60 min were recorded on a JEOL JES-RE1X spectrometer. The measurement conditions are as follows; temperature 25°C , microwave power 1 mW, field modulation 0.32 mT, time constant 0.1 s, and sweep rate 0.03 mT s^{-1} . The continuous light was obtained by passage of xenon light (HAL-302, Asahi Spectra) through a 510 nm long path filter. The reaction of 4-oxo-TEMP with $^1\text{O}_2$ produces a stable nitroxide radical (4-oxo-TEMPO), showing a characteristic 1 : 1 : 1 triplet signal.

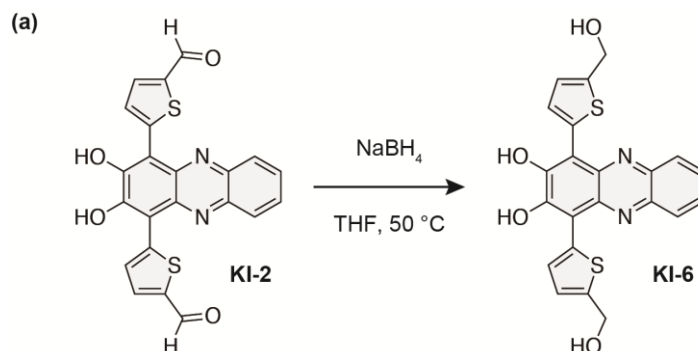
Theoretical calculations

The Gaussian 16 program⁸ was used for density functional theory (DFT) calculations. For the convenience of calculations, the *n*-hexyl groups of **KI-4** and **KI-5** were replaced with methyl groups. The S_0 geometries of these photosensitizers were optimized via frequency calculations at the B3LYP/6-31G(d,p)/THF-CPCM level. There are no imaginary frequencies for all optimized structures. The spin-orbit coupling (SOC) matrix elements were calculated at the B3LYP/6-31G(d,p)/THF-CPCM level using the ORCA 5.0.4 program.⁹ These calculations were performed using the optimized S_0 geometries of these photosensitizers.

Synthesis



Scheme 1 Synthetic route for phenazine derivatives **KI-1**, **KI-2**, **KI-3**, **KI-4**, and **KI-5**.



Scheme 2 Reduction of formyl groups in phenazine photosensitizer **KI-2** to produce **KI-6**.

Phenazine KI-1. A solution of compound **8** (44 mg, 94.7 μmol) in THF (20 mL) that was bubbled with N_2 for 15 min in advance was prepared and stirred at room temperature for 15 min. Concentrated HCl solution (1 mL) was added to the solution, and the mixture was stirred at room temperature with light blocking by aluminum foil cover. After disappearance of the reactant and stirring for additional 2 h, saturated NaHCO_3 solution was added to the mixture for neutralization. Then, Ethyl acetate was added to the mixture, and the extracted organic layer was washed with water once and saturated saline twice, dried over anhydrous Na_2SO_4 , filtered, concentrated, and washed with hexane and water. The crude product was dissolved in THF and precipitated in hexane to give phenazine **KI-1** as red solid (17 mg, 48% yield). ^1H NMR (500 MHz, acetone- d_6): δ (ppm) = 8.40 (br, 2H, OH), 8.04–8.13 (m, 2H, aromatic), 7.60 (dd, J = 6.3 and 3.3 Hz, 2H, aromatic), 7.44 (d, J = 4.0 Hz, 2H, aromatic), 7.16 (dd, J = 5.0 and 4.0 Hz, 2H, aromatic). ^{13}C NMR spectrum could not be obtained because of the low solubility in any solvents. HRMS (ESI): 375.02631 $[\text{M-H}]^-$, calculated for $\text{C}_{20}\text{H}_{11}\text{O}_2\text{N}_2\text{S}_2$ $[\text{M-H}]^-$: 375.02674.

Phenazine KI-2. A solution of compound **9** (0.228 g, 0.375 mmol) in THF (40 mL) that was bubbled with N_2 for 15 min in advance was prepared and stirred at room temperature for 15 min. Concentrated HCl solution (6 mL) was added to the solution, and the mixture was stirred at room temperature with light blocking by aluminum foil cover. After disappearance of the reactant and stirring for additional 2 h, saturated NaHCO_3 solution was added to the mixture for neutralization. Then, Ethyl acetate was added to the mixture, and the extracted organic layer was washed with water once and saturated saline twice, dried over anhydrous Na_2SO_4 , filtered, concentrated, and washed with hexane and water. The crude product was dissolved in THF and precipitated in hexane to give phenazine **KI-2** as red solid (0.145 g, 89% yield). ^1H NMR (500 MHz, acetone- d_6): δ (ppm) = 9.98 (s, 2H, CHO), 9.04 (d, J = 4.0 Hz, 2H, aromatic), 8.22 (dd, J = 6.5 and 3.3 Hz, 2H, aromatic), 7.90 (d, J = 4.0 Hz, 2H, aromatic), 7.66 (dd, J = 6.5 and 3.5 Hz, 2H, aromatic). ^{13}C NMR spectrum could not be obtained because of the

low solubility in any solvents. HRMS (ESI): 431.01642 $[M-H]^-$, calculated for $C_{22}H_{11}O_4N_2S_2$ $[M-H]^-$: 431.01657.

Phenazine KI-3. A solution of compound **10** (0.160 g, 0.245 mmol) in THF (30 mL) that was bubbled with N_2 for 15 min in advance was prepared and stirred at room temperature for 15 min. Concentrated HCl solution (5 mL) was added to the solution, and the mixture was stirred at room temperature with light blocking by aluminum foil cover. After disappearance of the reactant and stirring for additional 2 h, saturated $NaHCO_3$ solution was added to the mixture for neutralization. Then, Ethyl acetate was added to the mixture, and the extracted organic layer was washed with water once and saturated saline twice, dried over anhydrous Na_2SO_4 , filtered, concentrated, and washed with hexane and water. The crude product was dissolved in THF and precipitated in hexane to give phenazine **KI-3** as black solid (80 mg, 68% yield). 1H NMR (500 MHz, dimethyl sulfoxide ($DMSO$)- d_6): δ (ppm) = 9.98 (s, 1H, CHO), 9.93 (s, 1H, CHO), 9.04 (d, J = 4.0 Hz, 1H, aromatic), 8.88 (d, J = 2.5 Hz, 1H, aromatic), 8.75 (d, J = 4.0 Hz, 1H, aromatic), 8.41 (dd, J = 9.5 and 2.5 Hz, 1H, aromatic), 8.24 (d, J = 9.5 Hz, 1H, aromatic), 8.04 (d, J = 4.0 Hz, 1H, aromatic), 8.00 (d, J = 4.0 Hz, 1H, aromatic). ^{13}C NMR (125 MHz, $DMSO$ - d_6): δ (ppm) = 184.23, 183.80, 163.72, 158.39, 148.31, 146.33, 144.30, 142.16, 141.44, 141.22, 140.84, 139.13, 137.24, 136.94, 135.11, 128.59, 128.35, 127.03, 123.45, 120.80, 105.40, 105.26. HRMS (ESI): 476.00101 $[M-H]^-$, calculated for $C_{22}H_{10}O_6N_3S_2$ $[M-H]^-$: 476.00165.

Phenazine KI-4. A solution of compound **11** (0.171 g, 0.270 mmol) in THF (20 mL) that was bubbled with N_2 for 15 min in advance was prepared and stirred at room temperature for 15 min. Concentrated HCl solution (3.5 mL) was added to the solution, and the mixture was stirred at room temperature with light blocking by aluminum foil cover. After disappearance of the reactant and stirring for additional 2 h, saturated $NaHCO_3$ solution was added to the mixture for neutralization. Then, Ethyl acetate was added to the mixture, and the extracted organic layer was washed with water once and saturated saline twice, dried over anhydrous Na_2SO_4 , filtered, concentrated, and washed with hexane and water. The

crude product was dissolved in THF and precipitated in hexane to give phenazine **KI-4** as brown solid (66 mg, 45% yield). ^1H NMR (500 MHz, CDCl_3): δ (ppm) = 10.02 (s, 2H, OH), 8.25 (d, J = 8.0 Hz, 1H, aromatic), 8.08 (d, J = 4.0 Hz, 1H, aromatic), 7.63 (t, J = 7.3 Hz, 1H, aromatic), 7.53 (t, J = 7.8 Hz, 1H, aromatic), 7.40 (d, J = 8.0 Hz, 1H, aromatic), 7.13 (d, J = 3.5 Hz, 1H, aromatic), 6.93 (d, J = 3.0 Hz, 1H, aromatic), 6.91 (d, J = 3.5 Hz, 1H, aromatic), 2.87–2.95 (m, 4H, CH_2), 1.72–1.82 (m, 4H, CH_2), 1.31–1.49 (m, 12H, CH_2), 0.91 (t, J = 7.0 Hz, 6H, CH_3). ^{13}C NMR spectrum could not be obtained because of the low solubility in any solvents. HRMS (ESI): 543.21454 $[\text{M-H}]^-$, calculated for $\text{C}_{32}\text{H}_{35}\text{O}_2\text{N}_2\text{S}_2$ $[\text{M-H}]^-$: 543.21454.

Phenazine KI-5. A solution of compound **12** (0.140 g, 0.207 mmol) in THF (10 mL) that was bubbled with N_2 for 15 min in advance was prepared and stirred at room temperature for 15 min. Concentrated HCl solution (2.5 mL) was added to the solution, and the mixture was stirred at room temperature with light blocking by aluminum foil cover. After disappearance of the reactant and stirring for additional 2 h, saturated NaHCO_3 solution was added to the mixture for neutralization. Then, Ethyl acetate was added to the mixture, and the extracted organic layer was washed with water once and saturated saline twice, dried over anhydrous Na_2SO_4 , filtered, concentrated, and washed with hexane and water. The crude product was dissolved in THF and precipitated in hexane to give phenazine **KI-5** as black solid (0.100 g, 82% yield). ^1H NMR (500 MHz, acetone- d_6): δ (ppm) = 8.95 (d, J = 2.5 Hz, 1H, aromatic), 8.69 (d, J = 3.0 Hz, 1H, aromatic), 8.37 (d, J = 3.0 Hz, 1H, aromatic), 8.33 (dd, J = 9.0 and 2.5 Hz, 1H, aromatic), 8.16 (d, J = 9.0 Hz, 1H, aromatic), 6.85 (d, J = 3.5 Hz, 1H, aromatic), 6.80 (d, J = 3.5 Hz, 1H, aromatic), 2.85–2.94 (m, 4H, CH_2), 1.72–1.82 (m, 4H, CH_2), 1.31–1.52 (m, 12H, CH_2), 0.86–0.95 (m, 6H, CH_3). HRMS (ESI): 588.19849 $[\text{M-H}]^-$, calculated for $\text{C}_{32}\text{H}_{34}\text{O}_4\text{N}_3\text{S}_2$ $[\text{M-H}]^-$: 588.19962.

Phenazine KI-6. A solution of phenazine **KI-2** (50 mg, 0.116 mmol) and NaBH_4 (18 mg, 0.476 mmol) in THF (120 mL) that was bubbled with N_2 in advance was prepared and stirred at 50 °C for 18 h. After cooling to room temperature, ethyl acetate was added to the solution, and the mixture was

washed with saturated saline four times, dried over anhydrous Na₂SO₄, filtered, concentrated, and washed with hexane. Then, the crude product was dissolved in an ethyl acetate/acetone mixture, washed with saturated saline, dried over anhydrous Na₂SO₄, filtered, concentrated, dissolved in THF, and precipitated in hexane to give phenazine **KI-6** as black solid (12 mg, 24% yield). ¹H NMR (500 MHz, acetone-*d*₆): δ (ppm) = 8.65 (d, *J* = 3.5 Hz, 2H, aromatic), 8.12 (dd, *J* = 6.5 and 3.5 Hz, 2H, aromatic), 7.53 (dd, *J* = 6.8 and 3.3 Hz, 2H, aromatic), 6.97 (d, *J* = 4.0 Hz, 2H, aromatic), 4.81 (s, 4H, CH₂). HRMS (ESI): 435.04736 [M-H]⁻, calculated for C₂₂H₁₅O₄N₂S₂ [M-H]⁻: 435.04787.

Results and discussion

Synthesis

A new phenazine **KI-1** conjugated with two hydroxyl groups and two thiophenes was designed and synthesized to improve the photoabsorption property of phenazine (Fig. 1), because photoabsorption in the long-wavelength region (650–900 nm, particularly near-infrared, NIR) is required for photosensitizers to be available for the above applications. Formyl, *n*-hexyl, and nitro groups were introduced into **KI-1**, affording **KI-2**, **KI-3**, **KI-4**, and **KI-5**. These phenazine derivatives were synthesized by Stille coupling between dibromo-substituted precursor phenazines and the corresponding tributylstannyl thiophenes followed by deprotection of the hydroxyl and formyl groups (Scheme 1). Their ^1H and ^{13}C NMR spectra exclude the presence of their NH-form tautomers, as the previous studies on hydroxyl phenazines indicated.¹⁰ Therefore, we concluded that they exist in the OH forms as depicted in Fig. 1.

Photoabsorption properties

The photoabsorption spectra of phenazine and modified phenazines **KI-1**, **KI-2**, **KI-3**, **KI-4**, and **KI-5** in tetrahydrofuran (THF) are shown in Fig. 2, and their optical data are summarized in Table 1. The modified phenazines exhibited the photoabsorption over a wide range of wavelengths, and **KI-5** extended the photoabsorption edge up to 800 nm (NIR region), in contrast to phenazine, whose photoabsorption appeared below 420 nm. The broad photoabsorption bands of the modified phenazines above 420 nm are attributed to the formation of the phenoxide ion by the partial deprotonation of hydroxy groups,¹¹ in addition to their π -conjugation extended by the thiophene modification. In fact, these photoabsorption bands significantly decreased by addition of HCl and increased by addition of NaOH. Moreover, the protection of hydroxyl groups with methoxymethyl groups resulted in large hypsochromic shift, as observed in the previous studies, where a simple dihydroxy (catechol-type) phenazine showed a broad photoabsorption band from 300 to 600 nm

whereas the dialkoxy substitution rendered the photoabsorption spectrum similar to that of phenazine.^{10(e), 12} The modification of **KI-1** with two formyl groups (**KI-2**) significantly enhanced the photoabsorption from 500 to 600 nm while shifted the band edge to a shorter wavelength. The hexyl groups in **KI-4** slightly improved the photoabsorption above 600 nm. The strongly electron-withdrawing nitro group enabled **KI-3** and **KI-5** to exhibit photoabsorption in the visible long-wavelength and also NIR regions.

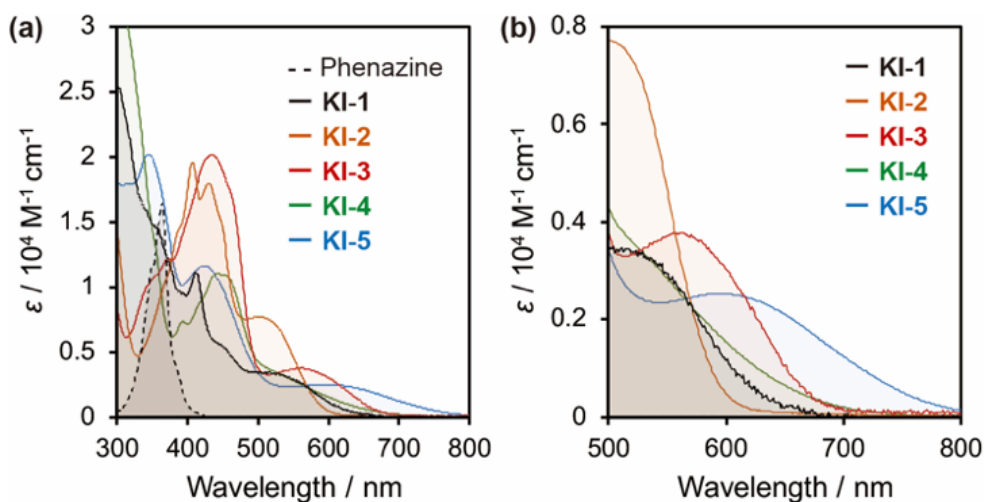


Fig. 2 (a) Photoabsorption spectra of phenazine and derivatives **KI-1**, **KI-2**, **KI-3**, **KI-4**, and **KI-5** in THF. (b) Magnification of the spectra above 500 nm.

Table 1 Optical data, $^1\text{O}_2$ quantum yields ($\Phi_{\Delta\text{S}}$), and first-order rate constants (k_{obsS}) for the photooxidation of DPBF using phenazine derivatives **KI-1**, **KI-2**, **KI-3**, **KI-4**, and **KI-5** in THF

Dye	$\lambda_{\text{max}}^{\text{abs}} / \text{nm}^a$ ($\epsilon / \text{M}^{-1} \text{cm}^{-1}$)	$\epsilon / \text{M}^{-1} \text{cm}^{-1}$ @509 nm	Φ_{Δ}^b	$k_{\text{obs}} / \text{min}^{-1}^c$
KI-1	500 (3500)	3400	0.02	0.006
KI-2	500 (7700)	7600	0.48	0.144
KI-3	560 (3800)	3300	0.05	0.011
KI-4	530 (3400)	3900	0.03	0.005
KI-5	600 (2500)	2900	0.02	0.002

^a Above 500 nm. ^b $^1\text{O}_2$ quantum yields (relative decomposition rate of DPBF), with RB as a standard ($\Phi_{\Delta} = 0.80$ in MeOH^{13}) and DPBF as a $^1\text{O}_2$ scavenger. The Φ_{Δ} values were estimated under an assumption that the reactivity of $^1\text{O}_2$ is independent of the kind of solvents. ^c First-order rate constants for the reaction of DPBF with $^1\text{O}_2$ generated upon photoexcitation of the phenazine derivatives. The k_{obs} for RB is 0.351 min^{-1} .

¹O₂ generation

Photosensitized ¹O₂ generation by phenazine derivatives **KI-1**, **KI-2**, **KI-3**, **KI-4**, and **KI-5** was evaluated by monitoring the changes in photoabsorption spectra of 1,3-diphenylisobenzofuran (DPBF), a known ¹O₂ scavenger, in THF (Fig. 4a–e). DPBF can trap the generated ¹O₂ through oxidation.¹⁴ THF was bubbled with air for 15 min, prior to preparing solutions. The air-saturated THF solutions containing DPBF and **KI-1**, **KI-2**, **KI-3**, **KI-4**, or **KI-5** were irradiated with monochromatic light at 509 nm (300 μW cm⁻², see Table 1 for ε/M⁻¹ cm⁻¹ @ 509 nm) that was obtained by passage of xenon light through a monochromator. In the solutions with **KI-1**, **KI-3**, **KI-4**, or **KI-5**, the photoabsorption band of DPBF peaked at *ca.* 410 nm slightly decreased but was almost unchanged upon light irradiation. In contrast, the DPBF photoabsorption band in the solution with **KI-2** markedly declined with increasing photoirradiation time, indicating the photosensitized ¹O₂ generation by **KI-2** and oxidation of DPBF by ¹O₂. The changes in optical density (ΔOD) of DPBF are plotted against photoirradiation time to obtain the slopes (*m*_{samS}, Fig. 4f), which are required for estimation of Φ_Δ values. The Φ_Δ values of the phenazine derivatives were determined by the relative method using RB (Φ_Δ = 0.80 in MeOH) as a standard (Table 1).¹⁵ Interestingly, **KI-2** exhibited a much higher Φ_Δ value (0.48) than those of the other phenazine derivatives (0.02–0.05). This result is attributed to the promoted ISC from singlet to triplet states by the introduction of formyl groups as explained by El-Sayed's rule.¹⁶ In aromatic carbonyl compounds, the ISC is facilitated by the accompanying change of molecular orbital type, *i.e.*, transitions of ¹(π, π*) to ³(n, π*) and ¹(n, π*) to ³(π, π*). The promoted ISC would enhance the energy transfer from the triplet state of **KI-2** to ground-state oxygen and result in a high Φ_Δ value. In fact, the fluorescence quantum yield (Φ_f) of **KI-2** (0.04) is smaller than that of **KI-4** (0.09). The low Φ_Δ value of **KI-3** in spite of the formyl substitution is probably due to the fast nonradiative decay of excited states by the nitro group,¹⁷ as discussed later. The modification of hexyl groups in **KI-4** and **KI-5** has no positive effect on the ¹O₂ generation.

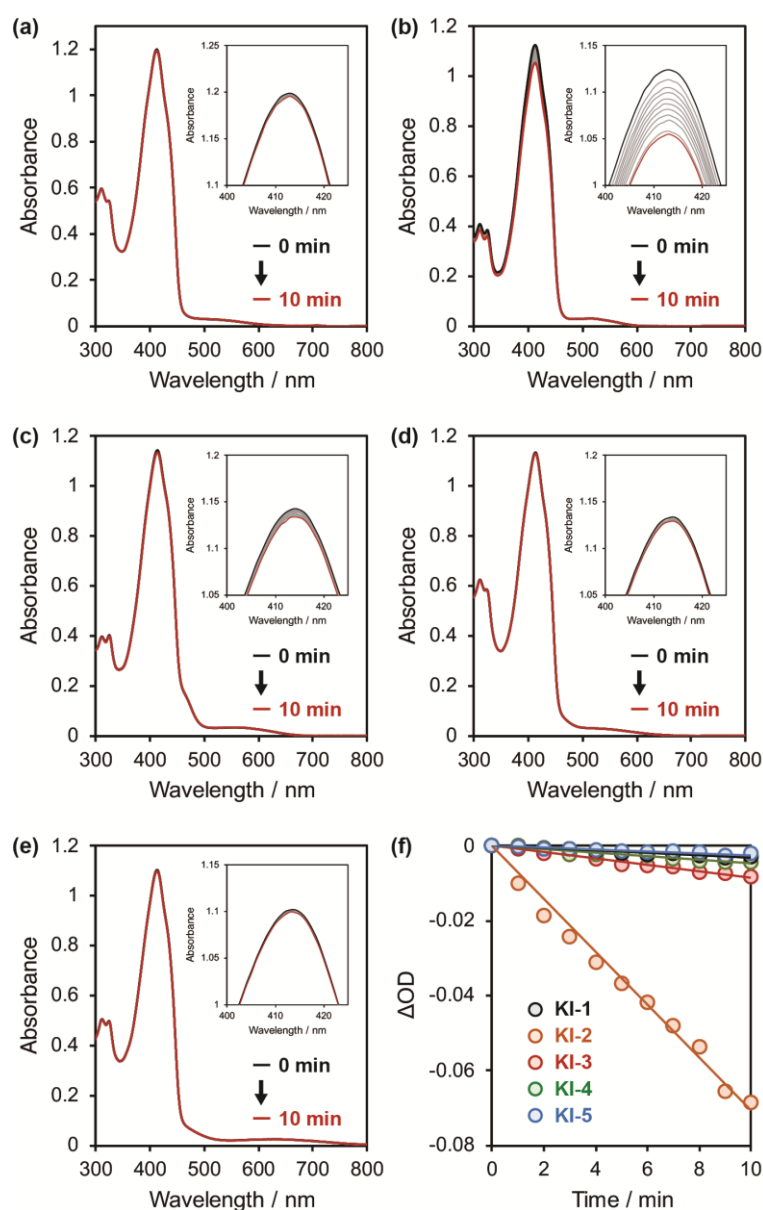


Fig. 4 Photoabsorption spectra of DPBF (Abs. @413 nm = ca. 1) in the presence of phenazine photosensitizer (a) **KI-1**, (b) **KI-2**, (c) **KI-3**, (d) **KI-4**, or (e) **KI-5** (Abs. @509 nm = ca. 0.03) upon irradiation with a monochromatic light (509 nm, $300 \mu\text{W cm}^{-2}$) in THF. Insets are magnifications of peak tops in the spectra around 410 nm. (f) Plots of ΔOD of DPBF at 413 nm against photoirradiation time (509 nm, $300 \mu\text{W cm}^{-2}$) in the presence of the phenazine photosensitizers in THF.

Photosensitizing ability

For further investigation of the photosensitizing abilities of the phenazine derivatives, the $^1\text{O}_2$ generation and DPBF degradation upon exposure to continuous visible light ($>510\text{ nm}$, 30 mW cm^{-2}) were evaluated in air-saturated THF solutions containing DPBF and **KI-1**, **KI-2**, **KI-3**, **KI-4**, or **KI-5**. The continuous light was obtained by passage of xenon light through a 510 nm long path filter. The photosensitized $^1\text{O}_2$ generation was clearly observed in the photoabsorption spectra of the solutions with **KI-1**, **KI-2**, **KI-3**, or **KI-4** as a gradual decrease of the DPBF photoabsorption band at *ca.* 410 nm with increasing photoirradiation time (Fig. 5a–d). The solution containing **KI-2** particularly exhibited a significant reduction of the photoabsorption band. However, the spectra of **KI-5** were almost unchanged similar to the behavior upon the monochromatic light irradiation (Fig. 5e). The $\ln(C_t/C_0)$ was plotted against photoirradiation time, where C_t is a concentration of DPBF at the reaction time (t) and C_0 is the initial concentration of DPBF before photoirradiation, and showed linear decreases (Fig. 5f), providing the first-order rate constants (k_{obs} s) for the oxidation of DPBF by $^1\text{O}_2$ generated using the phenazine derivatives as photosensitizers (Table 1). The large k_{obs} value of **KI-2** (0.144 min^{-1}) was obtained by the heavy atom effect of sulfur atoms and formyl substituents according to El-Sayed's rule.¹⁶ However, the modification of **KI-2** with a nitro group significantly lowered the k_{obs} value to 0.011 min^{-1} (**KI-3**). Additionally, **KI-5** with a nitro group but no formyl group showed an extremely low k_{obs} value (0.002 min^{-1}) despite the photoabsorption over a wide range of wavelengths above 510 nm . These results indicate that the modified nitro groups induced the photoexcited states to decay immediately without luminescence and energy transfer to ground-state oxygen,¹⁷ which strongly and negatively affected the photosensitized $^1\text{O}_2$ generation. Indeed, the weak fluorescence of **KI-2** and **KI-4** also disappeared by the modification with a nitro group (Φ_{fl} values of **KI-3** and **KI-5** < 0.02). The similar k_{obs} values of **KI-1** and **KI-4** (0.006 and 0.005 min^{-1} , respectively) indicate that the hexyl substitution hardly changed the photosensitizing ability.

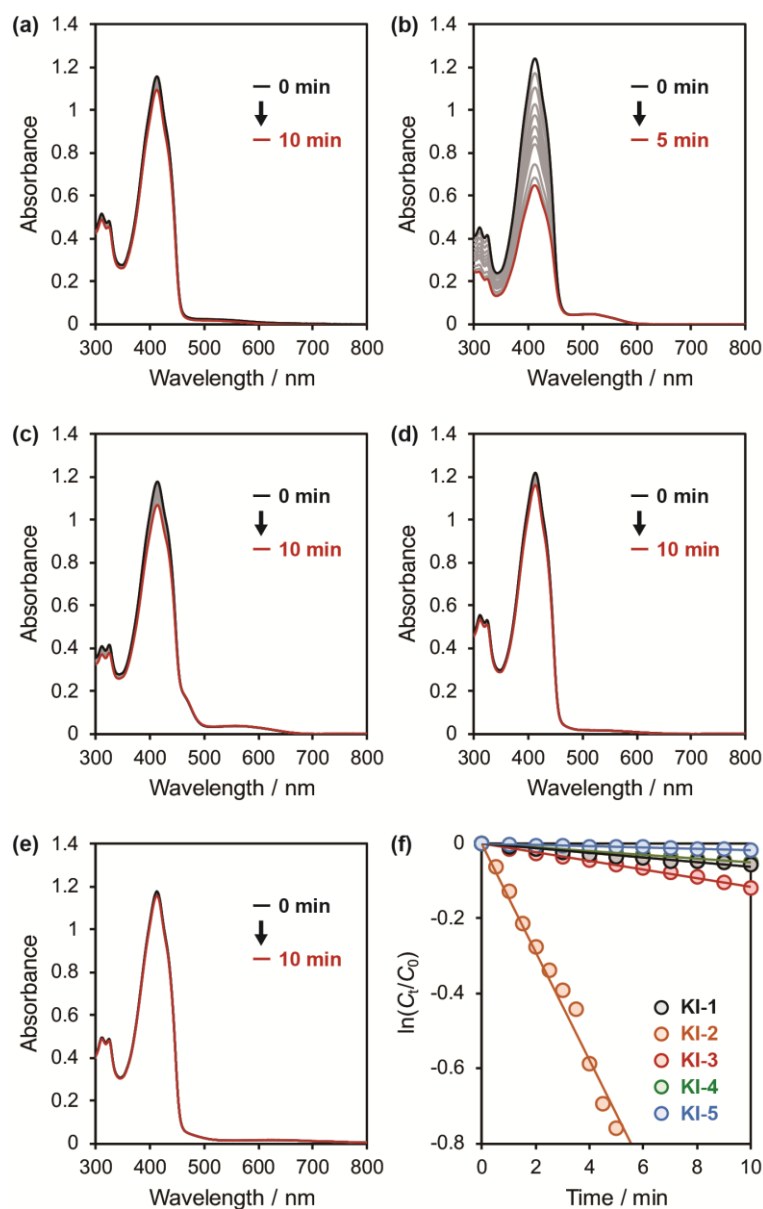


Fig. 5 Photoabsorption spectra of DPBF (50 μM) in the presence of phenazine photosensitizer (a) KI-1, (b) KI-2, (c) KI-3, (d) KI-4, or (e) KI-5 (5 μM) upon irradiation with a continuous light (>510 nm, 30 mW cm^{-2}) in THF. (f) Plots of $\ln(C_t/C_0)$ of DPBF against photoirradiation time (>510 nm, 30 mW cm^{-2}) in the presence of the phenazine photosensitizers in THF.

Investigation of the effect of formyl groups on $^1\text{O}_2$ generation

To verify that the superior photosensitizing ability of phenazine derivative **KI-2** stems from the modified formyl groups as explained by El-Sayed's rule, the formyl groups were almost completely reduced to hydroxyl groups by NaBH_4 to produce phenazine derivative **KI-6**, and its photosensitizing ability was examined by the above methods using DPBF and monochromatic light (509 nm, $300\ \mu\text{W cm}^{-2}$) or continuous light ($>510\ \text{nm}$, $30\ \text{mW cm}^{-2}$) in air-saturated THF (Fig. 6). The reduction significantly decreased the Φ_{Δ} value of **KI-2** from 0.48 to 0.05 and slowed the reaction rate (k_{obs}) from 0.144 to $0.009\ \text{min}^{-1}$. Therefore, we are convinced of the strongly enhancing effect of formyl groups in phenazine-based photosensitizers on their $^1\text{O}_2$ generation.

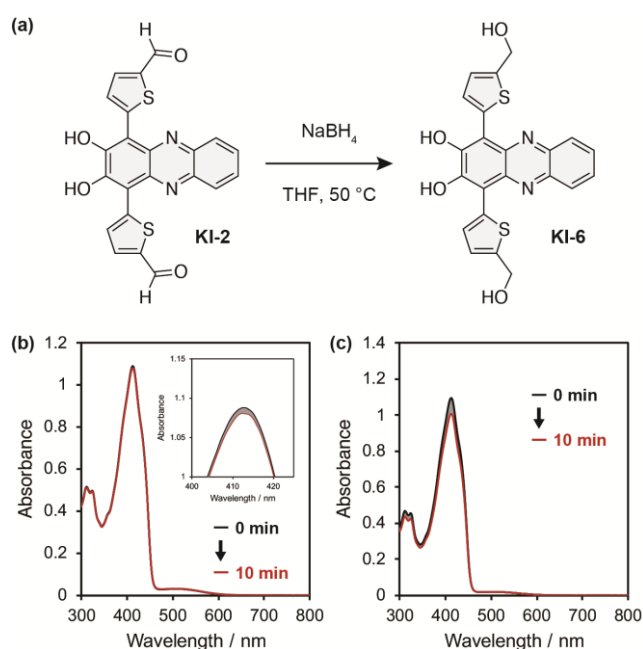


Fig. 6 (a) Reduction of formyl groups in phenazine photosensitizer **KI-2** to produce **KI-6**. (b) Photoabsorption spectra of DPBF (Abs. @413 nm = ca. 1) in the presence of **KI-6** (Abs. @509 nm = ca. 0.03) upon irradiation with a monochromatic light (509 nm, $300\ \mu\text{W cm}^{-2}$) in THF. Inset is magnification of peak tops in the spectra around 410 nm. (c) Photoabsorption spectra of DPBF (50 μM) in the presence of **KI-6** (5 μM) upon irradiation with a continuous light ($>510\ \text{nm}$, $30\ \text{mW cm}^{-2}$) in THF.

EPR measurements

The $^1\text{O}_2$ generation photosensitized by phenazine derivative **KI-2** was also confirmed by electron paramagnetic resonance (EPR) spectroscopy. 2,2,6,6-Tetramethyl-4-piperidone (4-oxo-TEMP) was employed as a spin-trapping agent to react with $^1\text{O}_2$ and produce a stable and detectable nitroxide radical (4-oxo-TEMPO).¹⁸ In the air-saturated THF solution containing **KI-2** and 4-oxo-TEMP, a characteristic 1 : 1 : 1 triplet signal of 4-oxo-TEMPO was observed and increased in intensity after exposure to continuous visible light ($>510\text{ nm}$, 30 mW cm^{-2}) (Fig. 7). The increased intensity was not observed in solutions with the other phenazine derivatives because of the small volume of photogenerated $^1\text{O}_2$.

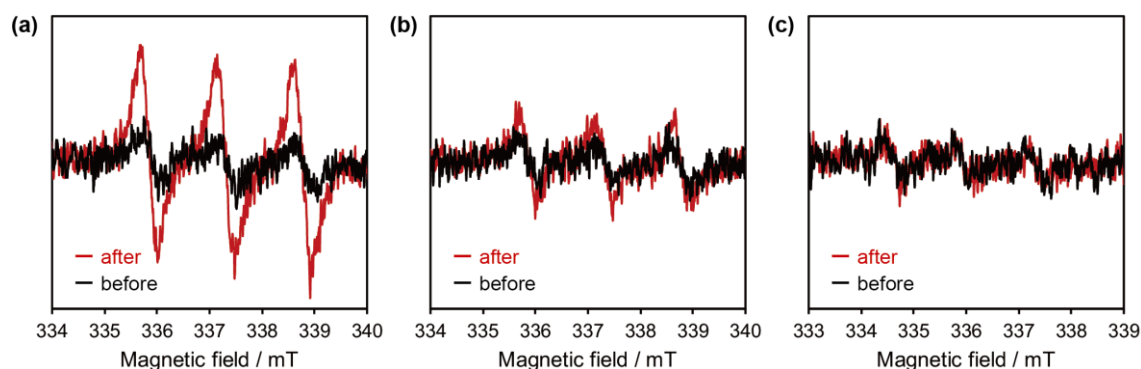


Fig. 7 Electron paramagnetic resonance (EPR) spectra of air-saturated THF solutions containing 4-oxo-TEMP and (a) RB, (b) **KI-2**, or (c) **KI-3** before and after exposure to a continuous visible light ($>510\text{ nm}$, 30 mW cm^{-2}) for 60 min. The characteristic 1:1:1 triplet signal originates from a stable nitroxide radical (4-oxo-TEMPO) formed by the reaction of 4-oxo-TEMP with $^1\text{O}_2$.

Theoretical calculations

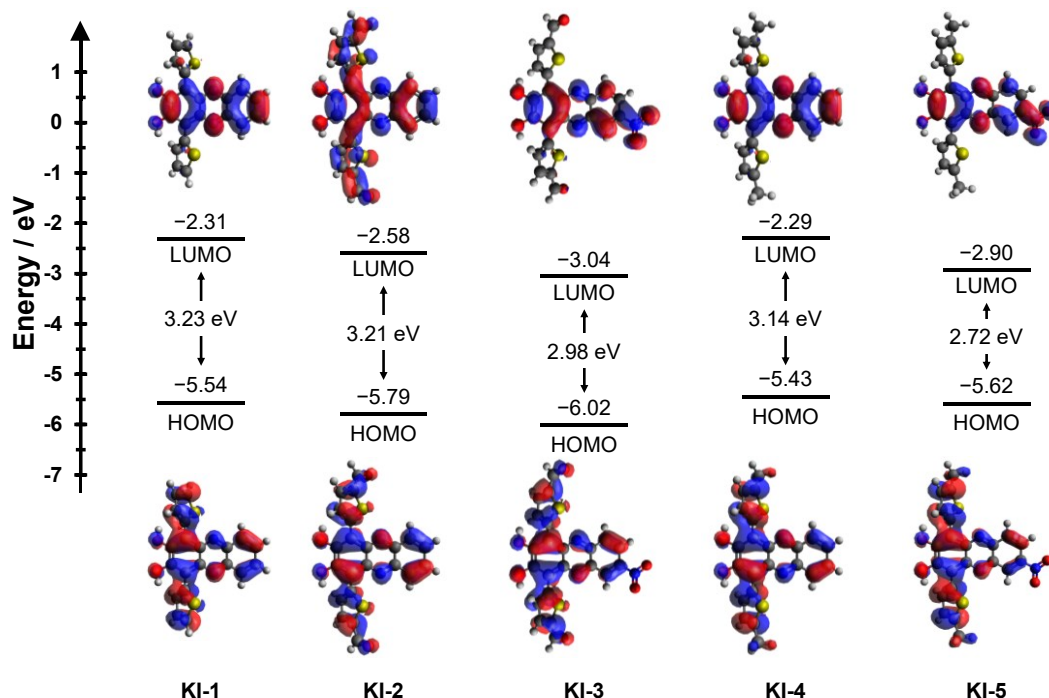


Fig. 8 Energy level diagram, HOMO and LUMO of **KI-1–5** at the B3LYP/6-31G(d,p)/THF-CPCM level using DFT calculations. The *n*-hexyl groups of **KI-4** and **KI-5** were replaced with the methyl groups for convenience of calculation.

The highest occupied molecular orbitals (HOMOs) and lowest unoccupied molecular orbitals (LUMOs) of phenazine derivatives **KI-1**, **KI-2**, **KI-3**, **KI-4**, and **KI-5** were examined by the calculation of their molecular orbitals using density functional theory (DFT) at the B3LYP/6-31G(d,p)/THF-CPCM level (Fig. 8).⁸ For the simple calculations of **KI-4** and **KI-5**, the *n*-hexyl groups were displaced by methyl groups. The DFT calculations indicate that their HOMOs are delocalized over the phenazine moiety and thiophene rings. The LUMOs of the derivatives except **KI-2** are mostly localized on the phenazine moiety. The formyl groups contribute to both the HOMOs and LUMOs of **KI-2**, and the nitro groups significantly contribute to the LUMOs of **KI-3** and **KI-5**. The introduction of moderately electron-withdrawing formyl groups into **KI-1** stabilized both the HOMO and LUMO

energy levels of **KI-2**, whereas the weakly electron-donating alkyl groups of **KI-4** caused the destabilization of both HOMO and LUMO. The strongly electron-withdrawing nitro groups of **KI-3** and **KI-5** lowered the HOMO and LUMO energy levels, but the extent in the LUMO was larger than that in the HOMO, resulting in narrow bandgaps, that is, photoabsorption in the long-wavelength region.

In order to gain insight into the $^1\text{O}_2$ generation properties of these photosensitizers based on the ISC efficiency, spin-orbit coupling (SOC) matrix elements were analyzed using time-dependent DFT (TD-DFT). The SOC constants and the vertical excitation energies from the S_0 state to the S_n and T_n states for these photosensitizers were calculated using their S_0 state geometries (Fig. 9 and Table 2). TD-DFT calculations suggested that the $S_0 \rightarrow S_1$ transitions of these photosensitizers are attributed to the transition from the HOMOs to the LUMOs with (π, π^*) characteristics and that HOMO-2 for **KI-2** and **KI-3**, HOMO-3 for **KI-5**, and HOMO-4 for **KI-1**, **KI-4**, and **KI-6** are attributed to the frontier n-orbitals consisting of the lone pair electrons on the nitrogen atoms of the phenazine skeleton (Fig. 9 insets). Meanwhile, for **KI-2** and **KI-3** possessing formyl groups, not only the lone pair electrons on the nitrogen atoms but also those on the formyl oxygens contributed to the frontier n-orbitals. Furthermore, it was revealed that these photosensitizers have several ISC pathways which meet the El-Sayed rule ($S_1 (\pi, \pi^*) \rightarrow T_3 (n, \pi^*)$ for **KI-1**, **KI-4**, and **KI-5**, $S_1 (\pi, \pi^*) \rightarrow T_4 (n, \pi^*)$ for **KI-3** and **KI-6**, and $S_1 (\pi, \pi^*) \rightarrow T_5 (n, \pi^*)$ for **KI-2**).¹⁶ In these major ISC pathways, these photosensitizers exhibited relatively large SOC matrix elements ($4.97\text{--}7.77 \text{ cm}^{-1}$). For the energy gaps (ΔE_{ST}), **KI-2** exhibited the smallest ΔE_{ST} (0.01 eV) among these photosensitizers (0.06 eV for **KI-1**, 0.15 eV for **KI-3**, 0.14 eV for **KI-4**, 0.39 eV for **KI-5**, and 0.14 eV for **KI-6**), leading to the highest Φ_{Δ} value (0.48) among these photosensitizers (0.02 for **KI-1**, 0.05 for **KI-3**, 0.03 for **KI-4**, 0.02 for **KI-5**, and 0.05 for **KI-6**). These results suggest that the modification of *n*-hexyl groups, the nitro group, and the hydroxymethyl groups in **KI-3**, **KI-4**, **KI-5**, and **KI-6** increased ΔE_{ST} values, resulting in inferior ISC

and Φ_{Δ} values. Considering that **KI-2** has three additional ISC pathways (T_2 – T_4 , 1.82–3.81 cm^{-1}), the low Φ_{Δ} value of **KI-1** suggests that multiple ISC pathways are required for efficient $^1\text{O}_2$ generation. Consequently, we revealed that the formyl groups play a key role in the $^1\text{O}_2$ generations on phenazine-based photosensitizers.

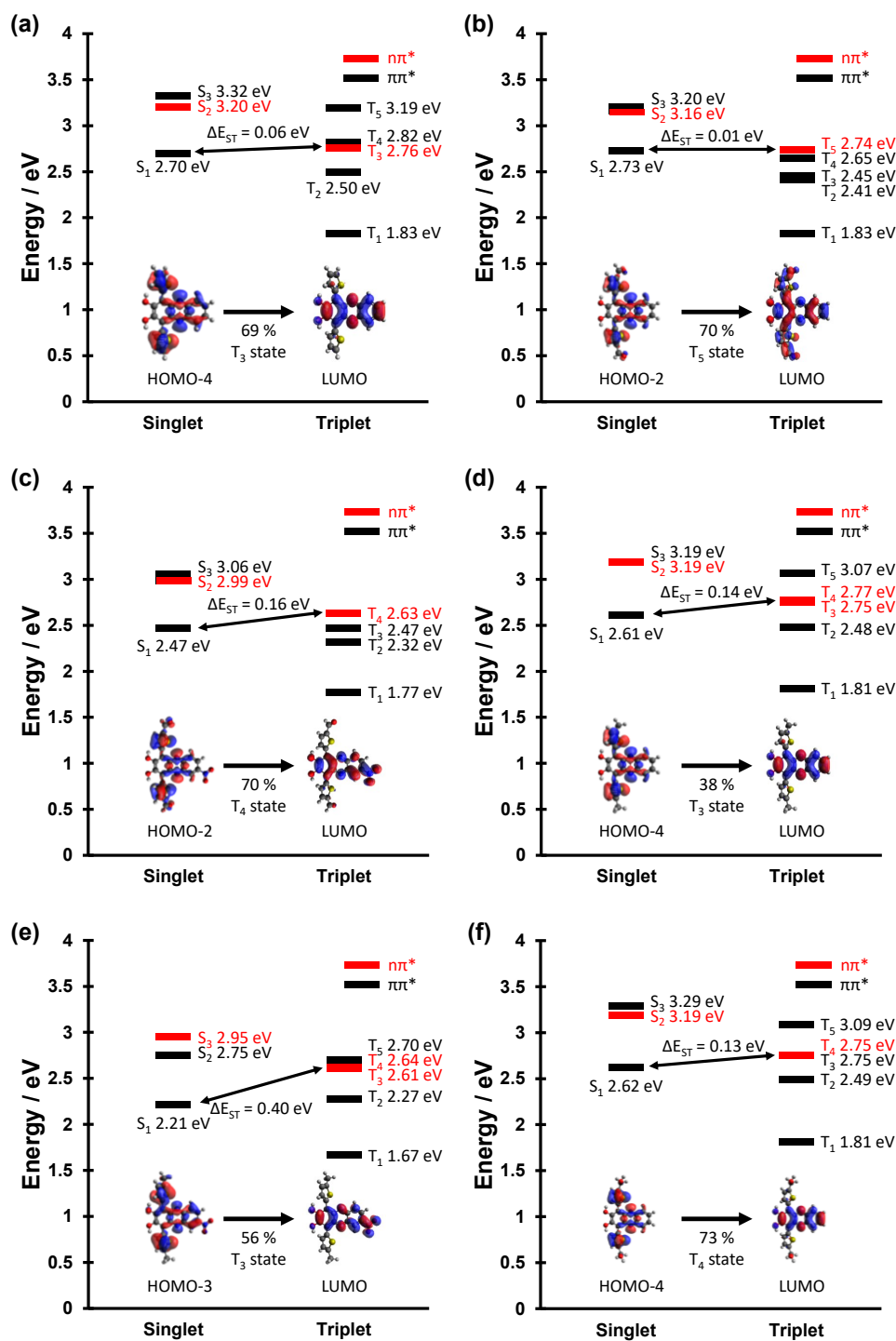


Fig. 9 Schematic diagrams showing vertical excitation energies of (a) KI-1, (b) KI-2, (c) KI-3, (d) KI-4, (e) KI-5, and (f) KI-6 for singlet and triplet excited states. The insets represent the frontier n-orbitals that contribute to the (n, π^*) triplet states. The *n*-hexyl groups of KI-4 and KI-5 were replaced with the methyl groups for convenience of calculation.

Table 2 Spin–orbit coupling (SOC) constants and the energy gaps (ΔE_{ST}) between the lowest excited singlet states (S_1) and the triplet states (T_n).

Dye	Triplet states	SOC / cm^{-1}	ΔE_{ST} / eV
KI-1	T ₁	0.49	-0.87
	T ₂	0.72	-0.20
	T ₃	7.77	0.06
	T ₄	0.60	0.12
	T ₅	3.58	0.49
KI-2	T ₁	0.78	-0.90
	T ₂	2.04	-0.32
	T ₃	1.82	-0.28
	T ₄	3.81	-0.08
	T ₅	7.70	0.01
KI-3	T ₁	0.29	-0.71
	T ₂	0.85	-0.15
	T ₃	0.93	0.00
	T ₄	7.29	0.15
	T ₅	2.36	0.16
KI-4	T ₁	0.08	-0.80
	T ₂	0.96	-0.13
	T ₃	4.97	0.14
	T ₄	4.71	0.16
	T ₅	2.15	0.46
KI-5	T ₁	0.18	-0.54
	T ₂	0.85	0.06
	T ₃	5.83	0.39
	T ₄	2.75	0.43
	T ₅	0.22	0.49
KI-6	T ₁	0.11	-0.81
	T ₂	1.39	-0.13
	T ₃	1.21	0.13
	T ₄	7.35	0.14
	T ₅	2.07	0.48

Conclusions

In this study, we developed new photosensitizers based on a phenazine structure conjugated with two hydroxyl groups and two thiophene rings. The photoabsorption properties were significantly improved in the long wavelength region compared with the plain phenazine. Further modification of the basic structure with several functional groups strongly affected the photophysical properties and photosensitizing ability to produce $^1\text{O}_2$. The introduction of a nitro group could extend the photoabsorption range up to the NIR region but inhibited the photosensitized $^1\text{O}_2$ generation by the fast nonradiative decay of excited states. On the other hand, a superior photosensitizing ability was achieved by the modification with formyl groups, according to El-Sayed's rule. The phenazine-based photosensitizers with improved photoabsorption properties and $^1\text{O}_2$ quantum yields promise future practical applications such as in photocatalytic synthesis, water purification, and PDT, and the findings obtained in this study will contribute to the establishment of synthetic guidelines for new photosensitizers that show excellent performance of $^1\text{O}_2$ generation.

Acknowledgements

Chapter 2 is reproduced from “Phenazine-based photosensitizers for singlet oxygen generation; K. Imato, K. Ohira, M. Yamaguchi, and Y. Ooyama, *Mater. Chem. Front.*, **2020**, 4, 589–596.” with permission from The Royal Society of Chemistry.

Reference

1. (a) M. C. DeRosa and R. J. Crutchley, *Coord. Chem. Rev.*, **2002**, 233–234, 351; (b) S. Lacombe and T. Pigot, *Catal. Sci. Technol.*, **2016**, 6, 1571.
2. (a) T. Montagnon, D. Kalaitzakis, M. Triantafyllakis, M. Stratakis and G. Vassilikogiannakis, *Chem. Commun.*, **2014**, 50, 15480; (b) B. M. Lamb and C. F. Barbas III, *Chem. Commun.*, **2015**, 51, 3196; (c) D. Kalaitzakis, M. Triantafyllakis, M. Sofiadis, D. Noutsias and G. Vassilikogiannakis, *Angew. Chem. Int. Ed.*, **2016**, 55, 4605; (d) T.-L. Lam, K.-C. Tong, C. Yang, W.-L. Kwong, X. Guan, M.-D. Li, V. Kar-Yan Lo, S. Lai-Fung Chan, D. Lee Phillips, C.-N. Lok and C.-M. Che, *Chem. Sci.*, **2019**, 10, 293.
3. (a) C. M. B. Carvalho, E. Alves, L. Costa, J. P. C. Tomé, M. A. F. Faustino, M. G. P. M. S. Neves, A. C. Tomé, J. A. S. Cavaleiro, A. Almeida, Â. Cunha, Z. Lin and J. Rocha, *ACS Nano*, **2010**, 4, 7133; (b) J. Almeida, J. P. C. Tomé, M. G. P. M. S. Neves, A. C. Tomé, J. A. S. Cavaleiro, Â. Cunha, L. Costa, M. A. F. Faustino and A. Almeida, *Photochem. Photobiol. Sci.*, **2014**, 13, 626; (c) M. Poß, H. Gröger and C. Feldmann, *Chem. Commun.*, **2018**, 54, 1245.
4. (a) Z. Zhou, J. Song, L. Nie and X. Chen, *Chem. Soc. Rev.*, **2016**, 45, 6597; (b) S. Callaghan and M. O. Senge, *Photochem. Photobiol. Sci.*, **2018**, 17, 1490.
5. (a) J. Ohshita, Y. Hayashi, K. Murakami, T. Enoki and Y. Ooyama, *Dalton Trans.*, **2016**, 45, 15679; (b) M. Dichiaro, O. Prezzavento, A. Marrazzo, V. Pittalà, L. Salerno, A. Rescifina and E. Amata, *Eur. J. Med. Chem.*, **2017**, 142, 459; (c) K. Liu, R. A. Lalancette and F. Jäkle, *J. Am. Chem. Soc.*,

2019, 141, 7453.

6. (a) J. M. Dąbrowski, B. Pucelik, A. Regiel-Futyr, M. Brindell, O. Mazuryk, A. Kyzioł, G. Stochel, W. Macyk and L. G. Arnaut, *Coord. Chem. Rev.*, **2016**, 325, 67; (b) F. Taba, A. Onoda, U. Hasegawa, T. Enoki, Y. Ooyama, J. Ohshita and T. Hayashi, *ChemMedChem*, **2018**, 13, 15.
7. (a) D. F. Gloster, L. Cincotta and J. W. Foley, *J. Heterocyclic Chem.*, **1999**, 36, 25; (b) M. Velusamy, J.-Y. Shen, J. T. Lin, Y.-C. Lin, C.-C. Hsieh, C.-H. Lai, C.-W. Lai, M.-L. Ho, Y.-C. Chen, P.-T. Chou and J.-K. Hsiao, *Adv. Funct. Mater.*, **2009**, 19, 2388; (c) A. Pinto, Y. Mace, F. Drouet, E. Bony, R. Boidot, N. Draoui, I. Lobysheva, C. Corbet, F. Polet, R. Martherus, Q. Deraedt, J. Rodríguez, C. Lamy, O. Schicke, D. Delvaux, C. Louis, R. Kiss, A. V. Kriegsheim, C. Dessy, B. Elias, J. Quetin-Leclercq, O. Riant and O. Feron, *Oncogene*, **2016**, 35, 3976.
8. Gaussian 16, Revision A.03, M. J. Frisch, G. W. Trucks, H. B. Schlegel, G. E. Scuseria, M. A. Robb, J. R. Cheeseman, G. Scalmani, V. Barone, G. A. Petersson, H. Nakatsuji, X. Li, M. Caricato, A. V. Marenich, J. Bloino, B. G. Janesko, R. Gomperts, B. Mennucci, H. P. Hratchian, J. V. Ortiz, A. F. Izmaylov, J. L. Sonnenberg, D. Williams-Young, F. Ding, F. Lipparini, F. Egidi, J. Goings, B. Peng, A. Petrone, T. Henderson, D. Ranasinghe, V. G. Zakrzewski, J. Gao, N. Rega, G. Zheng, W. Liang, M. Hada, M. Ehara, K. Toyota, R. Fukuda, J. Hasegawa, M. Ishida, T. Nakajima, Y. Honda, O. Kitao, H. Nakai, T. Vreven, K. Throssell, J. A. Montgomery, Jr., J. E. Peralta, F. Ogliaro, M. J. Bearpark, J. J. Heyd, E. N. Brothers, K. N. Kudin, V. N. Staroverov, T. A. Keith, R. Kobayashi, J. Normand, K. Raghavachari, A. P. Rendell, J. C. Burant, S. S. Iyengar, J. Tomasi, M. Cossi, J. M. Millam, M. Klene, C. Adamo, R. Cammi, J. W. Ochterski, R. L. Martin, K. Morokuma, O. Farkas, J. B. Foresman, and D. J. Fox, Gaussian, Inc., Wallingford CT, 2016.
9. F. Neese, *Wiley Interdiscip. Rev.: Comput. Mol. Sci.*, **2022**, 12, e1606.
10. (a) G. M. Badger, R. S. Pearce and R. Pettit, *J. Chem. Soc.*, **1951**, 3204; (b) J. F. Corbett, *Spectrochim. Acta*, **1964**, 20, 1665; (c) K. Ogawa, M. Miura, T. Nakayama and J. Harada, *Chem.*

- Lett.*, **2003**, *32*, 840; (d) C. Seillan, P. Marsal and O. Siri, *Org. Biomol. Chem.*, **2010**, *8*, 3882; (e) T.-B. Wei, W.-T. Li, Q. Li, J.-X. Su, W.-J. Qu, Q. Lin, H. Yao and Y.-M. Zhang, *Tetrahedron Lett.*, **2016**, *57*, 2767.
11. (a) K. Takagi, A. Mizuno, H. Yoshimura and M. Matsuoka, *Dyes Pigm.*, **1990**, *14*, 203; (b) Y. Ooyama, M. Kanda, K. Uenaka and J. Ohshita, *ChemPhysChem*, **2015**, *16*, 3049; (c) Y. Ooyama, K. Yamaji and J. Ohshita, *Mater. Chem. Front.*, **2017**, *1*, 2243.
 12. D.-C. Lee, B. Cao, K. Jang and P. M. Forster, *J. Mater. Chem.*, **2010**, *20*, 867.
 13. Y. Yamakoshi, N. Umezawa, A. Ryu, K. Arakane, N. Miyata, Y. Goda, T. Masumizu and T. Nagano, *J. Am. Chem. Soc.*, **2003**, *125*, 12803.
 14. K. Gollnick and A. Griesbeck, *Tetrahedron*, **1985**, *41*, 2057.
 15. W. Wu, J. Sun, X. Cui and J. Zhao, *J. Mater. Chem. C*, **2013**, *1*, 4577.
 16. (a) M. A. El-Sayed, *Acc. Chem. Res.*, **1968**, *1*, 8; (b) H. Ma, Q. Peng, Z. An, W. Huang and Z. Shuai, *J. Am. Chem. Soc.*, **2018**, *141*, 1010.
 17. (a) C. Reichardt, R. A. Vogt and C. E. Crespo-Hernández, *J. Chem. Phys.*, **2009**, *131*, 224518; (b) J.-M. Mewes, V. Jovanović, C. M. Marian and A. Dreuw, *Phys. Chem. Chem. Phys.*, **2014**, *16*, 12393.
 18. (a) Y. Yamakoshi, N. Umezawa, A. Ryu, K. Arakane, N. Miyata, Y. Goda, T. Masumizu and T. Nagano, *J. Am. Chem. Soc.*, **2003**, *125*, 12803; (b) S. Oriana, S. Aroua, J. O. B. Söllner, X.-J. Ma, Y. Iwamoto and Y. Yamakoshi, *Chem. Commun.*, **2013**, *49*, 9302.

Chapter 3

Development of phenazine-2,3-diol-based photosensitizers: effect of formyl groups on singlet oxygen generation

Introduction

Photosensitizers (PSs) possessing the ability to produce singlet oxygen ($^1\text{O}_2$) from triplet oxygen ($^3\text{O}_2$) under light irradiation have attracted considerable attention because of their useful applications such as photooxidation in organic and inorganic syntheses¹ and cancer treatment by photodynamic therapy (PDT).² PSs are excited by light, and then, their lowest excited singlet state (S_1) undergoes intersystem crossing (ISC) to become triplet excited states (T_n). Subsequent energy transfer from the lowest excited triplet state (T_1) to $^3\text{O}_2$ produces $^1\text{O}_2$.³ Therefore, high light-harvesting efficiency in the phototherapeutic window (650–900 nm) for PDT and efficient ISC leading to high $^1\text{O}_2$ quantum yields (Φ_Δ) are required for PSs. Previously, incorporation of heavy atoms (e.g., halogens and heavy metals) into PS skeletons has been adopted as an effective strategy to develop PSs with high Φ_Δ values.⁴ However, PSs containing heavy atoms frequently show high cytotoxicity despite the absence of light irradiation and are generally difficult to synthesize.⁵ Therefore, heavy atom-free PSs are required for PDT treatment. As PS skeletons, porphyrin dyes,⁶ phthalocyanine dyes,⁷ phenothiazine dyes,⁸ xanthene dyes,⁹ and fullerene (C_{60}) derivatives¹⁰ are known to show high Φ_Δ values. In particular, heteroanthracene analogs such as rose bengal (RB) and methylene blue (MB) are used as reference samples for evaluation of Φ_Δ (Fig. 1).¹¹ We have focused on phenazine, which is one of the heteroanthracene analogs with two nitrogen atoms at the 9, 10-positions, because of the relative ease of synthesis.¹² However, the photoabsorption of phenazine is limited below 400 nm and phenazine has no $^1\text{O}_2$ generation ability. In **Chapter 2**, in order to overcome the drawbacks of the phenazine

chromophore as a PS, we constructed a phenazine-2,3-diol skeleton having two thiophene rings and two hydroxy groups (**KI-1**).¹³ Actually, phenazine-2,3-diol derivatives (**KI-2–5**) further modified with formyl groups, hexyl groups, and a nitro group have been successfully synthesized by employing simple reactions (Fig. 2a). Interestingly, the photoabsorption onsets of the derivatives reach over 600 nm. Furthermore, we found that only **KI-2** with two formyl groups showed a high Φ_{Δ} (0.48). This result inspired us to investigate the effect of formyl groups in phenazine-2,3-diol-based PSs on their Φ_{Δ} .

Thus, in this study, to gain insight into the enhancement of ISC and $^1\text{O}_2$ generation by formyl groups, we developed phenazine-2,3-diol derivatives **KO-0–3** with zero to three formyl groups, respectively (Fig. 2b), and investigated the relationships between the number of formyl groups in the phenazine-2,3-diol derivatives and $^1\text{O}_2$ generation ability. This study demonstrates the superiority of phenazine-2,3-diol as a promising PS skeleton and suggests an approach for the development of PSs with excellent ability to generate $^1\text{O}_2$.

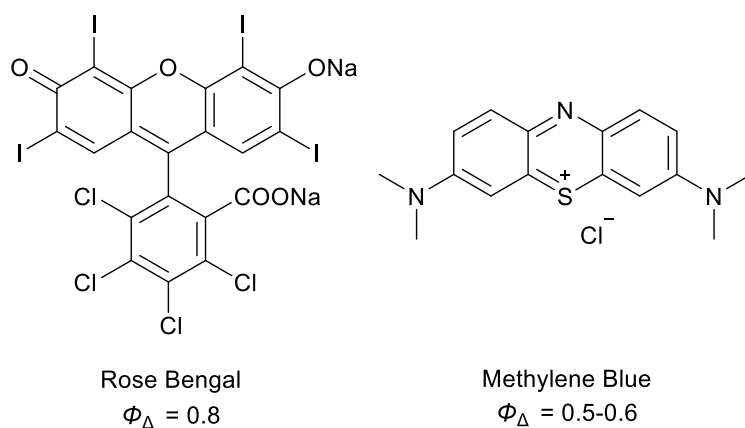


Fig. 1 Chemical structures of heteroanthracene analogs.

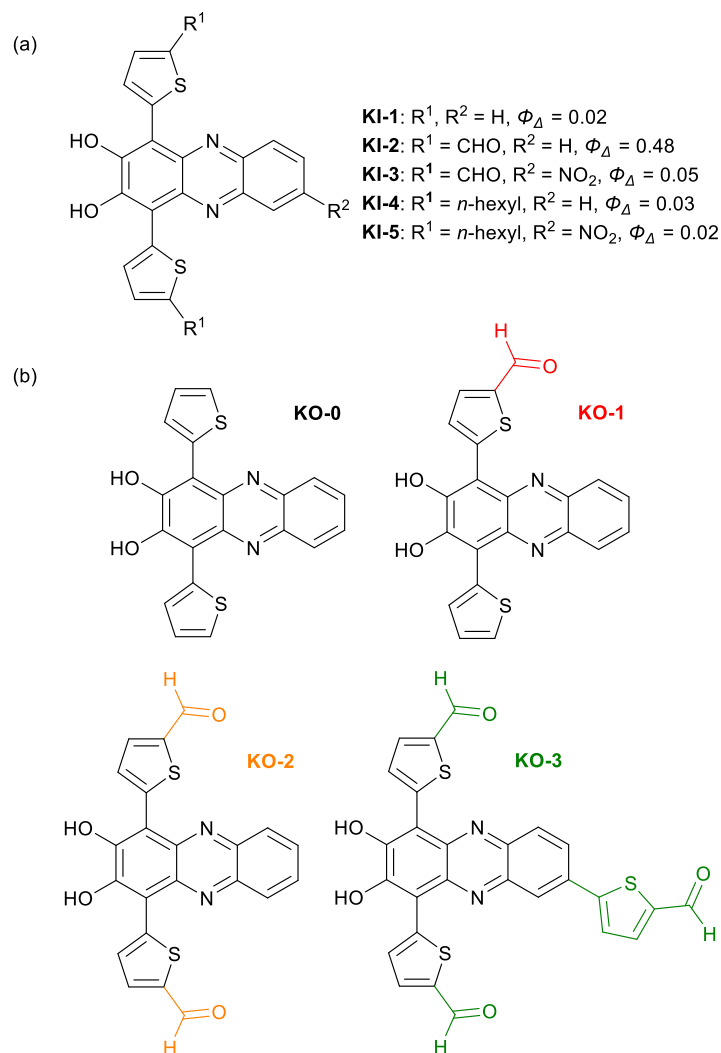


Fig. 2 (a) Chemical structures of phenazine-2,3-diol-based PSs **KI-1–5** with different functional groups and their Φ_{Δ} values employed in **Chapter 2**. (b) Chemical structures of phenazine-2,3-diol-based PSs **KO-0–3** with different numbers of formyl groups designed and synthesized in this study.

Experimental

Materials

All solvents and reagents were used as received, unless otherwise noted. Rose bengal (RB) was purchased from Sigma Aldrich and recrystallized from methanol twice. 1,3-Diphenylisobenzofuran (DPBF) was purchased from Tokyo Chemical Industry and recrystallized from a mixture of dichloromethane and methanol. 2,2,6,6-Tetramethyl-4-piperidone (4-oxo-TEMP) was purchased from FUJIFILM Wako Pure Chemical.

General

^1H NMR and ^{13}C NMR spectra were recorded using a Varian-500 (500 MHz) FT NMR spectrometer. FT-IR spectra were recorded using a Shimadzu IRTracer-100. High-resolution mass spectral data were acquired using a Thermo Fisher Scientific LTQ Orbitrap XL. Photoabsorption spectra were recorded using Shimadzu UV-3150 and UV-3600-plus spectrophotometers. Fluorescence spectra were measured using a Hitachi F-4500 spectrophotometer. The fluorescence quantum yields (Φ_{f}) were determined with a Hamamatsu C9920-01 instrument equipped with CCD by use of a calibrated integrating sphere system. Irradiance of monochromatic and continuous lights for photosensitizing reactions was adjusted using a Newport 1918-C optical power meter.

Evaluation of $^1\text{O}_2$ quantum yield

Quantum yields (Φ_{Δ}) for singlet oxygen ($^1\text{O}_2$) generation by **KO-0-3** and the corresponding precursors **5-8** were evaluated by monitoring the changes in the photoabsorption spectra of 1,3-diphenylisobenzofuran (DPBF), a $^1\text{O}_2$ scavenger, in tetrahydrofuran (THF) upon photoirradiation. DPBF traps the generated $^1\text{O}_2$ to be oxidized. THF was bubbled with air for 10 min, prior to preparation of the solutions. The concentration of DPBF was 50 mM in the air-saturated THF solutions. The concentration of the photosensitizers (PSs) and rose bengal (RB) was adjusted so that the absorbance was ca. 0.03 at the irradiation wavelength (509 nm). The THF solutions containing DPBF and **KO-0-**

3 or the corresponding precursors **5–8** were irradiated with monochromatic light (509 nm, and 300 mW cm⁻²) that was obtained by passage of a xenon light source (HAL-320, Asahi Spectra) through a monochromator (CMS-100, Asahi Spectra). Except for the nonirradiated solutions, each spectrum was measured immediately after photoirradiation for 1 min. The procedure was promptly repeated until the total photoirradiation time reached 10 min. The changes in optical density (ΔOD) of DPBF were plotted against photoirradiation time to obtain the slopes (m) and estimate Φ_{Δ} values. After confirming that there is no self-degradation of the PSs by the ¹O₂, the Φ_{Δ} values of **KO-0–3** and the corresponding precursors **5–8** were determined by the relative method using RB ($\Phi_{\Delta} = 0.80$ in MeOH) as a standard according to the following equation (1):

$$\Phi_{\Delta\text{sam}} = \Phi_{\Delta\text{ref}} \times [(m_{\text{sam}}/m_{\text{ref}}) \times (L_{\text{ref}}/L_{\text{sam}})] \quad (1)$$

where $\Phi_{\Delta\text{sam}}$ and $\Phi_{\Delta\text{ref}}$ are ¹O₂ quantum yields of phenazine PSs and RB, respectively, m_{sam} and m_{ref} are slopes in the plots of ΔOD at the photoabsorption maximum wavelength of DPBF (413 nm) against photoirradiation time, and L_{sam} and L_{ref} are light harvesting efficiencies, which are given by $L = 1 - 10^{-A}$ (“ A ” is the absorbance at the photoirradiation wavelength).

Photosensitizing ability

Photosensitizing ability of phenazine derivatives under continuous visible-light irradiation (>510 nm, 30 mW) was evaluated in THF solutions containing **KO-0–3** or the corresponding precursors **5–8** (5 μM) and DPBF as a ¹O₂ scavenger (50 μM). THF was bubbled with air for 10 min, prior to preparation of the solutions. The continuous light was obtained by passage of a xenon light source (HAL-302, Asahi Spectra) through a 510 nm long path filter. Except the nonirradiated solutions, each spectrum was measured immediately after photoirradiation for 1 min. The procedure was promptly repeated until the total irradiation time reached 10 min. Then, $\ln(C_t/C_0)$ was plotted against photoirradiation time, where C_t is a concentration of DPBF at the reaction time (t) and C_0 is the initial concentration of DPBF before photoirradiation. C_t was calculated based on Lambert–Beer law ($A_{\text{DPBF}} = \epsilon cl$) using the

maximum absorbance at 413 nm. Since the $\ln(C_t/C_0)$ plots showed linear decreases with the increase in photoirradiation time, the slopes were used to estimate the first-order rate constants (k_{obs}) of the DPBF oxidation by $^1\text{O}_2$ generated using the phenazine PSs. The k_{obs} value for RB was also obtained in a same manner.

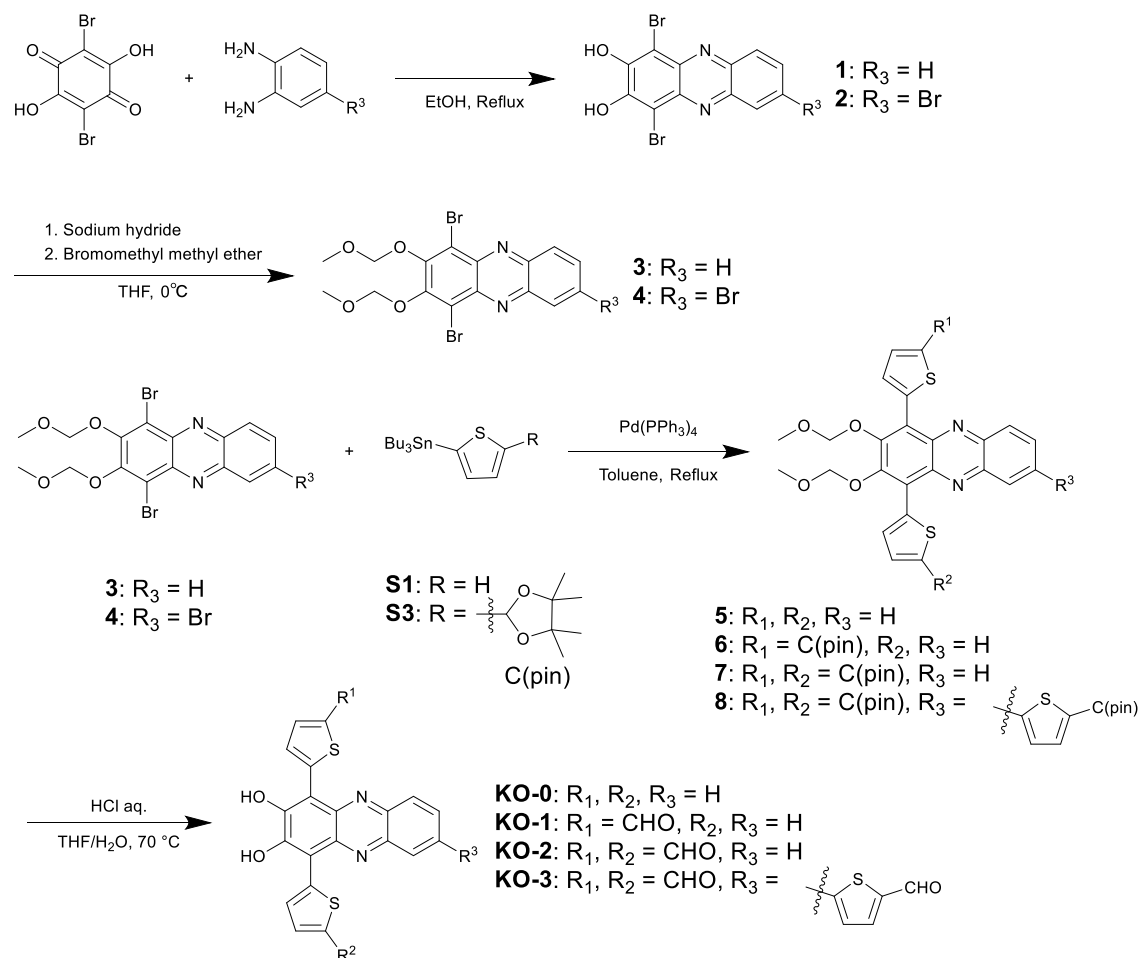
EPR measurements

Air-saturated THF solutions containing **KO-0-3** as a PS (5 μM) and 4-oxo-TEMP as a spin-trapping agent (50 mM) were prepared. THF was bubbled with air for 10 min, prior to preparation of the solutions. Their electron paramagnetic resonance (EPR) spectra were recorded before and after exposure to continuous visible light (>510 nm, and 30 mW cm^{-2}) for 60 min on a Bruker ELEXSYS E500 spectrometer. The continuous light was obtained by passage of a xenon light source (HAL-302, Asahi Spectra) through a 510 nm long path filter. The reaction of 4-oxo-TEMP with $^1\text{O}_2$ produces a stable nitroxide radical (4-oxo-TEMPO), showing a characteristic 1 : 1 : 1 triplet signal.

Theoretical calculations

The Gaussian 16 program¹⁴ was used for density functional theory (DFT) calculations. The S_0 geometries of these PSs were optimized via frequency calculations at the B3LYP/6-31G(d,p)/THF-CPCM level. There are no imaginary frequencies for all optimized structures. The spin-orbit coupling (SOC) matrix elements were calculated at the B3LYP/6-31G(d,p)/THF-CPCM level using the ORCA 5.0.4 program.¹⁵ These calculations were performed using the optimized S_0 geometries of these PSs.

Synthesis



Scheme 1 Synthetic route for phenazine-2,3-diol-based PSs **KO-0**, **KO-1**, **KO-2**, and **KO-3**.

Phenazine KO-0. **KO-0** was synthesized by the method reported in **Chapter 2**¹³; m.p. over 300 °C; IR (ATR): $\tilde{\nu}$ = 3065 (br), 1614, 1549, 1510, 1483 cm⁻¹.

Phenazine KO-1. A solution of compound **6** (0.015 g, 0.0253 mmol) and 1N HCl aq. (2 mL) in the mixture of THF (10 mL) and water (10 mL) was stirred at 70 °C. After disappearance of the reactants, saturated NaHCO₃ solution was added to the mixture for neutralization. Then, ethyl acetate was added to the mixture, and the extracted organic layer was washed with saturated saline once, dried over anhydrous Na₂SO₄, filtered, and concentrated. The crude product was dissolved in THF and precipitated in hexane to give phenazine **KO-1** as brown solid (0.010 g, 98% yield); m.p. over 300 °C; IR (ATR): $\tilde{\nu}$ = 3316 (br), 2924, 2851, 1597, 1551 cm⁻¹; ¹H NMR (500 MHz, DMSO-*d*₆): δ = 9.86 (s, 1H, CHO), 9.27 (d, *J* = 4.3 Hz, 1H, aromatic), 8.34 (d, *J* = 3.8 Hz, 1H, aromatic), 8.05–8.18 (m, 2H, aromatic), 7.92 (d, *J* = 4.3 Hz, 1H, aromatic), 7.65–7.75 (m, 1H, aromatic), 7.57–7.65 (m, 2H, aromatic), 7.20 (dd, *J* = 5.3 and 3.8 Hz, 1H, aromatic) ppm; ¹³C NMR spectrum could not be obtained because of the low solubility in any solvents; HRMS (APCI): *m/z* found 403.02133 [M-H]⁻, calculated for C₂₁H₁₁O₃N₂S₂ [M-H]⁻: 403.02166.

Phenazine KO-2. A solution of compound **7** (0.0506 g, 0.0702 mmol) and 1N HCl aq. (4 mL) in the mixture of THF (25 mL) and water (25 mL) was stirred at 70 °C until insoluble components precipitated. The precipitate was filtered and washed with hexane to give phenazine **KO-2** as black solid (0.0264 g, 87% yield); m.p. over 300 °C; IR (ATR): $\tilde{\nu}$ = 3177 (br), 1647, 1636, 1616, 1541 cm⁻¹; ¹H NMR (500 MHz, DMSO-*d*₆): δ = 9.97 (s, 2H, CHO), 8.56 (br, 2H, aromatic), 8.08–8.17 (m, 2H, aromatic), 8.05 (d, *J* = 4.1 Hz, 1H, aromatic), 7.68–7.77 (m, 2H, aromatic) ppm; ¹³C NMR spectrum could not be obtained because of the low solubility in any solvents; HRMS (APCI): *m/z* found 431.01569 [M-H]⁻, calculated for C₂₂H₁₁O₄N₂S₂ [M-H]⁻: 431.01657.

Phenazine KO-3. A solution of compound **8** (51.3 mg, 55.0 μmol) and 1N HCl aq. (4 mL) in the mixture of THF (25 mL) and water (25 mL) was stirred at 70 °C for 24 h. The precipitate was filtered

and washed with water and hexane to give phenazine **KO-3** as black solid (26.8 mg, 90% yield); m.p. over 300 °C; IR (ATR): $\tilde{\nu}$ = 3146 (br), 3092, 2924, 2847, 2124, 1896, 1653, 1616, 1545, 1516 cm^{-1} ; ^1H NMR (500 MHz, $\text{DMSO-}d_6$): δ = 9.97 (s, 2H, CHO), 9.96 (s, 1H, CHO), 8.58–8.99 (br, 2H, aromatic), 8.46 (d, J = 2.1 Hz, 1H, aromatic), 8.19 (d, J = 8.7 Hz, 1H, aromatic), 8.10–8.16 (2H, aromatic), 7.99–8.07 (m, 3H, aromatic) ppm; ^{13}C NMR spectrum could not be obtained because of the low solubility in any solvents; HRMS (APCI): m/z found 540.99799 $[\text{M-H}]^-$, calculated for $\text{C}_{27}\text{H}_{13}\text{O}_5\text{N}_2\text{S}_3$ $[\text{M-H}]^-$: 540.99921.

Results and discussion

Synthesis

Phenazine-2,3-diol-based PSs **KO-0–3** were synthesized by a stepwise synthetic protocol as shown in Scheme 1. Compounds **1** and **2** were prepared by the cyclodehydration of 2,5-dibromo-3,6-dihydroxy-*p*-quinone with 1,2-benzenediamine or 4-bromo-1,2-benzenediamine, respectively. However, it is difficult to use **1** and **2** in the subsequent reaction due to their low solubility. Thus, **1** and **2** were converted to methoxymethyl (MOM)-protected compounds **3** and **4**, which have good solubility in organic solvents. Indeed, the Stille coupling of **3** and **4** with the corresponding stannyl thiophene derivatives¹⁶ successfully gave compounds **5**, **7** and **8**. Unsymmetrical compound **6** was prepared by the Stille coupling of compound **3** with an equimolar mixture of compounds **S1** and **S3**. Finally, **5–8** were hydrolyzed by treatment with acid in a 1/1 (v/v) mixed solvent of tetrahydrofuran (THF)/water to produce **KO-0–3** with high purity. In **Chapter 2**,¹³ the hydrolysis of **6** was performed in pure THF, but the resulting **KI-2** (**KO-2** in this study) is of low purity. The impurities were successfully removed from **KO-2** by using the mixed solvent of THF/water, which would result in the difference in Φ_{Δ} values between **KO-2** in this study and **KI-2** in **Chapter 2**, as discussed below. **KO-0–3** were characterized by ¹H NMR, FT-IR, and high-resolution mass spectrometric analysis, although we could not obtain their ¹³C NMR spectra due to the low solubility in any organic solvents.

Photoabsorption properties

The UV-vis photoabsorption, excitation, and fluorescence spectra of **KO-0–3** and the corresponding precursors **5–8** in THF are shown in Fig. 3, and the optical data are summarized in Table 1. Phenazine derivatives **5**, **6**, and **7** show two photoabsorption peaks: a sharp band around 380 nm is ascribable to the $\pi \rightarrow \pi^*$ transition of the phenazine skeleton, and the other band at 410–550 nm is ascribable to the $\pi \rightarrow \pi^*$ transition of the phenazine skeleton containing two thiophene units at the 1,4-positions.¹⁷ The red shift of the bands in phenazine derivative **8** indicates that the additional introduction of a thiophene

unit at the 6-position onto the phenazine skeleton results in extended conjugation. Phenazine-2,3-diol-based PSs **KO-0-3** show two photoabsorption bands in longer wavelength regions of 300–500 nm and 500–650 nm, compared with those of **5-8**. The large red shifts of the photoabsorption from **5-8** to **KO-0-3** by the deprotection of the hydroxy and formyl groups are mainly attributed to the formation of phenoxide ions by the partial deprotonation of the hydroxyl groups.¹⁸ This was supported in **Chapter 2**¹³ and also demonstrated by the fact that the deprotection of only hydroxy groups in **5** caused the pronounced red shift as observed in **KO-0**. In addition, the broad photoabsorption band of phenazine-2,3-diol at around 400–550 nm was decreased upon addition of HCl and increased upon addition of NaOH. Although the photoabsorption onsets of **KO-1-3** are slightly red-shifted with increasing number of formyl groups, their deprotection of formyl groups contribute less to the large red shifts.

The phenazine derivatives **5-8** show fluorescence maxima ($\lambda_{\text{fl}}^{\text{fl}}_{\text{max}}$) at around 610–626 nm and moderate fluorescence quantum yields ($\Phi_{\text{fl}} = 0.34\text{--}0.46$). The fluorescence band of **8** is slightly red-shifted due to the extended conjugation by the additional introduction of a thiophene unit at the 6-position on the phenazine skeleton, as is the photoabsorption. The $\lambda_{\text{fl}}^{\text{fl}}_{\text{max}}$ of **KO-0-2** appear at around 574–609 nm and are gradually blue-shifted as the number of formyl groups increases. The pronounced blue shift in symmetric **KO-2** would be because its dipole moment in the excited state is smaller than those of the other asymmetric PSs, which makes the excited state less stable in THF as a moderately polar solvent. On the other hand, the fluorescence band of **KO-3** ($\lambda_{\text{fl}}^{\text{fl}}_{\text{max}} = 610$ nm) is red-shifted compared to those of **KO-0-2** ($\lambda_{\text{fl}}^{\text{fl}}_{\text{max}} = 609$ nm for **KO-0**, 598 nm for **KO-1**, and 574 nm for **KO-2**), indicating that the bathochromic effect by the thiophene ring surpasses the hypsochromic effect by the formyl group on $\lambda_{\text{fl}}^{\text{fl}}_{\text{max}}$. **KO-0-3** exhibit lower Φ_{fl} (0.024–0.097) than those of the corresponding precursors **5-8**, which is attributed to enhanced ISC and nonradiative decay, as discussed later.

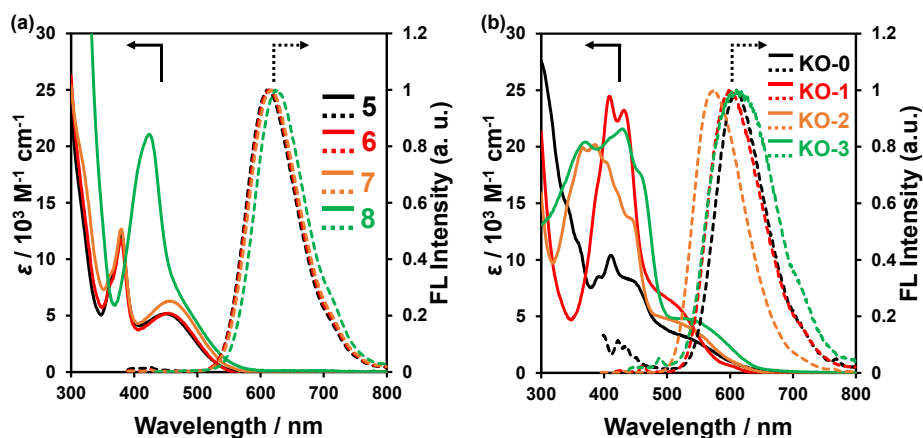


Fig. 3 (a) Photoabsorption (solid lines) and fluorescence (dashed lines) spectra of phenazine derivatives **5–8** in THF. (b) Photoabsorption (solid lines) and fluorescence (dashed lines) spectra of **KO-0–3** in THF.

Table 1 Optical data, fluorescence quantum yields (Φ_f), $^1\text{O}_2$ quantum yields (Φ_Δ), and first-order rate constants (k_{obs}) for photooxidation of DPBF of phenazine derivatives **5–8** and **KO-0–3** in THF

Dye	$\epsilon / \text{M}^{-1} \text{cm}^{-1}$ @509 nm	$\lambda_{\text{max}}^{\text{fl}} / \text{nm}$	Φ_f [a]	Φ_Δ [b]	$k_{\text{obs}} / \text{min}^{-1}$ [c]
5	1900	610	0.42	0.040	0.0046
6	2100	614	0.46	0.038	0.0031
7	3000	618	0.45	0.23	0.0025
8	3500	626	0.34	0.11	0.0087
KO-0	3600	609	0.053	0.036	0.0046
KO-1	6200	598	0.050	0.22	0.046
KO-2	4700	574	0.097	0.33	0.12
KO-3	4800	610	0.024	0.41	0.052

[a] Fluorescence quantum yields excited at 509 nm were determined by using a calibrated integrating sphere system. [b] $^1\text{O}_2$ quantum yields (relative decomposition rate of DPBF) using RB as a standard ($\Phi_\Delta = 0.80$ in MeOH¹⁹) and DPBF as a $^1\text{O}_2$ scavenger. The Φ_Δ values were estimated under an assumption that the reactivity of $^1\text{O}_2$ is independent of the kind of solvents. [c] First-order rate constants for the reaction of DPBF with $^1\text{O}_2$ generated upon photoexcitation of the phenazine derivatives. The k_{obs} for RB is 0.351 min^{-1} .¹³

¹O₂ generation

We evaluated the ¹O₂ generation ability of the phenazine derivatives as PSs. It is well known that 1,3-diphenylisobenzofuran (DPBF) acts as an efficient ¹O₂ scavenger to become its oxidized product, *o*-dibenzoylbenzene.²⁰ Thus, ¹O₂ generation by **KO-0-3** in THF was investigated, together with that of the corresponding precursors **5-8**, by monitoring the photoabsorption spectral changes of DPBF accompanied by the reaction of DPBF with the generated ¹O₂ (Fig. 4a–d and 5a–d). THF was bubbled with air for 10 min prior to preparing solutions. Air-saturated THF solutions containing DPBF and each phenazine derivative were irradiated with monochromatic light at 509 nm (300 μW cm⁻²) that was obtained by passage of a xenon light source through a monochromator. In all solutions, the photoabsorption band of DPBF peaked at around 410 nm decreased with the increase in photoirradiation time, which indicates that DPBF reacted with ¹O₂ generated by the photoexcitation of the phenazine derivatives. However, the decrements are significantly different between the solutions. Thus, the changes in optical density (ΔOD) of DPBF at 413 nm were plotted against photoirradiation time to estimate Φ_Δ values of the phenazine derivatives (Fig. 4e and 5e). The Φ_Δ values were calculated from the slopes (*m*_{sam}) of the plots using RB (Φ_Δ = 0.80 in MeOH) as a standard sample (Table 1).¹⁹ **KO-3** with three formyl groups exhibit the highest Φ_Δ value (0.41), and the Φ_Δ values increase in the order of **KO-0** (0.036) < **KO-1** (0.22) < **KO-2** (0.33) < **KO-3** (0.41). On the other hand, compounds **5-8** show no correlation between the number of protected formyl groups and the Φ_Δ values (0.038–0.23, Table 1). These results strongly suggest that the formyl groups additively facilitate the ISC from the singlet to triplet states and contribute to singlet oxygen generation. In aromatic carbonyl compounds, the ISC is facilitated by the accompanying change of molecular orbital type, such as transitions of ¹(nπ*) to ³(ππ*) and ¹(ππ*) to ³(nπ*) based on El-Sayed's rule.²¹ There have been several studies on the effect of the number of heavy atoms on Φ_Δ, based on heavy atom effect.²² To the best of our knowledge, however, the present study is the first report on the effect of the number of formyl

groups on Φ_{Δ} , based on El-Sayed's rule. The facilitated ISC by the formyl groups is also supported by the fact that the Φ_{fl} values of **KO-1-3** (0.024–0.097) are lower than those of compounds **6-8** (0.34–0.46), whose formyl groups are protected, as shown in Table 1.

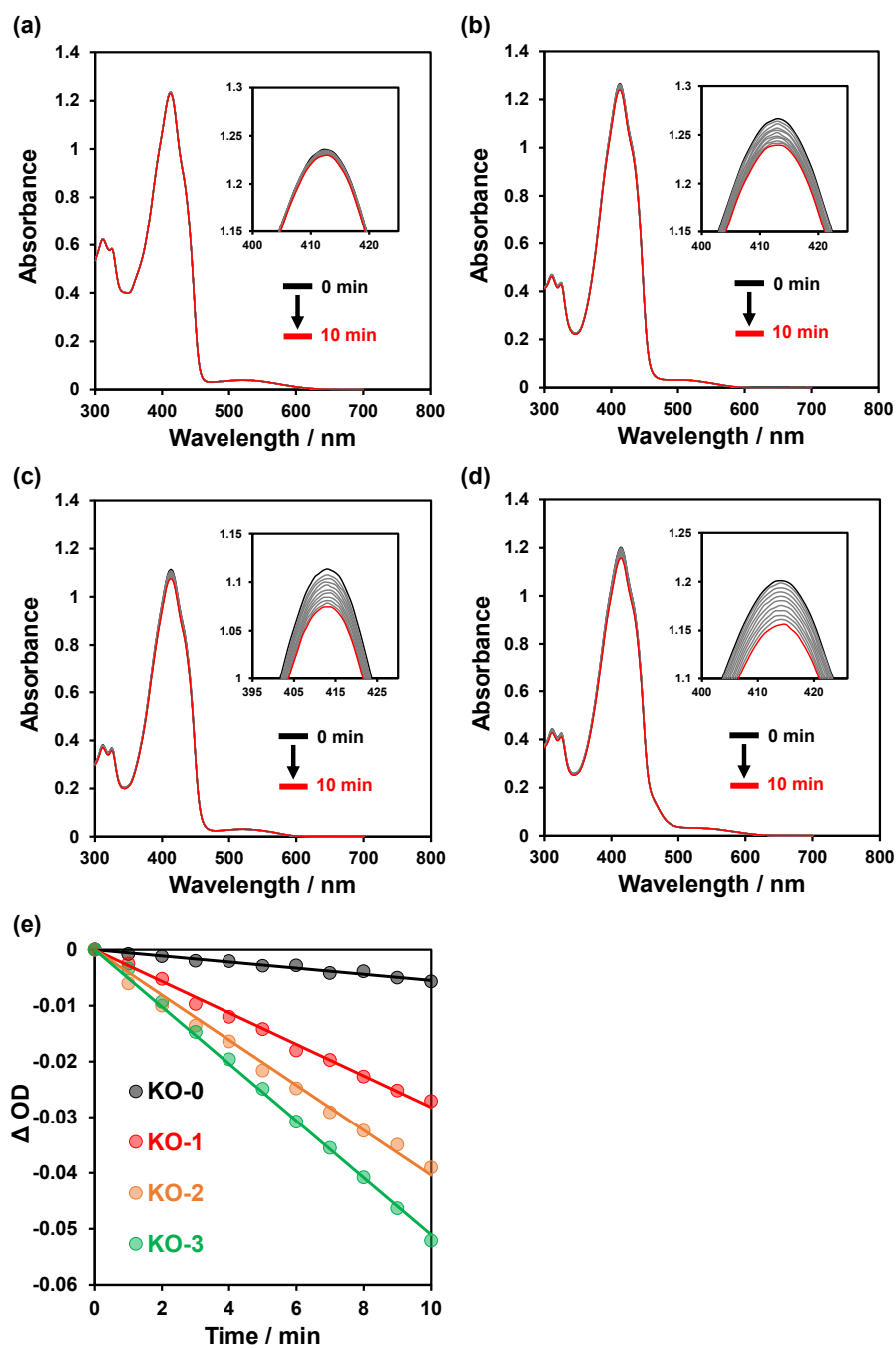


Fig. 4 Photoabsorption spectra of DPBF (50 μM) in the presence of phenazine-2,3-diol-based photosensitizers (a) **KO-0**, (b) **KO-1**, (c) **KO-2**, or (d) **KO-3** (Abs. @509 nm = ca. 0.03) upon irradiation with a monochromatic light (509 nm, 300 $\mu\text{W cm}^{-2}$) in THF. Insets are magnifications of peak tops in the spectra around 410 nm. Plots of ΔOD of DPBF at 413 nm against photoirradiation time (509 nm, 300 $\mu\text{W cm}^{-2}$) in the presence of (e) **KO-0–3** in THF.

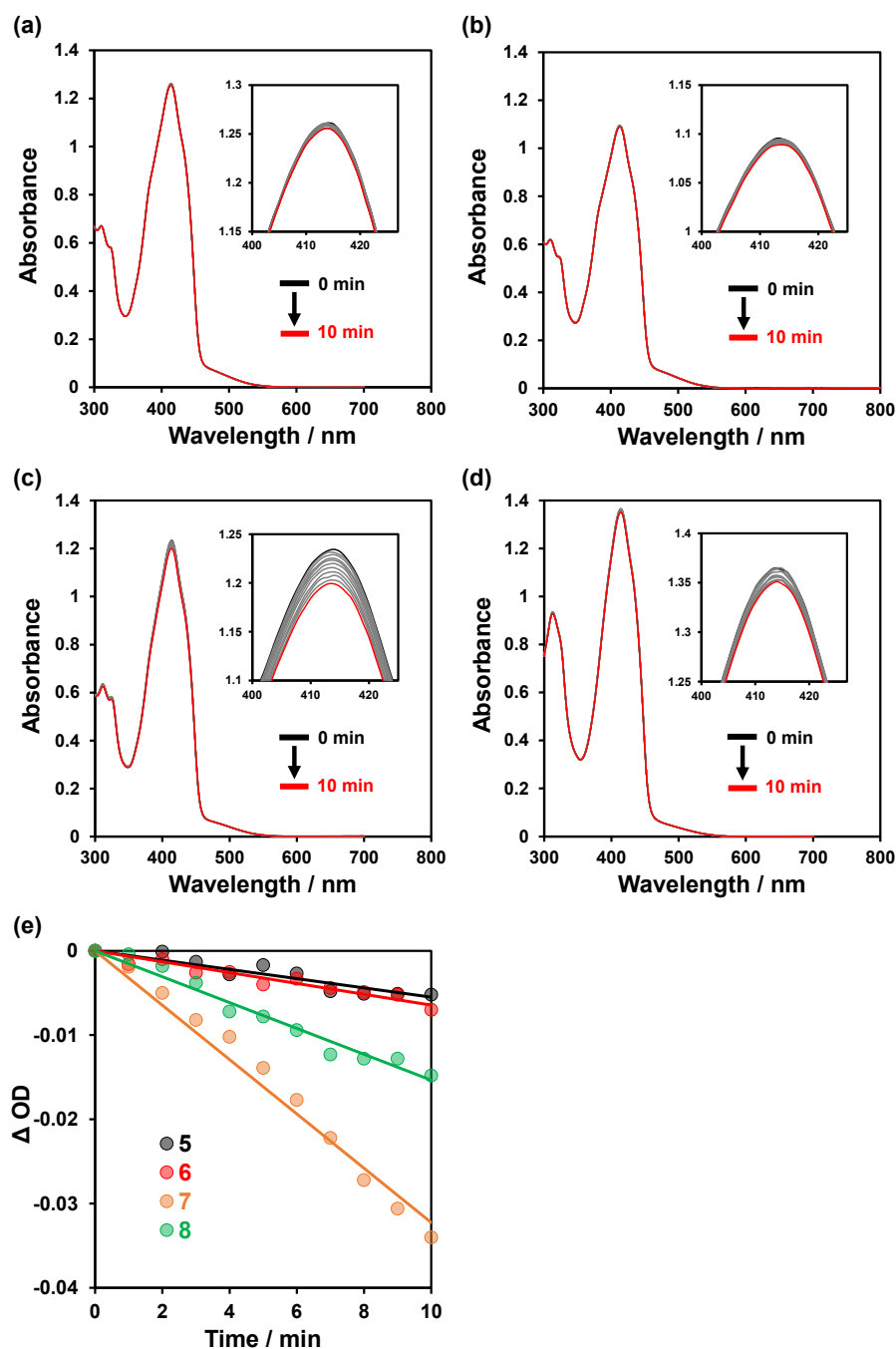


Fig. 5 Photoabsorption spectra of DPBF (50 μM) in the presence of phenazine-2,3-diol-based photosensitizers (a) **5**, (b) **6**, (c) **7** or (d) **8** (Abs. @509 nm = ca. 0.03) upon irradiation with a monochromatic light (509 nm, 300 $\mu\text{W cm}^{-2}$) in THF. Insets are magnifications of peak tops in the spectra around 410 nm. Plots of ΔOD of DPBF at 413 nm against photoirradiation time (509 nm, 300 $\mu\text{W cm}^{-2}$) in the presence of (e) compounds **5–8** in THF.

Photosensitizing ability

For further investigation of the photosensitizing ability of the PSs, the $^1\text{O}_2$ generation and DPBF degradation upon exposure to continuous visible light ($>510\text{ nm}$, and 30 mW cm^{-2}) were evaluated in air-saturated THF solutions containing DPBF and **KO-0-3** or **5-8**. The continuous light was obtained by passage of a xenon light source through a 510 nm long path filter. The photoabsorption spectra in the photooxidation of DPBF using **KO-0-3** or **5-8** are shown in Fig. 6a–d and 7a–d. To gain insight into the effect of the formyl substituents on the photosensitizing properties of the PSs, the $\ln(C_t/C_0)$ was plotted against photoirradiation time, where C_t is the concentration of DPBF at the reaction time (t) and C_0 is the initial concentration of DPBF before photoirradiation (Fig. 6e and 7e). In all PSs, the $\ln(C_t/C_0)$ shows a linear decrease with the increase in photoirradiation time, providing the first-order rate constants (k_{obs}) for the oxidation of DPBF by $^1\text{O}_2$ generated using the phenazine derivatives as PSs (Table 1). The k_{obs} values of **KO-1** (0.046 min^{-1}), **KO-2** (0.12 min^{-1}), and **KO-3** (0.052 min^{-1}) are greater than that of **KO-0** (0.0046 min^{-1}), according to El-Sayed's rule, although no correlation is found between the k_{obs} values and the number of formyl groups. The inconsistent k_{obs} values would be due to the difference in photoabsorbance (*i.e.*, light harvesting efficiency) above 510 nm . As shown in Fig. 5a–d, above 510 nm , **KO-2** has the highest light harvesting efficiency at this concentration ($5\text{ }\mu\text{M}$) among **KO-0-3**, resulting in the highest k_{obs} value. Obviously, the lower k_{obs} values of compounds **5-8** are due to no formyl groups and the weak or no photoabsorption above 510 nm . These results demonstrate that **KO-1-3** with formyl groups have more efficient photosensitizing ability according to El-Sayed's rule and improved photoabsorption properties, compared to those of **KO-0** and **5-8** with no formyl groups.

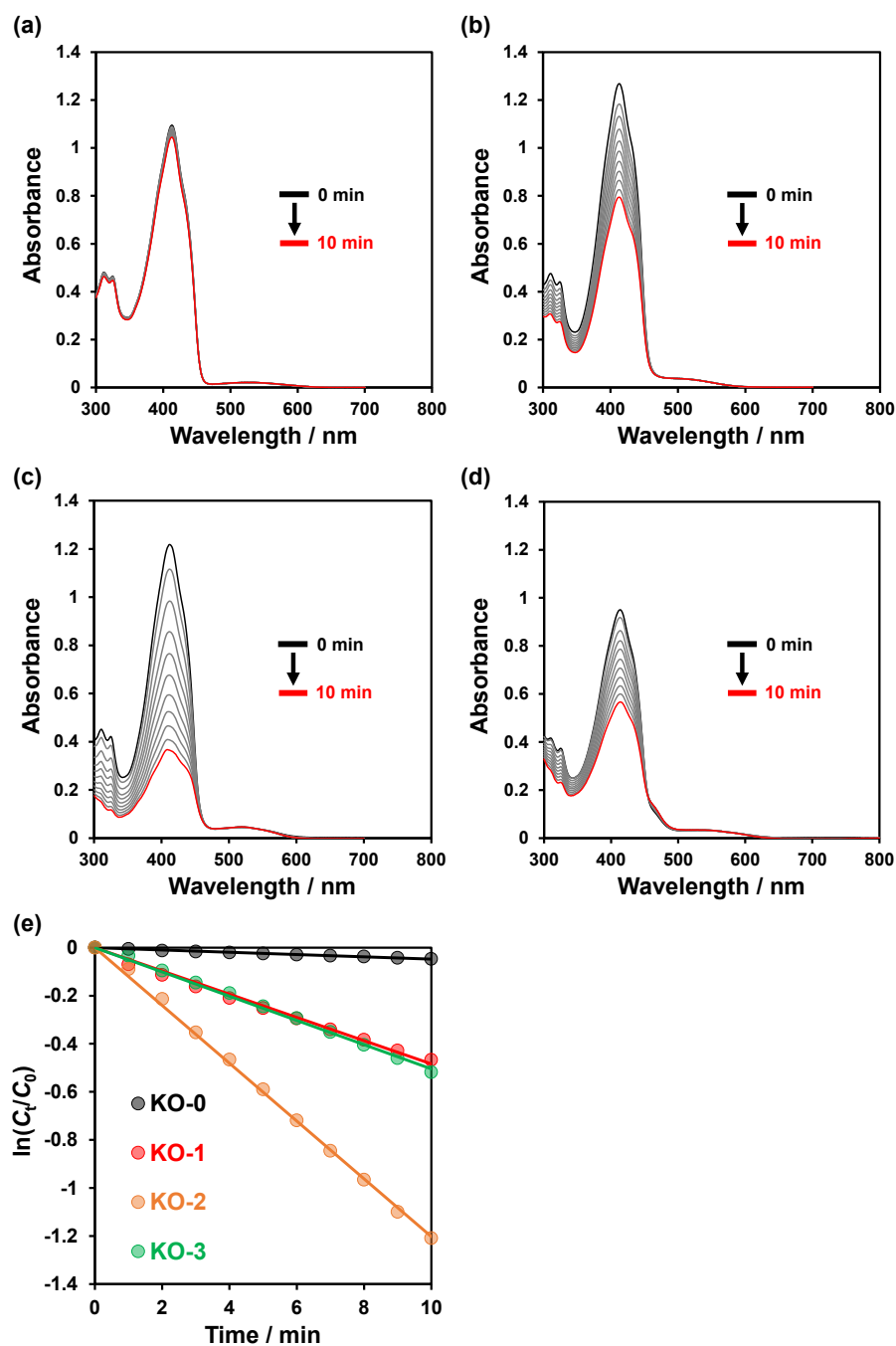


Fig. 6 Photoabsorption spectra of DPBF (50 μM) in the presence of phenazine photosensitizers (a) KO-0, (b) KO-1, (c) KO-2, or (d) KO-3 (5 μM) upon irradiation with a continuous light (>510 nm, 30 mW cm^{-2}) in THF. Plots of $\ln(C_t/C_0)$ of DPBF against photoirradiation time (>510 nm, 30 mW cm^{-2}) in the presence of (e) KO-0–3 in THF.

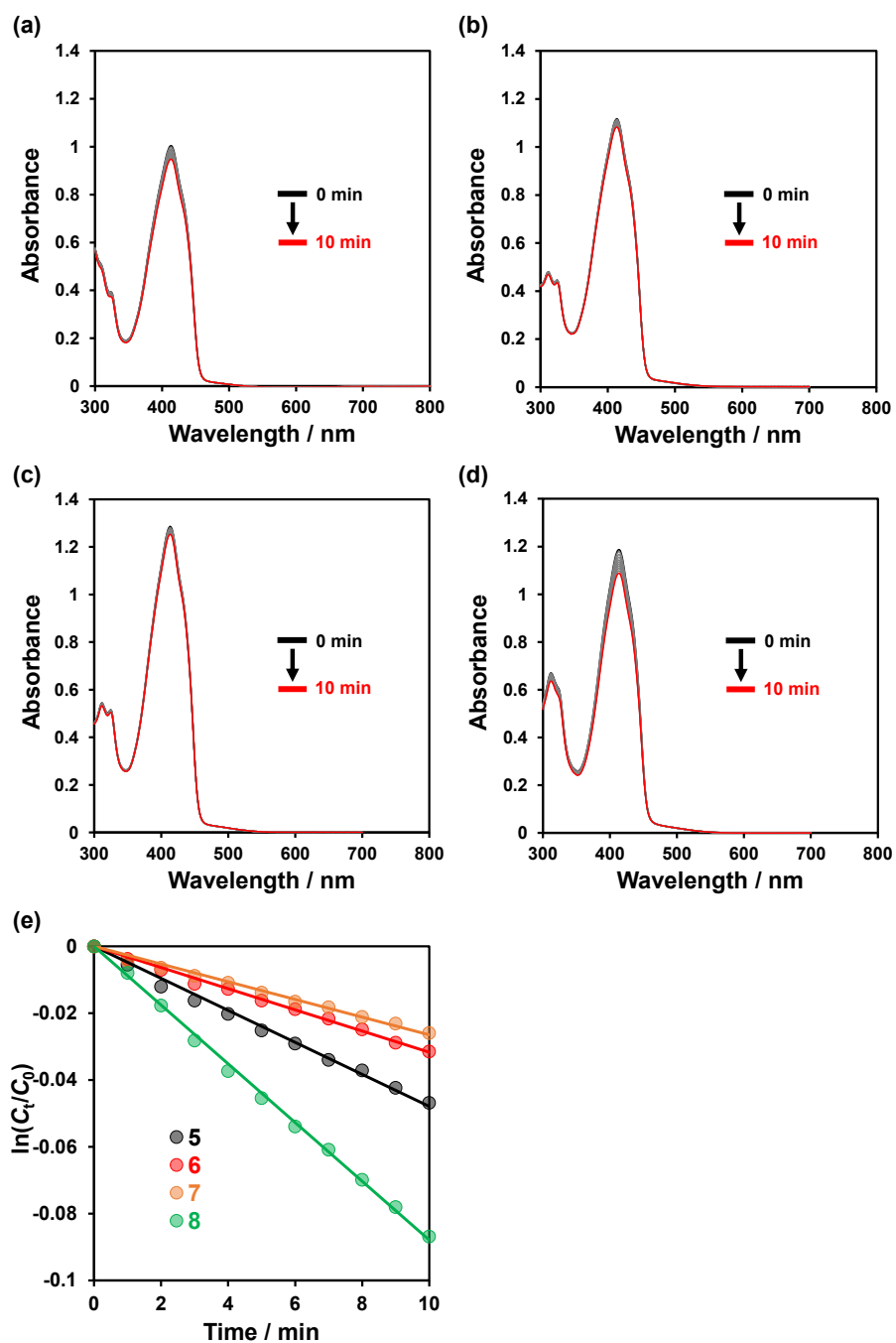


Fig. 7 Photoabsorption spectra of DPBF (50 μM) in the presence of phenazine photosensitizers (a) 5, (b) 6, (c) 7 or (d) 8 (5 μM) upon irradiation with a continuous light ($>510\text{ nm}$, 30 mW cm^{-2}) in THF. Plots of $\ln(C_t/C_0)$ of DPBF against photoirradiation time ($>510\text{ nm}$, 30 mW cm^{-2}) in the presence of (e) compounds 5–8 in THF.

EPR measurement

To confirm $^1\text{O}_2$ generated by the phenazine PSs, electron paramagnetic resonance (EPR) spectroscopy was also employed with 2,2,6,6-tetramethyl-4-piperidone (4-oxo-TEMP) as a spin-trapping agent, which can react with $^1\text{O}_2$ to produce 4-oxo-TEMPO, a stable nitroxide radical.²³ When the air-saturated solutions containing **KO-0-3** and 4-oxo-TEMP were irradiated with continuous visible light (>510 nm, and 30 mW cm^{-2}) obtained by passage of a xenon light source through a 510 nm long path filter, the EPR spectrum of 4-oxo-TEMPO was clearly observed as a characteristic 1 : 1 : 1 triplet signal (Fig. 8). The EPR intensity after light exposure increases in the order of **KO-0** < **KO-1** < **KO-2** < **KO-3**. This result also demonstrates that in **KO-0-3**, the photogenerated $^1\text{O}_2$ increases as the number of formyl groups increases, which is consistent with the trend of their Φ_{Δ} values.

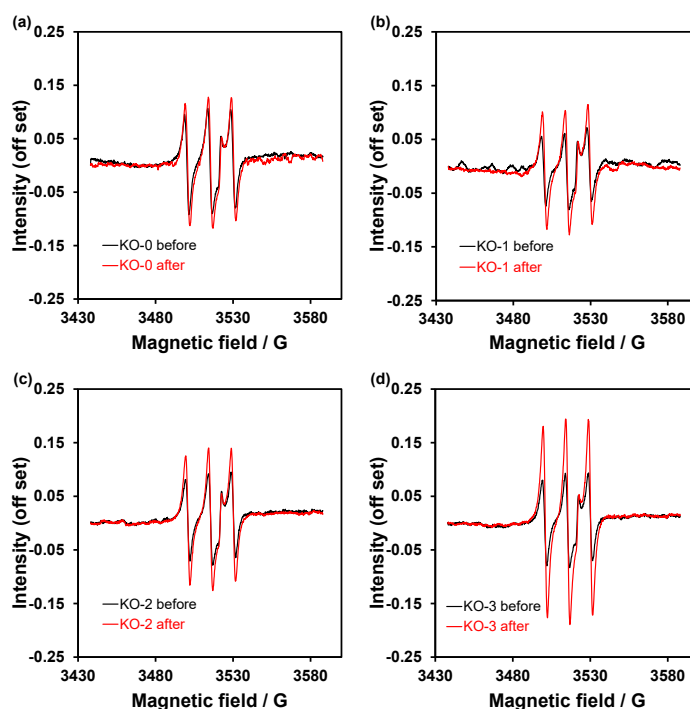


Fig. 8 EPR spectra of air-saturated THF solutions containing 4-oxo-TEMP (50 mM) and (a) **KO-0**, (b) **KO-1**, (c) **KO-2**, or (d) **KO-3** (5 μM) before and after exposure to continuous visible light (>510 nm, 30 mW cm^{-2}) for 60 min. The characteristic 1:1:1 triplet signal originates from a stable nitroxide radical (4-oxo-TEMPO) formed by the reaction of 4-oxo-TEMP with $^1\text{O}_2$.

Theoretical calculations

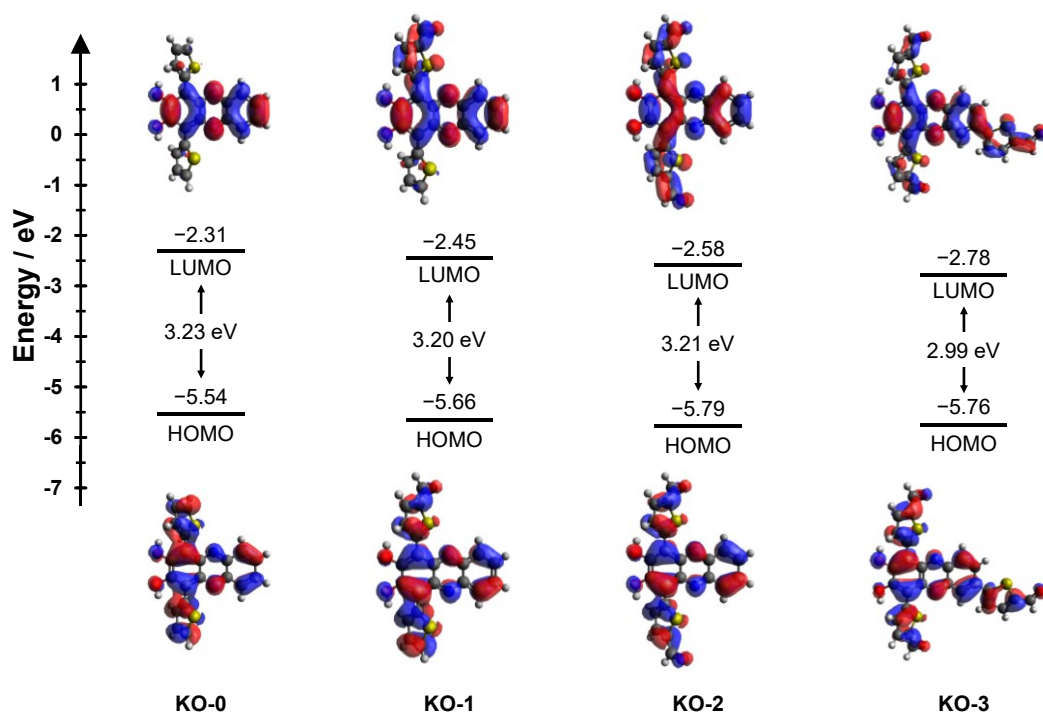


Fig. 9 Energy level diagram, HOMO and LUMO of **KO-0-3** at the B3LYP/6-31G(d,p)/THF-CPCM level using DFT calculations.

In order to investigate the electronic structures and molecular orbitals of phenazine-2,3-diol-based PSs, DFT calculations¹⁴ at the B3LYP/6-31G(d,p)/THF-CPCM level were performed (Fig. 9). The DFT calculations revealed that the highest occupied molecular orbitals (HOMOs) for these PSs are delocalized over the whole molecule. The lowest unoccupied molecular orbital (LUMO) for **KO-0** is delocalized on phenazine-2,3-diol moiety, but the LUMOs for **KO-1**, **KO-2**, and **KO-3** are delocalized over the whole molecule. Thus, it was found that the formyl groups on thiophene units expanded LUMO distributions, leading to the decrease of the LUMO energy levels (-2.31 eV for **KO-0**, -2.45 eV for **KO-1**, -2.58 eV for **KO-2**, and -2.78 eV for **KO-3**). Although the introduction of the electron-withdrawing formyl groups also lead to the lowering of the HOMO energy levels (-5.54 eV for **KO-0**, -5.66 eV for **KO-1**, -5.79 eV for **KO-2**, and -5.76 eV for **KO-3**), the lowering in the LUMOs are

larger than that in the HOMOs, and thus resulting in the decrease of HOMO-LUMO energy band gaps (3.23 eV for **KO-0**, 3.20 eV for **KO-1**, 3.21 eV for **KO-2**, and 2.99 eV for **KO-3**). These results are in good agreement with the experimental results about the photoabsorption spectra in the THF solutions (Fig. 3)

In order to gain insight into the $^1\text{O}_2$ generation properties of these PSs based on the ISC efficiency, spin-orbit coupling (SOC) matrix elements were analyzed using time-dependent DFT (TD-DFT).¹⁵ The SOC constants and the vertical excitation energies from the S_0 state to the S_n and T_n states for these PSs were calculated using their S_0 state geometries (Fig. 10 and Table 2). TD-DFT calculations suggested that the $S_0 \rightarrow S_1$ transitions of these PSs are attributed to the transition from the HOMOs to the LUMOs with $\pi\pi^*$ characteristics and that the HOMO-4 for **KO-0** and the HOMO-3 for **KO-1** and **KO-3**, the HOMO-2 for **KO-2** are attributed to the frontier n-orbitals consisting of the lone pair electrons on the nitrogen atoms of the phenazine skeleton (Fig. 10 insets). In particular, for **KO-1-3** possessing formyl groups, not only the lone pair electrons on the nitrogen atoms but also those on the formyl oxygens contribute to the frontier n-orbitals. However, contrary to our expectations, for **KO-3**, the formyl oxygen in the 6-formylthiophene scarcely contributes to the frontier n-orbitals (HOMO-3, Fig. 10d inset). Furthermore, it was revealed that, except for **KO-3**, these PSs have several ISC pathways which meet the El-Sayed rule ($S_1 (\pi\pi^*) \rightarrow T_3 (n\pi^*)$ for **KO-0**, $S_1 (\pi\pi^*) \rightarrow T_4 (n\pi^*)$ for **KO-1**, and $S_1 (\pi\pi^*) \rightarrow T_5 (n\pi^*)$ for **KO-2**). In these major ISC pathways, **KO-0-2** exhibited relatively large SOC matrix elements (7.66–7.77 cm^{-1}). As discussed in the theoretical calculations section of Chapter 1, **KO-0** has only one possible ISC pathway (S_1 to T_3), which results in the low Φ_Δ value of 0.040. The energy gap (ΔE_{ST}) of **KO-2** (0.01 eV) is slightly smaller than that of **KO-1** (0.05 eV), leading to efficient ISC. Indeed, these results are in good agreement with the order of Φ_Δ values ($\Phi_\Delta = 0.22$ for **KO-1** and 0.33 for **KO-2**). Although **KO-3** has no ISC pathways which meet the El-Sayed rule, there are several possible ISC pathways with the small ΔE_{ST} values (T_2-T_5 : -0.36–-0.01 eV,

1.10–2.27 cm^{-1}), leading to the efficient $^1\text{O}_2$ generation ($\Phi_{\Delta} = 0.41$). Consequently, we revealed that large SOC constants and many pathways for ISC triggered by the introduction of the formyl groups into the phenazine-2,3-diol chromophore result in efficient $^1\text{O}_2$ generations of **KO-1-3**.

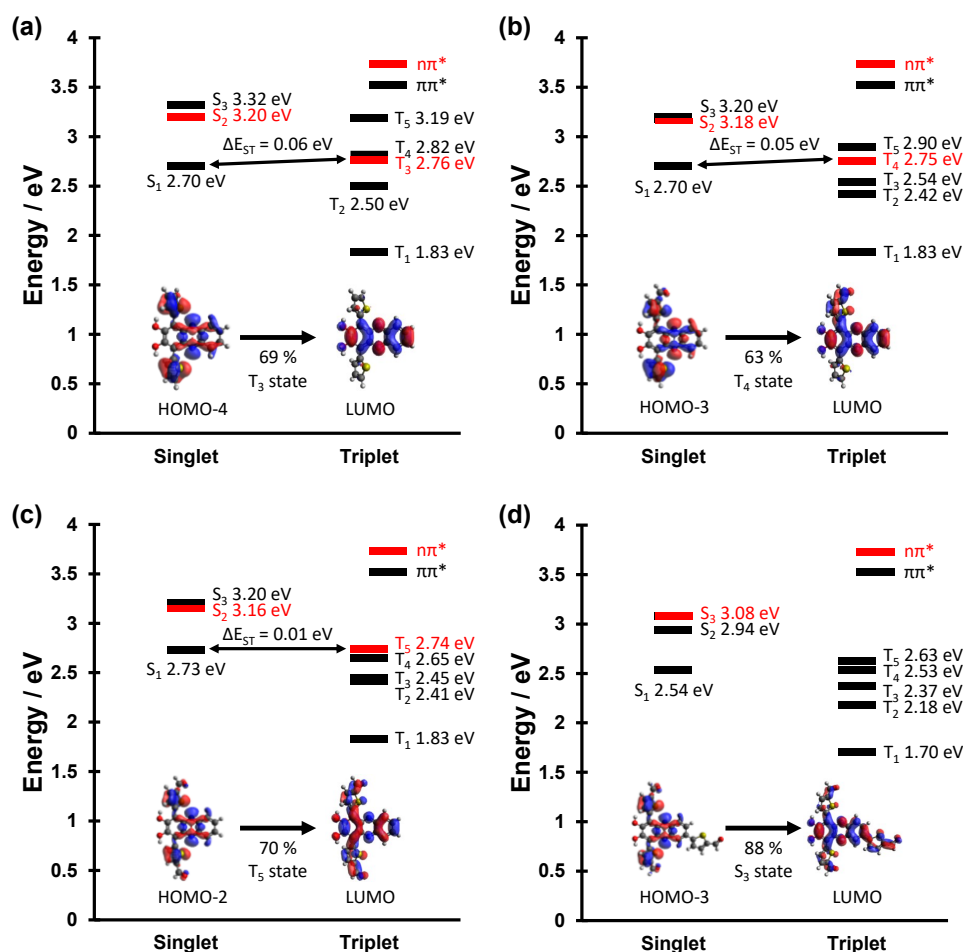


Fig. 10 Schematic diagrams showing vertical excitation energies of (a) **KO-0**, (b) **KO-1**, (c) **KO-2**, and (d) **KO-3** for singlet and triplet excited states. The insets represent the frontier n-orbitals that contribute to the ($n\pi^*$) triplet states.

Table 2 Spin–orbit coupling (SOC) constants and the energy gaps (ΔE_{ST}) between the lowest excited singlet states (S_1) and the triplet states (T_n).

Dye	Triplet states	SOC / cm^{-1}	ΔE_{ST} / eV
KO-0	T ₁	0.49	-0.87
	T ₂	0.72	-0.20
	T ₃	7.77	0.06
	T ₄	0.60	0.12
	T ₅	3.58	0.49
KO-1	T ₁	0.66	-0.87
	T ₂	1.93	-0.28
	T ₃	1.73	-0.16
	T ₄	7.66	0.05
	T ₅	2.39	0.20
KO-2	T ₁	0.78	-0.90
	T ₂	2.04	-0.32
	T ₃	1.82	-0.28
	T ₄	3.81	-0.08
	T ₅	7.70	0.01
KO-3	T ₁	0.27	-0.84
	T ₂	1.10	-0.36
	T ₃	1.36	-0.17
	T ₄	2.27	-0.01
	T ₅	1.60	-0.09

Conclusions

To gain insight into the promotion of ISC and $^1\text{O}_2$ generation by formyl groups, phenazine-2,3-diol-based dyes **KO-0-3** with zero to three formyl groups have been designed and developed as PSs. This work demonstrated that **KO-1-3** possess the photosensitizing ability to generate $^1\text{O}_2$ and that their Φ_Δ increase with increasing number of formyl groups, according to El-Sayed's rule. Although several studies reported the effect of the number of heavy atoms on Φ_Δ ,²² this is the first example that investigated the effect of the number of formyl groups. The key findings in this study will contribute to the development of heavy-atom-free PSs for PDT. Furthermore, **KO-0-3** showed the photoabsorption bands in the long wavelength region of 500–650 nm, and particularly, the additional introduction of a thiophene unit at the 6-position onto the phenazine skeleton (**KO-3**) results in extended conjugation, leading to the photoabsorption onset approaching the photodynamic window (650–900 nm). Further studies on the light-induced cytotoxicity of these PSs are now in progress to gain greater insight into the effect of formyl groups on $^1\text{O}_2$ generation under physiological conditions.

Acknowledgements

Chapter 3 is reproduced from “Development of phenazine-2,3-diol-based photosensitizers: effect of formyl groups on singlet oxygen generation; K Ohira, K. Imato, and Y. Ooyama, *Mater. Chem. Front.*, **2021**, 5, 5298–5304.” with permission from The Royal Society of Chemistry.

Reference

1. (a) S. Yakubov and J. P. Barham, *Beilstein J. Org. Chem.*, **2020**, 16, 2151–2192; (b) R. Gerdes, D. Wöhrle, W. Spiller, G. Schneider, G. Schnurpfeil and G. Schulz-Ekloff, *J. Photochem. Photobiol. A Chem.*, **1997**, 111, 65–74; (c) D. Kalaitzakis, A. Kouridaki, D. Noutsias, T. Montagnon and G. Vassilikogiannakis, *Angew. Chemie*, **2015**, 127, 6381–6385; (d) T. Luo, H. Wang, L. Chen, J. Li, F. Wu and D. Zhou, *J. Clean. Prod.*, **2021**, 280, 124374.
2. (a) D. van Straten, V. Mashayekhi, H. S. de Bruijn, S. Oliveira and D. J. Robinson, *Cancers (Basel)*, **2017**, 9, 1–54; (b) Y. Wen, C. L. Schreiber and B. D. Smith, *Bioconjug. Chem.*, **2020**, 31, 474–482; (c) M. Ethirajan, Y. Chen, P. Joshi and R. K. Pandey, *Chem. Soc. Rev.*, **2011**, 40, 340–362; (d) J. C. S. Simões, S. Sarpaki, P. Papadimitroulas, B. Therrien and G. Loudos, *J. Med. Chem.*, **2020**, 63, 14119–14150.
3. (a) M. C. DeRosa and R. J. Crutchley, *Coord. Chem. Rev.*, **2002**, 233–234, 351–371; (b) A. P. Castano, T. N. Demidova and M. R. Hamblin, *Photodiagnosis Photodyn. Ther.*, **2004**, 1, 279–293.
4. (a) Y. Ooyama, T. Enoki and J. Ohshita, *RSC Adv.*, **2016**, 6, 5428–5435; (b) J. Ohshita, Y. Hayashi, K. Murakami, T. Enoki and Y. Ooyama, *Dalt. Trans.*, **2016**, 45, 15679–15683.
5. L. A. Ortiz-Rodríguez and C. E. Crespo-Hernández, *Chem. Sci.*, **2020**, 11, 11113–11123.
6. (a) K. Hirakawa, S. Takai, H. Horiuchi and S. Okazaki, *ACS Omega*, **2020**, 27702–27707; (b) Y. Ooyama, T. Enoki, J. Ohshita, T. Kamimura, S. Ozako, T. Koide and F. Tani, *RSC Adv.*, **2017**, 7, 18690–18695; (c) F. Tani, A. Onoda, U. Hasegawa, T. Enoki, Y. Ooyama, J. Ohshita and T.

- Hayashi, *ChemMedChem*, **2018**, *13*, 15–19.
7. B. Barut, C. Ö. Yalçın and Ü. Demirbaş, *J. Photochem. Photobiol. A Chem.*, **2021**, *405*, 112946.
 8. K. Piwowar, A. Blacha-Grzechnik and J. Zak, *J. Electrochem. Soc.*, **2019**, *166*, G163–G169.
 9. T. M. Ebaston, F. Nakonechny, E. Talalai, G. Gellerman and L. Patsenker, *Dye. Pigment.*, **2021**, *184*, 108854.
 10. (a) M. Serda, G. Szewczyk, O. Krzysztyna-Kuleta, J. Korzuch, M. Dulski, R. Musioł and T. Sarna, *ACS Biomater. Sci. Eng.*, **2020**, *6*, 5930–5940; (b) D. M. Guldi and M. Prato, *Acc. Chem. Res.*, **2000**, *33*, 695–703.
 11. R. W. Redmond and J. N. Gamlin, *Photochem. Photobiol.*, **1999**, *70*, 391–475.
 12. M. A. Moris, C. Andrieu, P. Rocchi, C. Seillan, J. Acunzo, F. Brunel, F. Garzino, O. Siri and M. Camplo, *Tetrahedron Lett.*, **2015**, *56*, 2695–2698.
 13. K. Imato, K. Ohira, M. Yamaguchi, T. Enoki and Y. Ooyama, *Mater. Chem. Front.*, **2020**, *4*, 589–596.
 14. Gaussian 16, Revision A.03, M. J. Frisch, G. W. Trucks, H. B. Schlegel, G. E. Scuseria, M. A. Robb, J. R. Cheeseman, G. Scalmani, V. Barone, G. A. Petersson, H. Nakatsuji, X. Li, M. Caricato, A. V. Marenich, J. Bloino, B. G. Janesko, R. Gomperts, B. Mennucci, H. P. Hratchian, J. V. Ortiz, A. F. Izmaylov, J. L. Sonnenberg, D. Williams-Young, F. Ding, F. Lipparini, F. Egidi, J. Goings, B. Peng, A. Petrone, T. Henderson, D. Ranasinghe, V. G. Zakrzewski, J. Gao, N. Rega, G. Zheng, W. Liang, M. Hada, M. Ehara, K. Toyota, R. Fukuda, J. Hasegawa, M. Ishida, T. Nakajima, Y. Honda, O. Kitao, H. Nakai, T. Vreven, K. Throssell, J. A. Montgomery, Jr., J. E. Peralta, F. Ogliaro, M. J. Bearpark, J. J. Heyd, E. N. Brothers, K. N. Kudin, V. N. Staroverov, T. A. Keith, R. Kobayashi, J. Normand, K. Raghavachari, A. P. Rendell, J. C. Burant, S. S. Iyengar, J. Tomasi, M. Cossi, J. M. Millam, M. Klene, C. Adamo, R. Cammi, J. W. Ochterski, R. L. Martin, K. Morokuma, O. Farkas, J. B. Foresman, and D. J. Fox, Gaussian, Inc., Wallingford CT, 2016.

15. F. Neese, *Wiley Interdiscip. Rev.: Comput. Mol. Sci.*, **2022**, *12*, e1606.
16. S. Tsumura, K. Ohira, K. Hashimoto, K. Imato and Y. Ooyama, *Synthesis, Mater. Chem. Front.*, **2020**, *4*, 2762–2771.
17. (a) J. I. Nishida, S. Murakami, H. Tada and Y. Yamashita, *Chem. Lett.*, **2006**, *35*, 1236–1237; (b) L. V. Brownell, K. A. Robins, Y. Jeong, Y. Lee and D. C. Lee, *J. Phys. Chem. C*, **2013**, *117*, 25236–25247.
18. (a) K. Takagi, A. Mizuno, H. Yoshimura and M. Matsuoka, *Dye. Pigment.*, **1990**, *14*, 203–210; (b) Y. Ooyama, M. Kanda, K. Uenaka and J. Ohshita, *ChemPhysChem*, **2015**, *16*, 3049–3057; (c) Y. Ooyama, K. Yamaji and J. Ohshita, *Mater. Chem. Front.*, **2017**, *1*, 2243–2255.
19. W. Wu, J. Sun, X. Cui and J. Zhao, *J. Mater. Chem. C*, **2013**, *1*, 4577–4589.
20. K. Gollnick and A. Griesbeck, *Tetrahedron*, **1985**, *41*, 2057–2068.
21. (a) M. Baba, *J. Phys. Chem. A*, **2011**, *115*, 9514–9519; (b) M. A. El-Sayed, *Acc. Chem. Res.*, **1968**, *1*, 8–16.
22. (a) R. Acharya, S. Cekli, C. J. Zeman, R. M. Altamimi and K. S. Schanze, *J. Phys. Chem. Lett.*, **2016**, *7*, 693–697; (b) A. Mohan, E. Sebastian, M. Gudem and M. Hariharan, *J. Phys. Chem. B*, **2020**, *124*, 6867–6874.
23. S. Oriana, S. Aroua and O. Butz, *Chem. Commun.*, **2013**, *49*, 9302–9304

Chapter 4

Development of phenazine-2,3-diol-based photosensitizers: effect of substitution of cyano group for nitro group on singlet oxygen generation

Introduction

Singlet oxygen ($^1\text{O}_2$) produced by photosensitizers (PSs) has gained considerable interest due to their versatile applications, including an efficient oxidant of dienes and olefins for Diels–Alder [4 + 2]-cycloaddition reaction,¹ [2 + 2]-cycloaddition reaction,² and Schenck–Ene reaction in organic synthesis,³ degradation of water pollutants in environmental system,⁴ and cancer treatment in photodynamic therapy (PDT).⁵ PSs generally produce $^1\text{O}_2$ through the following processes: initially, the PS (S_0) absorbs light ($h\nu$) to generate the singlet excited state of the PS (S_n), and then the photoexcited PS (S_n) undergoes intersystem crossing (ISC) to generate the triplet excited state (T_n). After undergoing internal conversion (IC) to the lowest excited triplet state (T_1), the photoexcited PS (T_1) transfers energy to triplet oxygen ($^3\text{O}_2$), resulting in the generation of $^1\text{O}_2$. Thus, to achieve a high $^1\text{O}_2$ generation quantum yield (Φ_Δ), it is necessary to enhance the ISC efficiency of PSs. Porphyrin,⁶ phthalocyanine,⁷ xanthene,⁸ boron-dipyrromethene (BODIPY),⁹ and phenothiazine skeletons¹⁰ have been used as chromophores of PSs for producing $^1\text{O}_2$. For these PSs, halogen atoms such as iodide and bromide atoms are often introduced into the chromophores to promote ISC based on spin–orbit coupling.¹¹ However, it is well known that halogen atoms raise concerns about dark cytotoxicity in PDT.¹² Meanwhile, halogen-atom-free PSs such as a family of heteroanthracenes have been extensively studied.^{7, 8, 10, 13} Indeed, methylene blue (**MB**) without halogen atoms is commonly used not only as a standard PS for determining Φ_Δ values of the other PSs but also as a medication to treat methemoglobinemia.¹⁴ In addition, for efficient use in water purification systems and PDT, the PSs

are required to have photoabsorption in the longer wavelength region, that is, the visible light region (400–800 nm) and phototherapeutic window (650–900 nm).¹⁵

Thus, in **Chapter 2** and **3**,^{13b, 16} we have developed several phenazine-2,3-diol-based PSs (**KI-1–5**, **KO-1**, and **KO-3**) with thiophene units as halogen atom-free-heteroanthracene-based PSs (Fig. 1), and demonstrated that the introduction of formyl group into the phenazine-2,3-diol chromophore (**KI-2**, **KO-1**, and **KO-3**) could lead to efficient ¹O₂ generation (Φ_{Δ} = 0.22–0.41). It was suggested that the formyl group in the chromophore facilitates ISC by inducing changes of molecular orbital type, such as transitions from ¹(n π^*) to ³($\pi\pi^*$) and from ¹($\pi\pi^*$) to ³(n π^*) based on El-Sayed's rule.¹⁷ Moreover, it was found that the introduction of nitro group into the phenazine-2,3-diol chromophore (**KI-3** and **KI-5**) extended the photoabsorption edge (700 nm for **KI-3** and 800 nm for **KI-5**) to the phototherapeutic window owing to its strong electron-withdrawing effect. In addition, **KI-5** with electron-donating *n*-hexyl groups on thiophene units showed the redshift of photoabsorption bands compared to **KI-3** with electron-withdrawing formyl groups on thiophene units. However, the Φ_{Δ} values of **KI-3** and **KI-5** were significantly low (0.05 and 0.02) due to the rapid nonradiative decay of the excited states by the nitro group, although **KI-3** has formyl groups which meet the El-Sayed rule.

In this study, in order to further gain insight into the substituent effect on Φ_{Δ} values of phenazine-2,3-diol-based PSs, we have developed the derivative **YC-2** with a cyano group in place of the nitro group of **KI-3** (Fig. 2). It is expected that the substitution of the cyano group for the nitro group could reduce nonradiative decay. Furthermore, **YC-1** having a cyano group and two *n*-hexyl groups on thiophene units was synthesized and the substituent effect on the optical and ¹O₂ generation properties was investigated for comparison with **KI-5**. Herein we report that the introduction of the cyano group into the phenazine-2,3-diol chromophore improves the ¹O₂ generation capability.

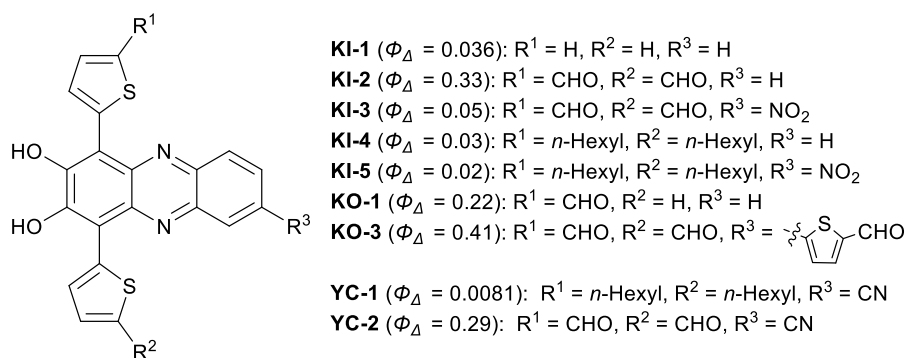


Fig. 3 Chemical structures of phenazine-based photosensitizers **KI-1–5**, **KO-1**, and **KO-3** in **Chapter 2** and **3**^{13b, 16} and **YC-1** and **YC-2** in this work and their singlet oxygen quantum yields (Φ_{Δ}).

Experimental

Materials

All solvents and reagents were used as received unless otherwise noted. Rose bengal (RB) was purchased from Sigma Aldrich and recrystallized from methanol twice. 1,3-diphenylisobenzofuran (DPBF) was purchased from Tokyo Chemical Industry and recrystallized from a mixture of dichloromethane and methanol. 2,2,6,6-Tetramethyl-4-piperidone (4-oxo-TEMP) was purchased from FUJIFILM Wako Pure Chemical.

General

^1H NMR and ^{13}C NMR spectra were recorded using Varian-400 (400 MHz) and Varian-500 (500 MHz) FT NMR spectrometers. FT-IR spectra were recorded using a Shimadzu IRTracer-100. High-resolution mass spectral data were acquired using a Thermo Fisher Scientific LTQ Orbitrap XL. Photoabsorption spectra were recorded using Shimadzu UV-3600-plus spectrophotometers. Fluorescence spectra were measured using a Hitachi F-4500 spectrophotometer. The fluorescence quantum yields (Φ_{f}) were determined with a Hamamatsu C9920-01 instrument equipped with CCD by use of a calibrated integrating sphere system. The irradiance of monochromatic light (509 nm) for photosensitizing reactions was adjusted using a Newport 1918-C optical power meter.

Evaluation of $^1\text{O}_2$ quantum yield

Quantum yields (Φ_{Δ}) for singlet oxygen ($^1\text{O}_2$) generation by **YC-1** and **YC-2** were evaluated by monitoring the changes in the photoabsorption spectra of DPBF, a $^1\text{O}_2$ scavenger, in THF upon photoirradiation. DPBF traps the generated $^1\text{O}_2$ to be oxidized. THF was bubbled with air for 10 min, prior to the preparation of the solutions. The concentration of DPBF was 50 μM in the air-saturated THF solutions. The concentration of the PSs and **RB** was adjusted so that the absorbance was ca. 0.03 at the irradiation wavelength (509 nm). The THF solutions containing DPBF and **YC-1** or **YC-2** were irradiated with monochromatic light (509 nm, 300 $\mu\text{W cm}^{-2}$) that was obtained by passage of a xenon

light source (HAL-320, Asahi Spectra) through a monochromator (CMS-100, Asahi Spectra). Except for the nonirradiated solutions, each spectrum was measured immediately after photoirradiation for 1 min. The procedure was promptly repeated until the total photoirradiation time reached 10 min. The changes in optical density (ΔOD) of DPBF were plotted against photoirradiation time to obtain the slopes (m) and estimate Φ_{Δ} values. W. Wu et. al. reported that **RB** shows a high 1O_2 generation with the $\Phi_{\Delta} = 0.80$ in MeOH.¹⁹ To correct the difference of Φ_{Δ} values between MeOH and THF, the Φ_{Δ} values in THF were estimated from the following equation.

$$\Phi_{\Delta RB, THF} = \Phi_{\Delta RB, MeOH} \times [(m_{RB, THF}/m_{RB, MeOH}) \times (L_{RB, MeOH}/L_{RB, THF})]$$

where $m_{RB, MeOH}$ and $m_{RB, THF}$ are slopes in the plots of ΔOD at the photoabsorption maximum wavelength (413 nm) of DPBF against photoirradiation time, and $L_{RB, THF}$ and $L_{RB, MeOH}$ are light harvesting efficiencies, which are given by $L = 1 - 10^{-A}$ (“ A ” is the absorbance at the photoirradiation wavelength). The $\Phi_{\Delta RB, THF}$ value was estimated to be 0.68.^{13a} The Φ_{Δ} values of **YC-1** and **YC-2** were determined by the relative method using **RB** ($\Phi_{\Delta} = 0.68$ in THF) as a standard according to the following equation:

$$\Phi_{\Delta sam} = \Phi_{\Delta ref} \times [(m_{sam}/m_{ref}) \times (L_{ref}/L_{sam})]$$

where $\Phi_{\Delta sam}$ and $\Phi_{\Delta ref}$ are 1O_2 quantum yields of phenazine-2,3-diol-based PSs and **RB**, respectively, m_{sam} and m_{ref} are slopes in the plots of ΔOD at the photoabsorption maximum wavelength of DPBF (413 nm) against photoirradiation time, and L_{sam} and L_{ref} are light harvesting efficiencies, which are given by $L = 1 - 10^{-A}$ (“ A ” is the absorbance at the photoirradiation wavelength).

Photosensitizing ability

The photosensitizing abilities of phenazine-2,3-diol-based PSs upon exposure to continuous visible light (>510 nm, 30 mW cm⁻²) were evaluated in THF solutions containing **YC-1**, **YC-2**, or **RB** (5 μ M) and DPBF as a 1O_2 scavenger (50 μ M). THF was bubbled with air for 15 min, prior to preparing the solutions. The continuous light was obtained by passing a xenon light (HAL-302, Asahi Spectra)

through a 510 nm long path filter. Each spectrum was recorded immediately after photoirradiation for either 10 seconds for **RB** or 1 minute for **YC-1** and **YC-2**. The procedure was repeated promptly until the total irradiation time reached 1 minute for **RB**, and 10 minutes for **YC-1** and **YC-2**. Then, $\ln(C_t/C_0)$ was plotted against photoirradiation time, where C_t is the concentration of DPBF at the reaction time (t) and C_0 is the initial concentration of DPBF before photoirradiation. C_t was calculated based on Lambert–Beer law ($A_{\text{DPBF}} = \epsilon cl$) using the maximum absorbance at 413 nm for DPBF. Because the $\ln(C_t/C_0)$ plots showed linear decreases with increasing photoirradiation time, the slopes were used to estimate the first-order rate constants (k_{obs}) of the DPBF oxidation by $^1\text{O}_2$ generated using the phenazine-2,3-diol-based PSs. The k_{obs} value for **RB** was also obtained in a similar way.

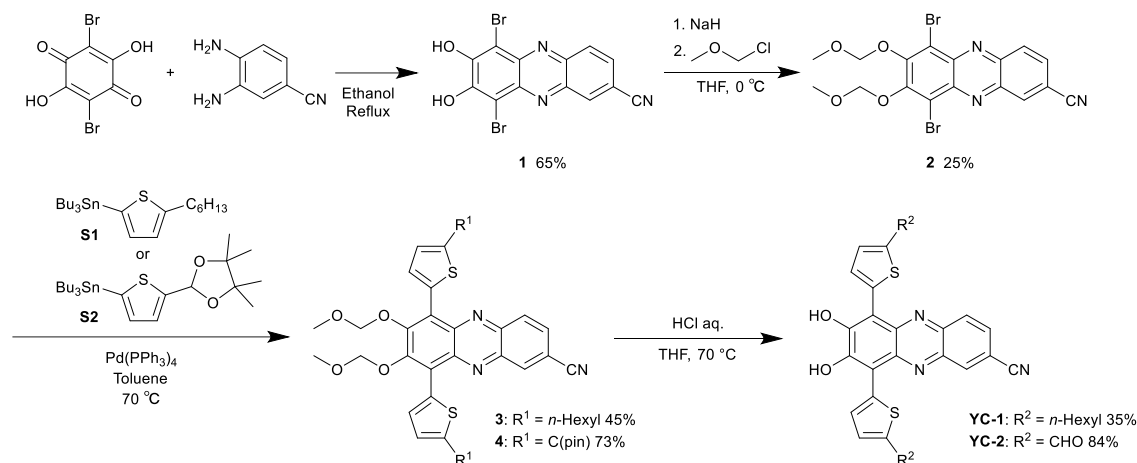
EPR measurements

Air-saturated THF solutions containing **YC-1** or **YC-2** as a PS (5 μM) and 4-oxo-TEMP as a spin-trapping agent (50 mM) were prepared. THF was bubbled with air for 15 min, prior to preparation of the solutions. Their electron paramagnetic resonance (EPR) spectra were recorded before and after exposure to continuous visible light (>510 nm, and 30 mW cm^{-2}) for 60 min on a Bruker ELEXSYS E500 spectrometer. The continuous light was obtained by passage of a xenon light source (HAL-302, Asahi Spectra) through a 510 nm long path filter. The reaction of 4-oxo-TEMP with $^1\text{O}_2$ produces a stable nitroxide radical (4-oxo-TEMPO), showing a characteristic 1 : 1 : 1 triplet signal.

Theoretical calculations

The Gaussian 16 program¹⁴ was used for density functional theory (DFT) calculations. The S_0 geometries of these PSs were optimized via frequency calculations at the B3LYP/6-31G(d,p)/THF-CPCM level. There are no imaginary frequencies for all optimized structures. The spin-orbit coupling (SOC) matrix elements were calculated at the B3LYP/6-31G(d,p)/THF-CPCM level using the ORCA 5.0.4 program.¹⁵ These calculations were performed using the optimized S_0 geometries of these PSs.

Synthesis



Scheme 1 Synthetic routes to **YC-1** and **YC-2**.

6,9-Bis(5-hexylthiophen-2-yl)-7,8-dihydroxyphenazine-2-carbonitrile (YC-1). A solution of compound **3** (0.22 g, 0.33 mmol) and 1N HCl aq. (5 mL) in THF (35 mL) was stirred at 70 °C until insoluble compounds precipitated. The precipitate was filtered and washed by hexane to give **YC-1** as black solid (35% yield); decomposition around 270–273°C; IR (ATR): $\tilde{\nu} = 2228$ (-CN), 2924 cm^{-1} ; ^1H NMR (500 MHz, DMSO- d_6): δ 8.51 (s, 1H), 8.11 (dd, $J = 8.6$ Hz, 1H), 7.91 (dd, $J = 8.52$ Hz, 1H), 6.94–6.88 (m, 2H), 2.87 (t, 4H), 1.71 (m, 4H), 1.33 (m, 12H), 0.89 (m, 6H); ^{13}C NMR spectrum could not be obtained because of the low solubility in any solvents; HRMS (ESI): m/z found 569.21631 [M^+], calculated for $\text{C}_{33}\text{H}_{35}\text{O}_2\text{N}_3\text{S}_2$ [M^+]: 569.21652.

6,9-Bis(5-formylthiophen-2-yl)-7,8-dihydroxyphenazine-2-carbonitrile (YC-2). A solution of compound **4** (0.132 g, 0.289 mmol) and 1N HCl aq. (5 mL) in THF (35 mL) was stirred at 70 °C until insoluble compounds precipitated. The precipitate was filtered and washed by hexane to give **YC-2** as black solid (84% yield); decomposition over 300°C; IR (ATR): $\tilde{\nu} = 2228$ (-CN), 3204 cm^{-1} ; ^1H NMR (500 MHz, DMSO- d_6): δ 9.97 (s, 1H), 9.93 (s, 1H), 8.96 (d, $J = 4.1$ Hz, 1H), 8.78 (d, $J = 4.2$ Hz, 1H), 8.60 (dd, $J = 1.82, 0.35$ and 0.5 Hz, 1H), 8.21 (d, $J = 8.55$ Hz, 1H), 8.02 (d, $J = 4.25$ Hz, 1H), 8.00 (d, $J = 4.25$ Hz, 1H), 7.93 (dd, $J = 8.65, 1.85$ and 1.85 Hz, 1H); ^{13}C NMR spectrum could not be obtained

because of the low solubility in any solvents; HRMS (ESI): m/z found 458.02640 $[M+H]^+$, calculated for $C_{23}H_{12}O_4N_3S_2$ $[M+H]^+$: 458.02637.

Results and discussion

Synthesis

The cyano-substituted phenazine-2,3-diol-based PSs **YC-1** and **YC-2** were synthesized via a stepwise synthetic protocol as shown in Scheme 1. Compound **1** was prepared by the cyclodehydration of 2,5-dibromo-3,6-dihydroxy-*p*-quinoline with 4-cyano-1,2-benzenediamine. For ease of handling in the subsequent Stille couplings, **1** was converted to its methoxymethyl (MOM)-protected derivative **2** with good solubility in solvent. Indeed, the Stille coupling of **2** with the corresponding stannyl thiophene (**S1** or **S2**)^{13b, 16} gave compounds **3** and **4** in moderate yield (45% and 73%, respectively). Finally, **3** and **4** were hydrolyzed by treatment with acid in the tetrahydrofuran (THF) to produce **YC-1** and **YC-2**, respectively. **YC-1** and **YC-2** were fully characterized by ¹H and ¹³C NMR, FT-IR, and high-resolution mass spectrometric (HRMS) analysis.

Optical properties

The photoabsorption and fluorescence spectra of **KI-3**, **KI-5**, **YC-1** and **YC-2** in THF are shown in Fig. 3, and their optical data of are summarized in Table 1. These phenazine-2,3-diol-based PSs exhibited two photoabsorption bands in the range of 300–500 nm and 500–800 nm. The photoabsorption bands in 300–500 nm are attributed to the $\pi\pi^*$ transition of the phenazine-2,3-diol skeleton containing thiophene units. Meanwhile, for the photoabsorption bands in 500–800 nm, the photoabsorption edge ($\lambda_{\text{edge}}^{\text{abs}}$) of **YC-1** reached at 700 nm which is in a longer wavelength region by 50 nm in comparison with that (650 nm) of **YC-2**, as with the case of **KI-3** ($\lambda_{\text{edge}}^{\text{abs}} = 700$ nm) with formyl groups and **KI-5** ($\lambda_{\text{edge}}^{\text{abs}} = 800$ nm) with *n*-hexyl groups (Fig. 1a inset). Furthermore, the photoabsorption edges of **YC-1** and **YC-2** exhibited blue-shifts, compared to that of **KI-3** and **KI-5**. Thus, it was found that the substitutions of electron-donating *n*-hexyl group for electron-withdrawing formyl group on thiophene units and moderate electron-withdrawing cyano group for stronger electron-withdrawing nitro group on phenazine-2,3-diol skeleton lead to red-shift and blue-shift,

respectively, for the photoabsorption edges. This result is due to the stabilizations of the highest occupied molecular orbital (HOMO) energy levels from **YC1** and **KI-5** to **YC-2** and **KI-3** and the lowest unoccupied molecular orbital (LUMO) energy levels from **YC-1** and **YC-2** to **KI-5** and **KI-3**, as discussed later in the section of density functional theory (DFT) and time-dependent DFT (TDDFT) calculations. Meanwhile, keep in mind that the photoabsorption characteristics of **YC-2** in the range of 500–800 nm is superior to those of **YC-1**, **KI-3**, and **KI-5**; in fact the molar extinction coefficient ($\varepsilon = 5000 \text{ M}^{-1}\text{cm}^{-1}$) at 509 nm for **YC-2** is which is higher than those ($\varepsilon = 2400\text{--}3300 \text{ M}^{-1}\text{cm}^{-1}$) of **YC-1**, **KI-3**, and **KI-5** (Table 1).

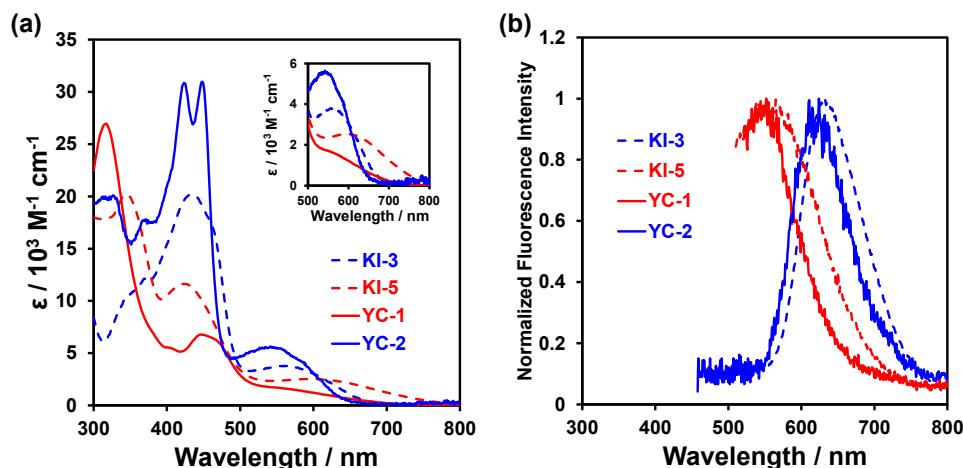


Fig. 2 (a) Photoabsorption and (b) fluorescence spectra ($\lambda_{\text{ex}} = 430$ nm for **KI-3** and **KI-5**, $\lambda_{\text{ex}} = 446$ nm for **YC-1**, and $\lambda_{\text{ex}} = 448$ nm for **YC-2**) of **KI-3**, **KI-5**, **YC-1**, and **YC-2** in THF (10 μM for **KI-3**, **KI-5**, and **YC-1**, and 4.9 μM for **YC-2**).

Table 1 Optical data of **KI-3**, **KI-5**, **YC-1**, and **YC-2**, and $^1\text{O}_2$ quantum yields (Φ_{Δ}) and first-order rate constants (k_{obs}) for the photooxidation of DPBF using **KI-3**, **KI-5**, **YC-1**, and **YC-2**.

PS	$\epsilon / \text{M}^{-1} \text{cm}^{-1}$ @509 nm	$\lambda_{\text{max}}^{\text{fl}} / \text{nm}$	Φ_{fl}^a	Φ_{Δ}^b	$k_{\text{obs}} / \text{min}^{-1c}$
KI-3 ^d	3300	632	< 0.01	0.05	1.1×10^{-2}
KI-5 ^d	2900	544	< 0.01	0.02	2.0×10^{-3}
YC-1	2400	552	< 0.01	0.0081	9.6×10^{-4}
YC-2	5000	644	0.022	0.29	2.8×10^{-2}

^a Fluorescence quantum yields (Φ_{fl}) were determined by using a ^a Fluorescence quantum yields (Φ_{fl}) were determined by using a calibrated integrating sphere system at $\lambda_{\text{ex}} = 430$ nm for **KI-3** and **KI-5**, 446 nm for **YC-1**, and 448 nm for **YC-2**. ^b $^1\text{O}_2$ quantum yields (relative decomposition rate of DPBF), with **RB** as a standard ($\Phi_{\Delta} = 0.68$ in THF) and DPBF as a $^1\text{O}_2$ scavenger. ^c First-order rate constants for the reaction of DPBF with $^1\text{O}_2$ generated upon photoexcitation of **KI-3**, **KI-5**, **YC-1**, and **YC-2**. The k_{obs} for **RB** is estimated to be 2.0 min^{-1} . ^d In **Chapter 2**. ^e Non fluorescence.

In **Chapter 2**,¹⁶ we demonstrated that for **KI-3** and **KI-5** the above-mentioned photoabsorption bands in the range of 500–800 were attributed to their phenoxide forms by the partial deprotonation of hydroxy groups, based on the photoabsorption spectral changes upon the addition of acid or base to the solution. For **YC-1**, the photoabsorption spectrum did not undergo appreciable changes in the absorbance and shape upon the addition of trifluoroacetic acid (TFA) as an acid to the THF solution (Fig. 3a). On the other hand, with the increase in content of triethylamine (TEA) as a base in the THF solution, the photoabsorption band at around 570 nm increases with the simultaneous disappearance of photoabsorption band at around 450 nm with an isosbestic point at 510 nm (Fig. 3b), which suggests a presence of the phenoxide as dominant species. Meanwhile, for **YC-2**, with the increase in content of TFA in the THF solution, the photoabsorption band at around 550 nm decreases with the simultaneous decrease in absorbance at around 420 nm with an isosbestic point at 490 nm (Fig. 3c), indicating a decrease in the phenoxide species, whereas there is no appreciable changes in the photoabsorption spectrum upon the addition of TEA to the THF solution (Fig. 3d). In addition, the photoabsorption spectra with the addition of NaOH aq. as a base were similar to that of TEA. Thus, in order to confirm the presence of the phenoxide forms for **YC-1** and **YC-2**, we performed ¹H NMR spectral measurements of the two PSs in THF-*d*₈ with and without the addition of TFA-*d*₁ or TEA-*d*₁₅. For both the ¹H NMR spectra of **YC-1** and **YC-2**, the signals for aromatic protons H_A–H_E of the phenazine-2,3-diol skeleton and thiophene units were broadened and complicated in the THF-*d*₈ solutions without the additives and with TFA-*d*₁, but these signals became clear in the THF-*d*₈ solutions with TEA-*d*₁₅ (Fig. 4a and b). Consequently, these results indicate that **YC-1** and **YC-2** exist in an equilibrium between the diol form and the phenoxide form in the solution and dominantly as the phenoxide species under the basic condition (Fig. 4c), although the ¹H NMR spectra of the solution with and without the addition of TFA-*d*₁ or TEA-*d*₁₅ are not entirely coincident with the photoabsorption spectral changes upon addition of TFA and TEA to the solution.

In the corresponding fluorescence spectra (Fig. 2b), these dyes showed feeble fluorescence bands with a fluorescence maximum wavelength ($\lambda_{\text{max}}^{\text{fl}}$) at 632 nm and 644 nm for **KI-3** and **YC-2**, respectively, originating from their phenoxide forms, and at 544 nm and 552 nm for **KI-5** and **YC-1**, respectively, originating from their diol forms. Thus, the fluorescence quantum yields (Φ_{fl}) of these dyes are significantly low (< 0.01 for **KI-3**, **KI-5**, and **YC-1**, and 0.022 for **YC-2**), which are attributed to the efficient ISC and IC, as discussed later.

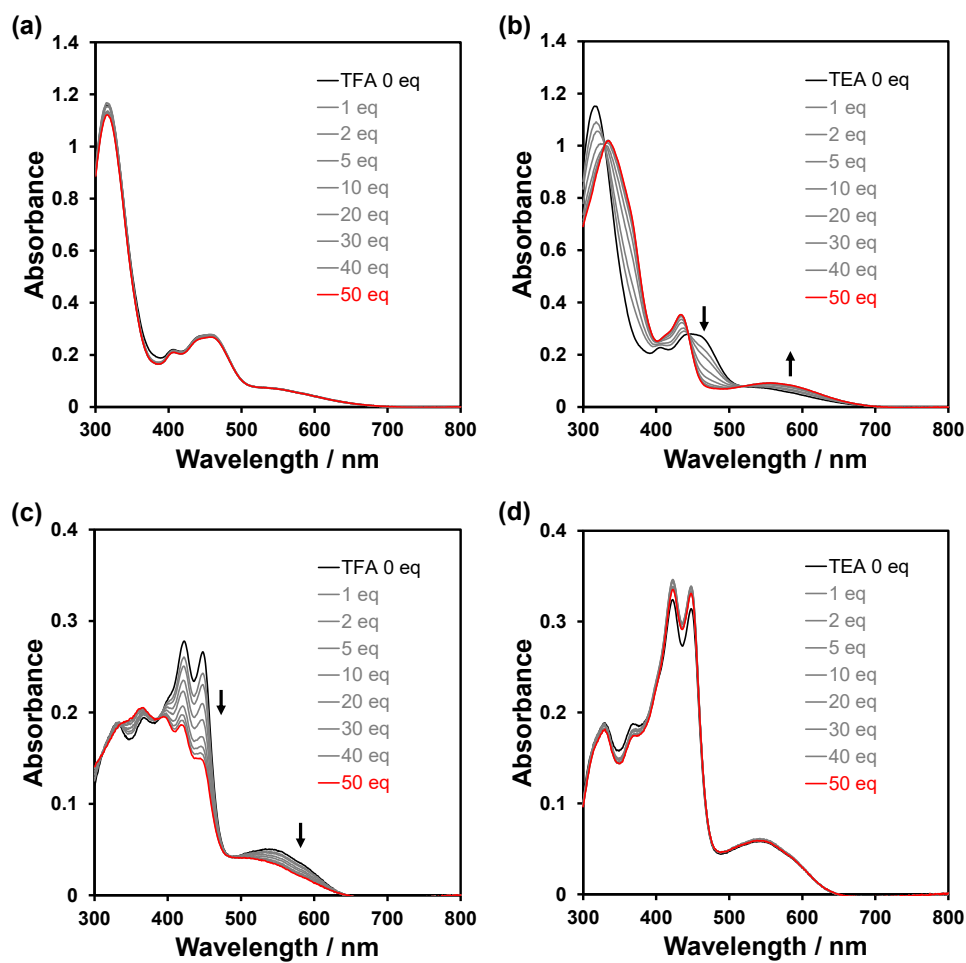


Fig. 3 Photoabsorption spectral changes of (a) YC-1 and (c) YC-2 upon the addition of trifluoroacetic acid (TFA) in THF (30 μ M for YC-1 and 10 μ M for YC-2), and (b) YC-1 and (d) YC-2 upon the addition of triethylamine (TEA) in THF (30 μ M for YC-1 and 10 μ M for YC-2).

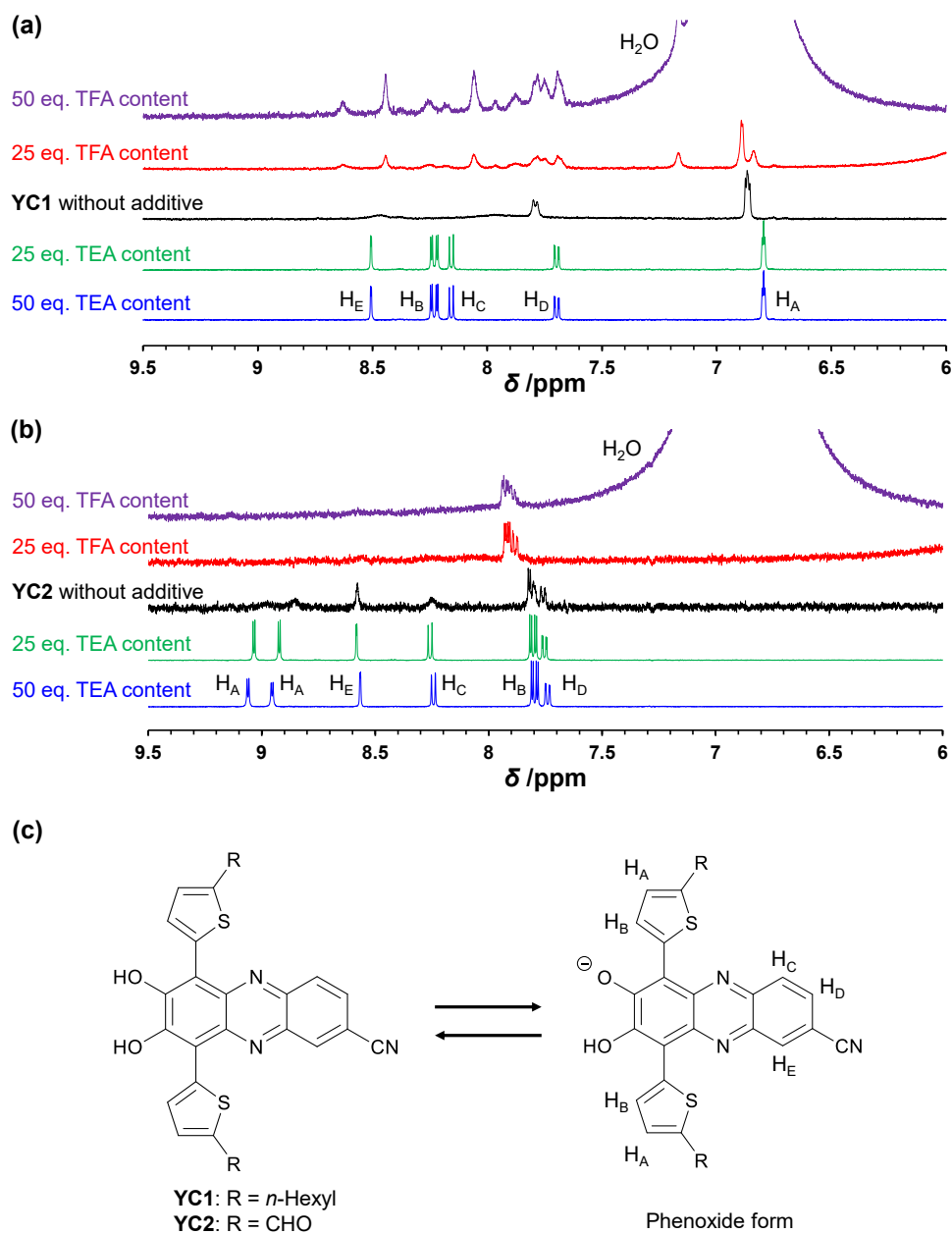


Fig. 4 ^1H NMR spectra of (a) **YC-1** (1.0 mM) and (b) **YC-2** (1.0 mM) in $\text{THF-}d_8$ with and without TFA- d_1 and TEA- d_{15} , and (c) their chemical structures of diol form and phenoxide form.

¹O₂ generation

We evaluated the ¹O₂ generation ability of PSs **YC-1** and **YC-2** by using 1,3-diphenylisobenzofuran (DPBF) as an efficient ¹O₂ scavenger to produce its oxidized product, *o*-dibenzoylbenzene.¹⁸ ¹O₂ generation by the two PSs was investigated by monitoring the photoabsorption spectral changes of DPBF in THF solution of each PS under photoirradiation, accompanying the reaction between DPBF and the generated ¹O₂ (Fig. 5). THF was bubbled with air for 10 minutes prior to preparing the solutions. Air-saturated THF solutions containing DPBF and each PS were irradiated with monochromatic light at 509 nm (300 μW cm⁻²) which was obtained by passing a xenon light source through a monochromator. For the **YC-2** solution, the photoabsorption band of DPBF peaked at 413 nm decreased with the increase in photoirradiation time, which indicates that DPBF reacted with ¹O₂ generated by the photoexcitation of **YC-2** to produce *o*-dibenzoylbenzene. However, such observable photoabsorption spectral changes was not observed in the case of **YC-1**. Therefore, in order to make clear the difference in ¹O₂ generation ability between the two PSs, the changes in optical density (ΔOD) at 413 nm of DPBF are plotted against the photoirradiation time (Fig. 5d), and the slope (m_{sam}) is used to estimate the ¹O₂ quantum yield (Φ_{Δ}): the Φ_{Δ} values for PSs were determined by the relative method using the slope value ($m_{\text{ref}} = -8.30 \times 10^{-3} \text{ min}^{-1}$) of the plot for rose bengal **RB** ($\Phi_{\Delta} = 0.68$ in THF)^{19, 13a} as a standard (see Fig. 5c for ¹O₂ generation by **RB**). The calibration curve for **YC-2** shows good linearity with the R^2 value of 0.9976, but that for **YC-1** has mediocre R^2 value (0.5085) which may be due to a small change in the ΔOD. In fact, the m_{sam} value ($-3.60 \times 10^{-3} \text{ min}^{-1}$) for **YC-2** is an order of magnitude greater than that ($-2.10 \times 10^{-4} \text{ min}^{-1}$) for **YC-1**. The Φ_{Δ} value of **YC-2** with cyano group is estimated to be 0.29, which is much higher than that (0.05) of **KI-3**¹⁶ with nitro group, indicating that replacing the nitro group with the cyano group in the phenazine-2,3-diol-based chromophore reduces the rapid nonradiative decay of the excited states, resulting in efficient ISC. On the other hand, **YC-1** with *n*-hexyl groups shows a significantly low Φ_{Δ} value (0.0081) similar to that

(0.02) of the corresponding derivative **KI-5**.¹⁶ It was suggested that for **YC-1** and **KI-5** the flexible *n*-hexyl groups accelerate nonradiative decay of the excited state which is responsible for the low Φ_{fl} values, thus resulting in inferior ISC. While these values are lower than those reported in literature for **RB** and **MB** (0.68^{19, 13a} and 0.5^{14b}), the extended $\lambda_{\text{edge}}^{\text{abs}}$ of **YC-1** and **YC-2** (700 nm and 650 nm) are comparable to those of **RB** and **MB** (650 nm and 700 nm), making them desirable for the efficient use of light sources. Furthermore, the generation of $^1\text{O}_2$ by **YC-1** and **YC-2** was confirmed through electron paramagnetic resonance (EPR) spectral measurements. These measurements were taken from air-saturated THF solutions containing 2,2,6,6-tetramethyl-4-piperidone (4-oxo-TEMP) as a spin-trapping agent and **YC-1** or **YC-2** before and after exposure to a continuous visible light (> 510 nm, 30 mW cm^{-2}) for 60 min (Fig. 6). In the THF solution containing 4-oxo-TEMP and **YC-1**, or **YC-2**, characteristic 1:1:1 triplet signals of 4-oxo-TEMPO were observed and increased in intensity after exposure to continuous light. The EPR intensity after light exposure increases in the order of **YC-1** < **YC-2**, which is consistent with the trend of their Φ_{Δ} values.

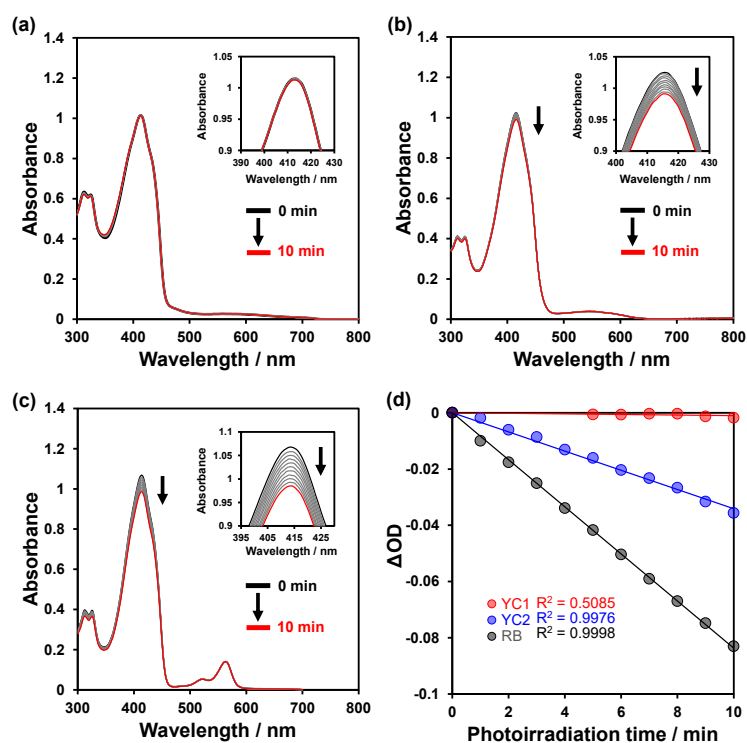


Fig. 5 Photoabsorption spectra of DPBF (50 μM) in the presence of (a) YC-1, (b) YC-2, and (c) RB (abs. @509 nm = ca. 0.03) upon irradiation with monochromatic light (509 nm, 300 $\mu\text{W cm}^{-2}$) in THF. Insets are magnifications of peak tops in the spectra around 410 nm. (d) Plots of ΔOD of DPBF at 413 nm against photoirradiation (509 nm, 300 $\mu\text{W cm}^{-2}$) time in the presence of YC-1, YC-2, and RB.

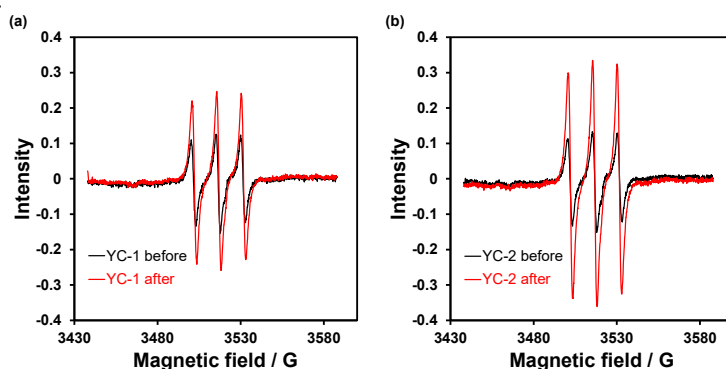


Fig. 6 EPR spectra of air-saturated THF solutions containing 4-oxo-TEMP (50 mM) and (a) YC-1, and (b) YC-2 (5 μM) before and after exposure to continuous visible light (>510 nm, and 30 mW cm^{-2}) for 60 min. The characteristic 1:1:1 triplet signal originates from a stable nitroxide radical (4-oxo-TEMPO) formed by the reaction of 4-oxo-TEMP with $^1\text{O}_2$.

Photosensitizing ability

To investigate the photosensitizing ability of the PSs, we evaluated the $^1\text{O}_2$ generation and DPBF degradation upon exposure to continuous visible light ($>510\text{ nm}$, and 30 mW cm^{-2}) in air-saturated THF solutions containing DPBF and **YC-1** and **YC-2**, or **RB**. The continuous light was obtained by passing a xenon light source through a 510 nm long path filter. The photoabsorption spectra during the photooxidation of DPBF using **YC-1** and **YC-2**, or **RB** are shown in Fig. 7a-c. To clarify the difference in photosensitizing abilities between the PSs, the $\ln(C_t/C_0)$ was plotted against photoirradiation time, where C_t is a concentration of DPBF at the reaction time (t) and C_0 is the initial concentration of DPBF before photoirradiation (Fig. 7d). Indeed, the $\ln(C_t/C_0)$ shows a linear decrease with the increase in photoirradiation time, providing the first-order rate constants (k_{obs}) for the oxidation of DPBF by $^1\text{O}_2$; the calibration curves have good R^2 values (0.9887 for **YC-1** and 0.9989 for **YC-2**). The k_{obs} values are in the order of **YC2** ($2.8 \times 10^{-2}\text{ min}^{-1}$) $>$ **KI-3** ($1.1 \times 10^{-2}\text{ min}^{-1}$)¹⁶ $>$ **KI-5** ($2.0 \times 10^{-3}\text{ min}^{-1}$)¹⁶ $>$ **YC-1** ($6.9 \times 10^{-4}\text{ min}^{-1}$), where k_{obs} value for **RB** is 2.0 min^{-1} . This order is consistent with that of the Φ_{Δ} values: **YC-2** (0.29) $>$ **KI-3** (0.05) $>$ **KI-5** (0.02) $>$ **YC-1** (0.0081). These results indicated that the highest k_{obs} value for **YC-2** among the four PSs can be attributed to both the efficient ISC characteristics and the intense photoabsorption properties in the range of $500\text{--}800\text{ nm}$. Consequently, it was found that **YC-2** with not only formyl groups for meeting the El-Sayed rule but also cyano group for reducing the nonradiative decay of the excited states exhibits superior $^1\text{O}_2$ generation and photosensitizing abilities to **YC-1**, **KI-3**, and **KI-5** with nitro and n -hexyl groups leading to the rapid nonradiative decay, as discussed later in the next section.

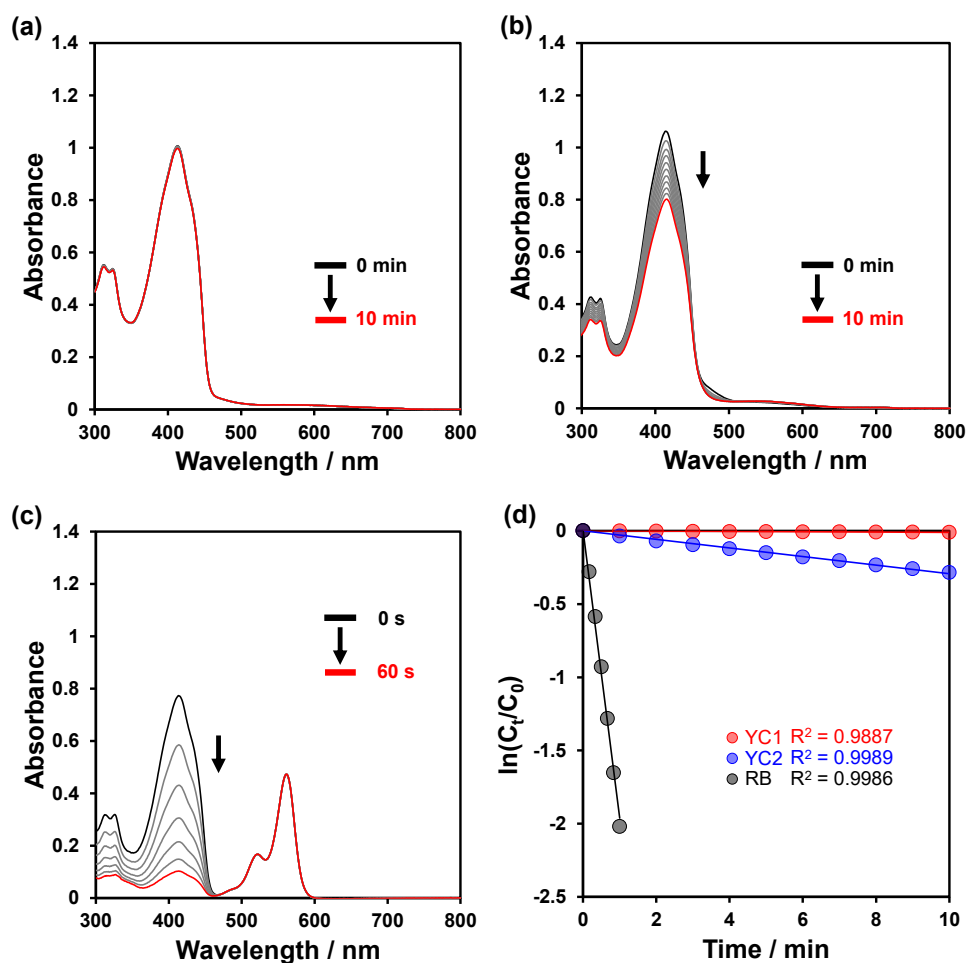


Fig. 7 Photoabsorption spectra of DPBF (50 μM) in the presence of (a) YC-1, (b) YC-2, and (c) RB (5 μM) upon irradiation with continuous light ($>510\text{ nm}$, 30 mW cm^{-2}) in THF. (d) Plots of $\ln(C_t/C_0)$ of DPBF against photoirradiation ($>510\text{ nm}$, 30 mW cm^{-2}) time in the presence of YC-1, YC-2, and RB.

Theoretical calculations

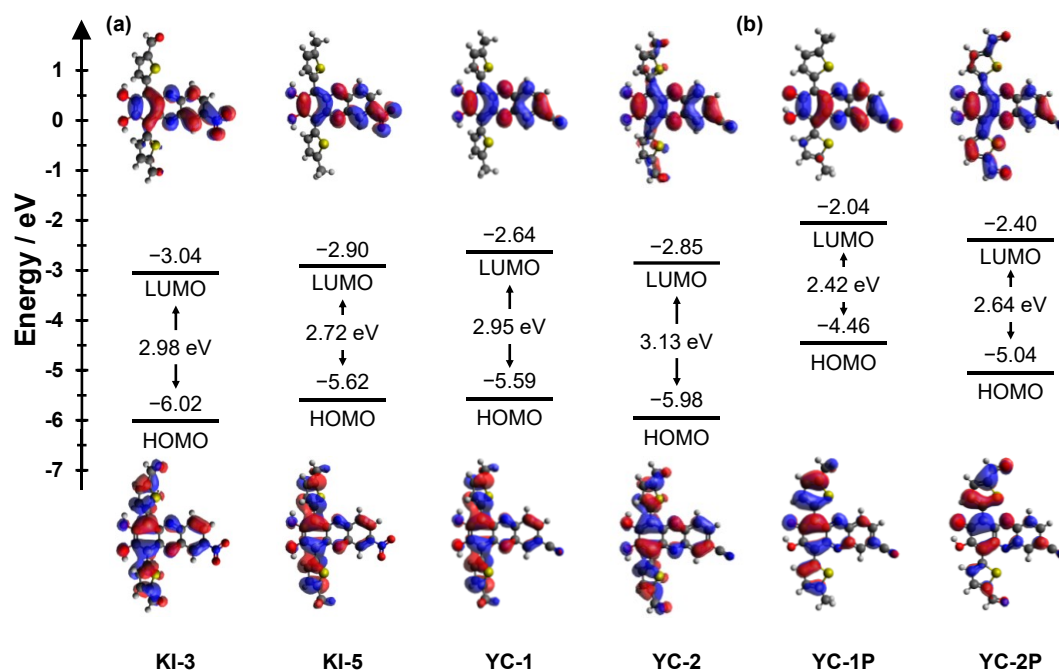


Fig. 8 Energy level diagram, HOMO and LUMO of (a) **KI-3**, **KI-5**, **YC-1**, and **YC-2** at the B3LYP/6-31G(d,p)/THF-CPCM level and (b) **YC-1P** and **YC-2P** at the B3LYP/6-31+G(d,p)/THF-CPCM level using DFT calculations. The *n*-hexyl groups of **KI-5**, **YC-1**, and **YC-1P** were replaced with the methyl groups for convenience of calculation.

In order to investigate the electronic structures and molecular orbitals of phenazine-2,3-diol-based PSs, DFT calculations²⁰ at the B3LYP/6-31G(d,p)/THF-CPCM level for **KI-3**, **KI-5**, **YC-1**, and **YC-2** and the B3LYP/6-31+G(d,p)/THF-CPCM level for the phenoxide forms (**YC-1P** and **YC-2P**) of **YC-1** and **YC-2** were performed (Fig. 8). For convenience of calculations, the *n*-hexyl groups of **KI-5**, **YC-1**, and **YC-1P** were replaced with methyl groups. The DFT calculations demonstrated that the HOMOs for these PSs are delocalized over the whole molecule. The LUMOs for **KI-3**, **KI-5**, **YC-1**, and **YC-1P** are localized on each phenazine-2,3-diol moiety, but the LUMOs for **YC-2** and **YC-2P** are delocalized over the whole molecule. The HOMO and LUMO energy levels (−6.02 eV and −3.04 eV, −5.98 eV and −2.85 eV, respectively) of **KI-3** and **YC-2** with formyl groups are lower than those

(−5.62 eV and −2.90 eV, −5.59 eV and −2.64 eV, respectively) of the corresponding **KI-5** and **YC-1** with methyl groups. Meanwhile, the LUMO energy levels (−3.04 eV and −2.90 eV, respectively) of **KI-3** and **KI-5** with the nitro group are lower than those (−2.85 eV and −2.64 eV, respectively) of the corresponding **YC-2** and **YC-1** with the cyano group. Consequently, the HOMO-LUMO energy band gaps of these PSs are 2.98 eV for **KI-3**, 2.72 eV for **KI-5**, 2.95 eV for **YC-1**, and 3.13 eV for **YC-2**. From these results, it is considered that the substitution of electron-donating *n*-hexyl group for electron-withdrawing formyl group on thiophene units lead to the rising of the HOMO and LUMO energy levels, but the rising in the HOMO is larger than that in the LUMO, and thus resulting in the decrease of HOMO-LUMO energy band gaps. On the other hand, the substitution of moderate electron-withdrawing cyano group for stronger electron-withdrawing nitro group on phenazine-2,3-diol skeleton lead to the rising of the LUMO energy levels, resulting in the increase of HOMO-LUMO energy band gaps. Furthermore, the HOMO-LUMO energy band gaps (2.42 eV and 2.64 eV, respectively) of **YC-1P** and **YC-2P** are smaller than those of (2.95 eV and 3.13 eV, respectively) of **YC-1** and **YC-2**. Thus, the DFT calculations are in good agreement with the experimental results about the photoabsorption spectra in the THF solutions (Fig. 2a and 3).

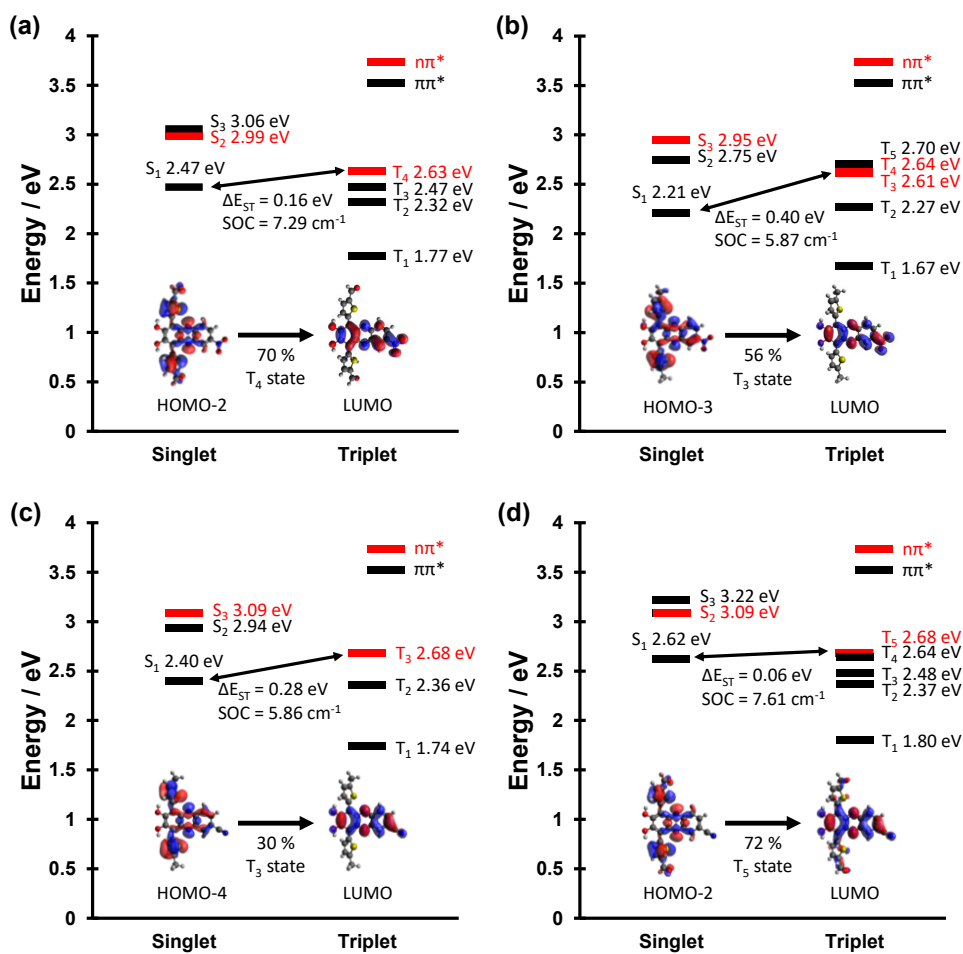


Fig. 9 Schematic diagrams showing vertical excitation energies of (a) **KI-3**, (b) **KI-5**, (c) **YC-1**, and (d) **YC-2** singlet and triplet excited states. The insets represent the frontier n-orbitals that contribute to the (n, π^*) triplet states. The *n*-hexyl groups of **KI-5** and **YC-1** were replaced with the methyl groups for convenience of calculation.

Table 2 Spin–orbit coupling (SOC) constants and the energy gaps (ΔE_{ST}) between the lowest excited singlet states (S_1) and the triplet states (T_n).

Dye	Triplet states	SOC / cm^{-1}	ΔE_{ST} / eV
KI-3	T ₁	0.29	-0.71
	T ₂	0.85	-0.15
	T ₃	0.93	0.00
	T ₄	7.29	0.15
	T ₅	2.36	0.16
KI-5	T ₁	0.18	-0.54
	T ₂	0.85	0.06
	T ₃	5.83	0.39
	T ₄	2.75	0.43
	T ₅	0.22	0.49
YC-1	T ₁	0.19	-0.67
	T ₂	0.98	-0.04
	T ₃	5.86	0.28
	T ₄	2.83	0.32
	T ₅	1.06	0.56
YC-2	T ₁	0.42	-0.82
	T ₂	1.29	-0.25
	T ₃	1.22	-0.14
	T ₄	3.10	0.03
	T ₅	7.61	0.06
YC-1P	T ₁	0.35	-0.44
	T ₂	0.69	0.01
	T ₃	0.48	0.48
	T ₄	6.25	0.91
	T ₅	0.15	0.97
YC-2P	T ₁	0.34	-0.56
	T ₂	0.88	-0.28
	T ₃	1.93	-0.11
	T ₄	1.38	0.29
	T ₅	12.1	0.64

Furthermore, in order to gain insight into the $^1\text{O}_2$ generation properties of these PSs based on the ISC efficiency, spin-orbit coupling (SOC) matrix elements were analyzed using time-dependent DFT (TD-DFT) calculations.²¹ The SOC constants and the vertical excitation energies from the S_0 state to the S_n and T_n states for these PSs were calculated using their S_0 state geometries (Fig. 9 and Table 2). TD-DFT calculations suggested that these PSs have the frontier n-orbitals that consist of the lone pair electrons on nitrogen atom of the phenazine skeleton. In particular, for **KI-3** and **YC-2** with formyl groups, the lone pair electrons on the formyl oxygens also contribute to the frontier n-orbitals (Fig. 9 insets). Therefore, it was revealed that these PSs have several ISC pathways which meet the El-Sayed rule ($S_1 (\pi, \pi^*) \rightarrow T_3 (n, \pi^*)$ for **KI-5** and **YC-1**, $S_1 (\pi, \pi^*) \rightarrow T_4 (n, \pi^*)$ for **KI-3**, and $S_1 (\pi, \pi^*) \rightarrow T_5 (n, \pi^*)$ for **YC-2**).¹⁷ In these major ISC pathways, these PSs exhibited relatively large SOC matrix elements (7.29 cm^{-1} for **KI-3**, 5.83 cm^{-1} for **KI-5**, 5.86 cm^{-1} for **YC-1**, and 7.61 cm^{-1} for **YC-2**). For the energy gaps (ΔE_{ST}) between the $S_1 (\pi\pi^*)$ states and T_n states with $n\pi^*$ characteristic, **YC-2** have the smallest ΔE_{ST} (-0.06 eV) among these PSs (-0.16 eV for **KI-3**, -0.40 eV for **KI-5**, and -0.28 eV for **YC-1**), leading to the efficient ISC according to the El-Sayed rule.¹⁷ Indeed, the large SOC and small ΔE_{ST} values of **YC-2** are consistent with the experimental results that **YC-2** exhibited the highest Φ_{Δ} value (0.29) among these PSs (0.05 for **KI-3**, 0.02 for **KI-5**, and 0.0081 for **YC-1**). Although **YC-1P** and **YC-2P** possess ISC pathways with relatively large SOC constants (S_1-T_4 , 6.25 cm^{-1} for **YC-1P** and S_1-T_5 , 12.1 cm^{-1} for **YC-2P**), there's little change in their orbital type. As discussed in the **Chapter 2**,¹⁶ the low Φ_{Δ} value of **KI-3**, despite the relatively small ΔE_{ST} value, is due to the rapid nonradiative decay of the excited states by the nitro group. In addition, the TDDFT calculations suggested that the low Φ_{Δ} values of **YC-1** and **KI-5** are due to the relatively large ΔE_{ST} values as well as the flexible *n*-hexyl groups which accelerate IC from S_1 to S_0 state, as evidenced by the low Φ_{I} values, resulting in inferior ISC. Consequently, we revealed that the substitution of the cyano group

for the nitro group in phenazine-2,3-diol-based chromophore reduces the rapid nonradiative decay of the excited states and the ΔE_{ST} values, leading to the efficient ISC.

Conclusions

We have designed and developed the cyano-substituted phenazine-2,3-diol-based dyes, **YC-1** and **YC-2** which have *n*-hexyl and formyl groups, respectively, on thiophene units, as halogen-atom-free-heteroanthracene-based photosensitizers (PSs) possessing the ability to generate singlet oxygen ($^1\text{O}_2$). The photoabsorption edges ($\lambda_{\text{edge}}^{\text{abs}}$) of **YC-1** and **YC-2** reached at 700 nm and 650 nm, respectively, but these exhibited blue-shifts, compared to those (700 nm and 800 nm) of nitro-substituted phenazine-2,3-diol-based dyes **KI-3** and **KI-5** with formyl groups and *n*-hexyl group, respectively, on thiophene units. **KI-3** and **KI-5** show low $^1\text{O}_2$ generation quantum yields ($\Phi_{\Delta} = 0.05$ and 0.02, respectively) due to the rapid nonradiative decay of the excited states by the nitro group. On the other hand, it was found that **YC-2** exhibits a moderate Φ_{Δ} value (0.29), but the Φ_{Δ} value (0.0081) of **YC-1** is significantly lower than those of the other PSs. Time-dependent density functional theory (TDDFT) calculations revealed that **YC-2** with the formyl groups has a small energy gap ΔE_{ST} (-0.06 eV) between the S_1 ($\pi\pi^*$) state and the T_5 ($n\pi^*$) state with relatively large spin-orbit coupling (SOC) constants (7.61 cm^{-1}) compared to the other PSs. This results in efficient intersystem crossing (ISC) of **YC-2** according to the El-Sayed rule. The low Φ_{Δ} value of **YC-1** with *n*-hexyl groups is attributed to the relatively large ΔE_{ST} value (0.28 eV) as well as the flexible *n*-hexyl groups which accelerate internal conversion (IC) from S_1 to S_0 state, resulting in inferior ISC. Consequently, we demonstrated that the substitution of the cyano group for the nitro group in phenazine-2,3-diol-based chromophore reduces the rapid nonradiative decay of the excited states and the ΔE_{ST} values, leading to the efficient ISC for $^1\text{O}_2$ generation.

Acknowledgements

Chapter 4 is reproduced from “Development of phenazine-2,3-diol-based photosensitizers: effect of substitution of the cyano group for the nitro group on singlet oxygen generation; K Ohira, C. Yu, K. Imato, and Y. Ooyama, *New J. Chem.*, **2023**, 47, 16799–16808.” with permission from The Royal Society of Chemistry.

Reference

1. (a) X. Li, G. Zhang, H. Ma, D. Zhang, J. Li, and D. Zhu, *J. Am. Chem. Soc.* **2004**, 126, 11543–11548; (b) L. Wang, L. Tang, Y. Liu, H. Wu, Z. Liu, J. Li, Y. Pan and E. U. Akkaya, *Chem. Commun.*, **2022**, 58, 1902–1905; (c) M. Bauch, W. Fudickar and T. Linker, *Molecules*, **2021**, 26, 804; (d) T. Montagnon, D. Kalaitzakis, M. Triantafyllakis, M. Stratakisa and G. Vassilikogiannakis, *Chem. Commun.*, **2014**, 50, 15480–15498.
2. (a) H. J. Shen, Z. N. Hu, and C. Zhang, *J. Org. Chem.* **2022**, 87, 3885–3894; (b) L. Burchill and J. H. George, *J. Org. Chem.* **2020**, 85, 2260–2265.
3. (a) P. Bayer, J. Schachtner, M. Májeka and A. J. v. Wangelin, *Org. Chem. Front.*, **2019**, 6, 2877–2883; (b) M. Prein and W. Adam, *Angew. Chem. Int. Ed. Engl.*, **1996**, 35, 471–494.
4. M. Jaramillo, J. A. Joens, and K. E. O’Shea, *Environ. Sci. Technol.*, **2020**, 54, 6073–6081.
5. M. Deiana, P. Josse, C. Dalinot, A. Osmolovskyi, P. S. Marqués, J. M. A. Castán, L. A. Galán, M. Allain, L. Khrouz, O. Maury, T. L. Bahers, P. Blanchard, S. D.-Seignon, C. Monnereau, N. Sabouri and C. Cabanetos, *Commun. Chem.*, **2022**, 5, 142.
6. (a) K. Hirakawa, S. Takai, H. Horiuchi and S. Okazaki, *ACS Omega*, **2020**, 5, 27702–27707; (b) Y. Ooyama, T. Enoki, J. Ohshita, T. Kamimura, S. Ozako, T. Koide and F. Tani, *RSC Adv.*, **2017**, 7, 18690–18695; (c) F. Taba, A. Onoda, U. Hasegawa, T. Enoki, Y. Ooyama, J. Ohshita and T. Hayashi, *ChemMedChem*, **2018**, 13, 15–19.

7. B. Barut , C. Ö. Yalçın and Ü. Demirbaş, *J. Photochem. Photobiol., A*, **2021**, *405*, 112946.
8. T. M. Ebaston , F. Nakonechny , E. Talalai , G. Gellerman and L. Patsenker , *Dyes Pigm.*, **2021**, *184*, 108854.
9. (a) L. Wang, J. Bai and Y. Qian, *New J. Chem.*, **2019**, *43*, 16829–16834; (b) H. Wang, C. Li, Q. Wu, H. Wen, T. Sun and Z. Xie, *J. Mater. Chem. B*, **2022**, *10*, 4967–4973; (c) M. Liu, C. Wang and Y. Qian, *New J. Chem.*, **2021**, *45*, 18082–18089; (d) J. Chen, Y. Cui, K. Song, T. Liu, L. Zhou, B. Bao, R. Wang and L. Wang, *Biomater. Sci.*, **2021**, *9*, 2115–2123; (e) I. J. Gomez, M. Russo, O. A. Arcidiacono, E. M. Sanchez-Carnerero, P. Klan and L. Zajickova, *Mater. Chem. Front.*, **2022**, *6*, 1719–1726.
10. (a) K. Piwowar, A. Blacha-Grzechnik and J. Zak, *J. Electrochem. Soc.*, **2019**, *166*, G163–G169; (b) F. Ronzani, A. Trivella, E. Arzoumanian, S. Blanc, M. Sarakha, C. Richard, E. Oliveros and S. Lacombe, *Photochem. Photobiol. Sci.*, **2013**, *12*, 2160–2169.
11. (a) Y. Ooyama, T. Enoki and J. Ohshita, *RSC Adv.*, **2016**, *6*, 5428–5435; (b) J. Ohshita, Y. Hayashi, K. Murakami, T. Enoki and Y. Ooyama, *Dalton Trans.*, **2016**, *45*, 15679–15683.
12. O. J. Stacey and S. J. A. Pope, *RSC Adv.*, 2013, **3**, 25550–25564.
13. (a) K. Ohira, M. Yamamoto, K. Imato and Y. Ooyama, *New J. Chem.*, **2023**, *47*, 2711–2718; (b) K. Ohira, K. Imato and Y. Ooyama, *Mater. Chem. Front.*, **2021**, *5*, 5298–5304; (c) K. Yagi, K. Ohira, K. Yamana, K. Imato, R. Kawasaki, A. Ikeda and Y. Ooyama, *Org. Biomol. Chem.*, **2023**, *21*, 5194–5202.
14. (a) N. M. Senozan, *J. Chem. Educ.*, **1985**, *62*, 181; (b) J. P. Tardivo, A. D. Giglio, C. S. d. Oliveira, D. S. Gabrielli, H. C. Junqueira, D. B. Tada, D. Severino, R. d. F. Turchiello and M. S. Baptista, *Photodiagnosis Photodyn Ther*, **2005**, *2*, 175–191.
15. (a) D. van Straten, V. Mashayekhi, H. S. de Bruijn, S. Oliveira and D. J. Robinson, *Cancers*, **2017**, *9*, 1–54; (b) Y. Wen, C. L. Schreiber and B. D. Smith, *Bioconjugate Chem.*, **2020**, *31*, 474–482;

- (c) M. Ethirajan, Y. Chen, P. Joshi and R. K. Pandey, *Chem. Soc. Rev.*, **2011**, *40*, 340–362; (d) J. C. S. Simões, S. Sarpaki, P. Papadimitroulas, B. Therrien and G. Loudos, *J. Med. Chem.*, **2020**, *63*, 14119–14150.
16. K. Imato, K. Ohira, M. Yamaguchi, T. Enoki and Y. Ooyama, *Mater. Chem. Front.*, **2020**, *4*, 589–596.
17. (a) M. A. El-Sayed *Acc. Chem. Res.*, **1968**, *1*, 8; (b) M. Baba *J. Phys. Chem. A*, **2011**, *115*, 9514–9519; (c) S. Tsumura, K. Ohira, K. Hashimoto, K. Imato and Y. Ooyama, *Mater. Chem. Front.*, **2020**, *4*, 2762–2771; (d) H. Shu, H. Li, J. Rao, L. Chen, X. Wang, X. Wu, H. Tian, H. Tong and L. Wang, *J. Mater. Chem. C*, **2020**, *8*, 14360–14364.
18. J. Zou, Z. Yin, P. Wang, D. Chen, J. Shao, Q. Zhang, L. Sun, W. Huang and X. Dong, *Chem. Sci.*, **2018**, *9*, 2188–2194.
19. W. Wu, J. Sun, X. Cui and J. Zhao, *J. Mater. Chem. C*, **2013**, *1*, 4577–4589.
20. Gaussian 16, Revision A.03, M. J. Frisch, G. W. Trucks, H. B. Schlegel, G. E. Scuseria, M. A. Robb, J. R. Cheeseman, G. Scalmani, V. Barone, G. A. Petersson, H. Nakatsuji, X. Li, M. Caricato, A. V. Marenich, J. Bloino, B. G. Janesko, R. Gomperts, B. Mennucci, H. P. Hratchian, J. V. Ortiz, A. F. Izmaylov, J. L. Sonnenberg, D. Williams-Young, F. Ding, F. Lipparini, F. Egidi, J. Goings, B. Peng, A. Petrone, T. Henderson, D. Ranasinghe, V. G. Zakrzewski, J. Gao, N. Rega, G. Zheng, W. Liang, M. Hada, M. Ehara, K. Toyota, R. Fukuda, J. Hasegawa, M. Ishida, T. Nakajima, Y. Honda, O. Kitao, H. Nakai, T. Vreven, K. Throssell, J. A. Montgomery, Jr., J. E. Peralta, F. Ogliaro, M. J. Bearpark, J. J. Heyd, E. N. Brothers, K. N. Kudin, V. N. Staroverov, T. A. Keith, R. Kobayashi, J. Normand, K. Raghavachari, A. P. Rendell, J. C. Burant, S. S. Iyengar, J. Tomasi, M. Cossi, J. M. Millam, M. Klene, C. Adamo, R. Cammi, J. W. Ochterski, R. L. Martin, K. Morokuma, O. Farkas, J. B. Foresman, and D. J. Fox, Gaussian, Inc., Wallingford CT, 2016.
21. F. Neese, *Wiley Interdiscip. Rev.: Comput. Mol. Sci.*, **2022**, *12*, e1606.

Chapter 5

Development of water-soluble phenazine-2,3-diol-based photosensitizers for singlet oxygen generation

Introduction

Singlet oxygen ($^1\text{O}_2$) generated by light irradiation to photosensitizers (PSs),¹ which is one of the reactive oxygen species (ROS), has gained more and more attention as an effective and convenient oxidant of alkenes and dienes for Schenck–ene reactions and [2 + 2]- and [4 + 2]-cycloadditions in organic synthesis,^{2–5} degradation of water pollutants in environmental and quality control monitoring systems,⁶ inactivation of microbiological contamination in point-of-use water disinfection systems,⁷ and cancer treatment in photodynamic therapy (PDT).⁸ $^1\text{O}_2$ is generally produced through the following processes: initially, the PS (^1PS) absorbs light ($h\nu$) to generate the singlet excited state ($^1\text{PS}^*$), and then the $^1\text{PS}^*$ undergoes intersystem crossing (ISC) to generate the triplet excited state ($^3\text{PS}^*$). Subsequent energy transfer from the photoexcited PS ($^3\text{PS}^*$) to triplet oxygen ($^3\text{O}_2$) produces $^1\text{O}_2$. Thus, in order to obtain a high $^1\text{O}_2$ quantum yield (Φ_Δ), it is necessary to enhance the ISC efficiency of PSs. Moreover, for use in water purification systems and PDT, the PSs are required to possess high solubility in water as well as efficient ISC. Methylene blue (**MB**),⁹ Rose Bengal (**RB**),¹⁰ and hydrophobically modified porphyrin derivatives¹¹ have been used as water-soluble PSs with high $^1\text{O}_2$ Φ_Δ values (0.50–0.60 for **MB**,^{9b,c} 0.70–0.80 for **RB**,^{9b,10b} and 0.50–0.60 for free base 5,10,15,20-tetrakis(4-carboxylatophenyl)porphyrin,^{11a,b} respectively). Meanwhile, halogen atoms such as iodide and bromide atoms are often introduced into chromophores (*e.g.* **RB**) to promote ISC based on spin–orbit coupling,¹¹ but they cause dark cytotoxicity.¹² Indeed, **MB** as a halogen atom-free-heteroanthracene-based PS¹³ is used as not only a reference water-soluble PS for the evaluation of

Φ_{Δ} ,^{9b,c} but also a fungicide and antidote in aquaculture.^{9f,g}

Thus, in **Chapter 3**, we have designed and developed phenazine-2,3-diol-based dyes (**KO-0-3**)¹⁴ as halogen atom-free-heteroanthracene-based PSs and demonstrated that the modification of the phenazine-2,3-diol chromophore with formyl groups promotes ISC, leading to efficient ¹O₂ generation (Fig. 1a). According to the El-Sayed rule, formyl and carbonyl substituents in a chromophore skeleton facilitate the ISC from the singlet (S_n) to triplet (T_n) states, that is, by the change in the molecular orbital type such as transitions of ¹($n\pi^*$) to ³($\pi\pi^*$) and ¹($\pi\pi^*$) to ³($n\pi^*$). In fact, **KO-1-3** exhibited moderate ¹O₂ generation ability ($\Phi_{\Delta} = 0.22\text{--}0.41$) in THF.

In this work, in order to attain the solubility of phenazine-2,3-diol-based PSs in water, we have developed **KY-1Na** and **KY-2Na** bearing one and two carboxylic acid sodium salts, respectively, as the water-soluble derivatives of **KO-2** exhibiting a moderate Φ_{Δ} value (0.17) in DMSO (Fig. 1b). Actually, in order to evaluate the solubility of **KY-1Na** and **KY-2Na** in water, the hydrophobicity/hydrophilicity of the two PSs was investigated by experimental measurement of the logarithms ($\log P_{o/w}$) of the 1-octanol/water partition coefficient ($P_{o/w}$) for the PS. Both the PSs in water show a broad photoabsorption band in the range of 500 to 600 nm. It was found that in water **KY-2Na** exhibits a moderate Φ_{Δ} value, which is higher than that of **KY-1Na**. Density functional theory (DFT) and time-dependent DFT (TD-DFT) calculations were performed to gain insight into the ¹O₂ generation properties of **KY-1Na** and **KY-2Na** based on the ISC efficiency. Herein we report that the introduction of carboxylic acid salts into the phenazine-2,3-diol chromophore is effective in yielding solubility in water and a small energy gap (ΔE_{ST}) between the S_1 state and the T_1 state for efficient ISC, leading to the development of water-soluble halogen-atom-free-heteroanthracene-based PSs.

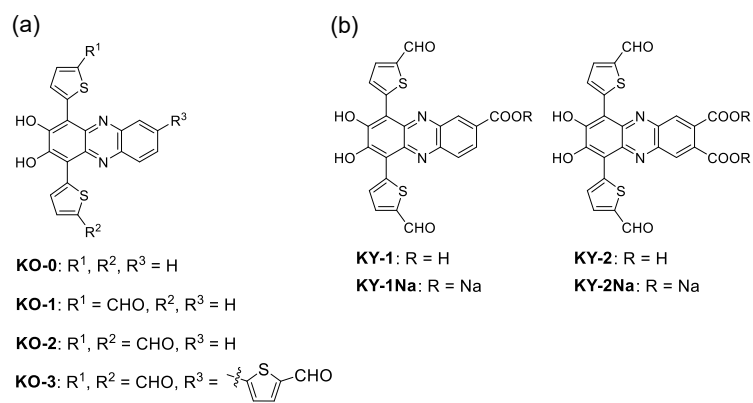


Fig. 1 (a) Chemical structures of phenazine-2,3-diol-based PSs, **KO-0–3** in Chapter 3 and **KY-1**, **KY-2**, **KY-1Na**, and **KY-2Na** in this study.

Experimental

Materials

All solvents and reagents were used as received unless otherwise noted. Rose bengal (RB) was purchased from Sigma Aldrich and recrystallized from methanol twice. 1,3-Diphenylisobenzofuran (DPBF) was purchased from Tokyo Chemical Industry and recrystallized from a mixture of dichloromethane and methanol. Bromanilic acid was purchased from Tokyo Chemical Industry.

General

^1H NMR and ^{13}C NMR spectra were recorded using a Varian-500 (500 MHz) FT NMR spectrometer. FT-IR spectra were recorded using a Shimadzu IRTracer-100. High-resolution mass spectral data were acquired using a Thermo Fisher Scientific LTQ Orbitrap XL. Photoabsorption spectra were recorded using Shimadzu and UV-3600-plus spectrophotometers. Fluorescence spectra were measured using a Hitachi F-4500 spectrophotometer. The fluorescence quantum yields (Φ_{f}) were determined with a Hamamatsu C9920-01 instrument equipped with CCD by use of a calibrated integrating sphere system. The irradiance of monochromatic and continuous lights for photosensitizing reactions was adjusted using a Newport 1918-C optical power meter.

n-Octanol/water partition coefficient

The log $P_{\text{o/w}}$ values were determined from the concentration of PSs partitioned into water (100 mL) and *n*-octanol (100 mL) and the concentration of PSs partitioned into each phase.

Evaluation of the $^1\text{O}_2$ quantum yield

$^1\text{O}_2$ generation by **KO-2**, **KY-1**, **KY-2**, **KY-1Na**, and **KY-2Na** was investigated by monitoring the changes in photoabsorption spectra of DPBF in DMSO solution of each PS and ABDA in aqueous solution ($\text{D}_2\text{O}/\text{DMSO}$ 99:1, v/v) of **KY-1Na** and **KY-2Na** under photoirradiation. DMSO and water were bubbled with air for 15 min prior to preparing solutions. Air-saturated DMSO containing DPBF or aqueous solutions containing ABDA and each PS were irradiated with monochromatic light at 532

nm ($300 \mu\text{W cm}^{-2}$) that was obtained by passage of a xenon light source (HAL-320, Asahi Spectra) through a monochromator (CMS-100, Asahi Spectra). The concentration of DPBF and ABDA was 5×10^{-5} M in the air-saturated DMSO or aqueous solutions. The concentration of the photosensitizers (PSs) and rose bengal (**RB**) was adjusted so that the absorbance was ca. 0.03 at the irradiation wavelength (532 nm). Except for the nonirradiated solutions, each spectrum was measured immediately after photoirradiation for 1 min. The procedure using DPBF and ABDA was promptly repeated until the total photoirradiation time reached 10 min and 60 min, respectively. The changes in optical density (ΔOD) of DPBF were plotted against photoirradiation time to obtain the slopes (m) and estimate Φ_{Δ} values. The Φ_{Δ} values of **KO-2**, **KY-1**, **KY-2**, **KY-1Na**, and **KY-2Na** were determined by the relative method using **RB** ($\Phi_{\Delta} = 0.76$ in DMSO and 0.75 in water) as a standard according to the following equation:

$$\Phi_{\Delta\text{sam}} = \Phi_{\Delta\text{ref}} \times [(m_{\text{sam}}/m_{\text{ref}}) \times (L_{\text{ref}}/L_{\text{sam}})]$$

where $\Phi_{\Delta\text{sam}}$ and $\Phi_{\Delta\text{ref}}$ are $^1\text{O}_2$ quantum yields of phenazine-2,3-diol-based PSs and **RB**, respectively, m_{sam} and m_{ref} are slopes in the plots of ΔOD at the photoabsorption maximum wavelength of DPBF (415 nm) and ABDA (400 nm) against photoirradiation time, and L_{sam} and L_{ref} are light harvesting efficiencies, which are given by $L = 1 - 10^{-A}$ (“ A ” is the absorbance at the photoirradiation wavelength).

Evaluation of the cellular uptake of KY-2Na

Colon26 cells were seeded on glass bottom dishes at a density of 1×10^5 cells per well and incubated overnight. The cells were treated with **KY-2Na** for 24 h. The medium was collected and the fluorescence spectrum was recorded. Then, the cells were observed under a confocal laser scanning microscope (LSM700, Carl Zeiss, Germany).

Photodynamic activity against cancer cell lines

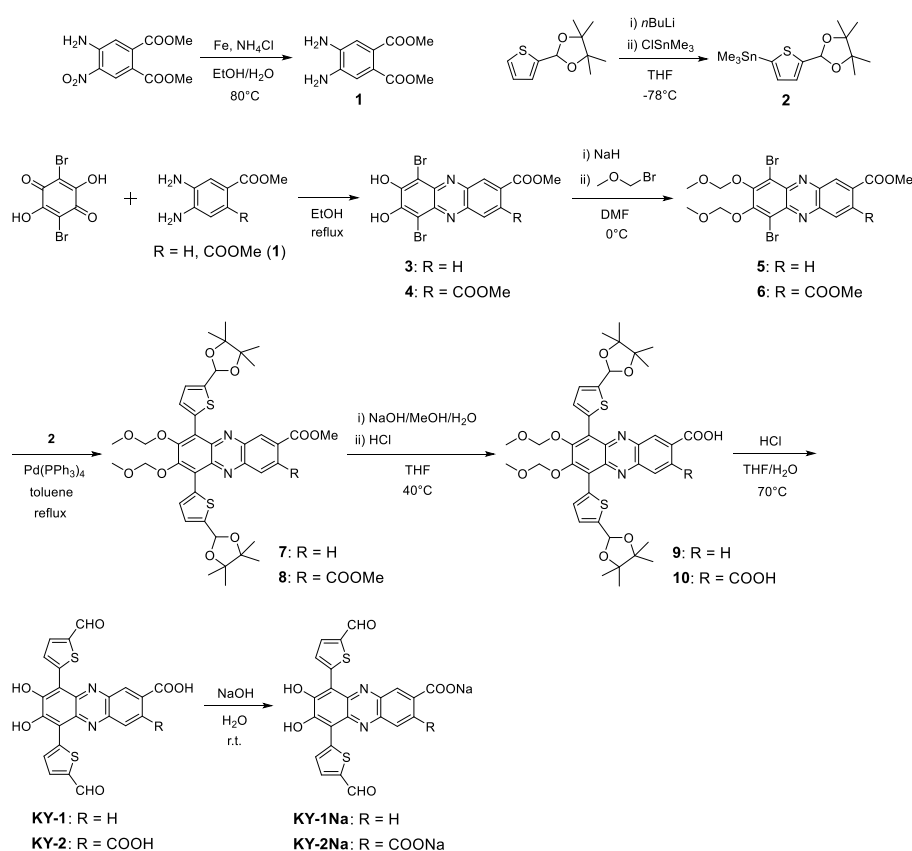
Colon26 cells were seeded on 48-well plates (Thermo Fischer Science) at 1.71×10^4 cells ($N = 3$) and incubated overnight (approximately 18 h). The cells were exposed to **KY-1Na** or **KY-2Na** at varying

concentrations. After 24 h of incubation, the cells were washed with PBS thrice, and photoirradiation (>510 nm, 9 mW cm^{-2}) was carried out for 30 min. Afterward, the cells were incubated for 24 h, and the Cell Counting Kit-8 solution was added to the cells. After 30 min of incubation, the absorbance at 450 nm was measured using a microplate reader.

Theoretical calculations

The Gaussian 16 program²¹ was used for density functional theory (DFT) calculations and time-dependent DFT (TD-DFT) calculations. DFT and TD-DFT calculations at the B3LYP/6-311G(d,p)/DMSO-IEFPCM level for **KO-2**, **KY-1**, and **KY-2**, the B3LYP/6-311+G(d,p)/DMSO-IEFPCM level for **KY-1Na** and **KY-2Na** in carboxylate anion forms, and the B3LYP/6-311+G(d,p)/Water-IEFPCM level for **KY-1Na** and **KY-2Na** in carboxylate anion forms were performed. Geometrical optimizations of the S_0 state at each calculation level were performed with frequency calculations. There are no imaginary frequencies for all optimized structures. The TD-DFT calculations of both excited singlet and triplet states were performed using optimized S_0 geometries.

Synthesis



Scheme 1 Synthetic route to phenazine-2,3-diol-based PSs **KY-1**, **KY-2**, **KY-1Na**, and **KY-2Na**.

6,9-Bis(5-formylthiophen-2-yl)-7,8-dihydroxyphenazine-2-carboxylic acid (KY-1). A solution of **9** (175 mg) and 1N HCl aq. (0.5 mL) in the mixture of THF (100 mL) and water (100 mL) was stirred at 70 °C overnight. The precipitate was filtered and washed with hexane to give **KY-1** as black solid (70 mg, 64% yield); m.p. over 300°C; IR (ATR): $\tilde{\nu}$ = 3505, 3159, 2961, 2799, 2737, 2349, 2085, 1996, 1989, 1703, 1643, 1614, 1557, 1520, 1508 cm⁻¹; ¹H NMR (500 MHz, DMSO-*d*₆): δ = 9.97 (s, 1H, CHO), 9.93 (s, 1H, CHO), 8.96 (s, 1H, aromatic), 8.76 (d, *J*=3,20 Hz, aromatic), 8.71–8.70 (m, 1H, aromatic), 8.19–8.16 (m, 2H, aromatic), 8.04–8.00 (m, 2H, aromatic) ppm; ¹³C NMR spectrum could not be obtained because of the low solubility in any solvents; HRMS (APCI): *m/z* found 477.02100 [M+H]⁺, calculated for C₂₃H₁₃O₆N₂S₂ [M+H]⁺ : 477.02095.

6,9-Bis(5-formylthiophen-2-yl)-7,8-dihydroxyphenazine-2,3-dicarboxylic acid (KY-2). A solution

of **10** (63.0 mg, mmol) and 1N HCl aq. (2 mL) in the mixture of THF (50 mL) and water (50 mL) was stirred at 70 °C overnight. The precipitate was filtered and washed with hexane to give **KY-2** as black solid (8.00 mg, 20% yield); m.p. over 300°C; IR (ATR): $\tilde{\nu}$ = 3198, 2376, 2347, 2160, 1726, 1701, 1697, 1678, 1655, 1612, 1595, 1535 cm^{-1} ; ^1H NMR (500 MHz, DMSO- d_6): δ = 9.95 (s, 2H, CHO), 8.91–8.87 (m, 2H, aromatic), 8.34 (s, 2H, aromatic), 8.01 (d, J = 4.25 Hz, 2H, aromatic) ppm; ^{13}C NMR spectrum could not be obtained because of the low solubility in any solvents; HRMS (ESI): m/z found 518.99603 $[\text{M}-\text{H}]^-$, calculated for $\text{C}_{24}\text{H}_{11}\text{O}_8\text{N}_2\text{S}_2$ $[\text{M}-\text{H}]^-$: 518.99513.

Sodium 6,9-bis(5-formylthiophen-2-yl)-7,8-dihydroxyphenazine-2-carboxylate (KY-1Na). A solution of **KY-1** (42 mg, 0.881 mmol) and 1N NaOH aq. (70 μL) in the water (100 mL) was stirred at room temperature for 10 min and concentrated to give **KY-1Na** as red solid (46% yield); m.p. over 300°C; IR (ATR): $\tilde{\nu}$ = 3200, 2303, 2110, 1994, 1846, 1578 cm^{-1} ; ^1H NMR (500 MHz, D_2O): δ = 9.51 (s, 1H, CHO), 9.36 (s, 1H, CHO), 8.71 (s, 1H, aromatic), 8.59 (s, 1H, aromatic), 8.43 (s, 1H, aromatic), 8.00 (d, J = 8.62 Hz, 1H, aromatic), 7.93 (d, J = 8.50 Hz, 1H, aromatic), 7.84 (s, 1H, aromatic), 7.68 (s, 1H, aromatic) ppm; ^{13}C NMR spectrum could not be obtained because of the low solubility in any solvents; HRMS (ESI): m/z found 475.00620 $[\text{M}-\text{Na}]^-$, calculated for $\text{C}_{23}\text{H}_{11}\text{O}_6\text{N}_2\text{S}_2$ $[\text{M}-\text{Na}]^-$: 475.00530.

Sodium 6,9-bis(5-formylthiophen-2-yl)-7,8-dihydroxyphenazine-2,3-dicarboxylate (KY-2Na). A solution of **KY-2** (8.00 mg, 0.0154 mmol) and 1N NaOH aq. (31.0 μL) in the water (50 mL) was stirred at room temperature for 10 min and concentrated to give **KY-2Na** as red solid (10 mg, quant.); m.p. over 300°C; IR (ATR): $\tilde{\nu}$ = 3318, 1560 cm^{-1} ; ^1H NMR (500 MHz, D_2O): δ = 9.84 (s, 1H, CHO), 9.78 (s, 1H, CHO), 8.45 (m, 1H, aromatic), 8.39 (m, 1H, aromatic), 8.27 (s, 1H, aromatic), 8.14 (s, 1H, aromatic), 8.03 (s, 2H, aromatic) ppm; ^{13}C NMR spectrum could not be obtained because of the low solubility in any solvents; HRMS (APCI): m/z found 518.99615 $[\text{M}+\text{H}-2\text{Na}]^-$, calculated for $\text{C}_{24}\text{H}_{11}\text{O}_8\text{N}_2\text{S}_2$ $[\text{M}+\text{H}-2\text{Na}]^-$: 518.99513.

Results and discussion

Synthesis

Phenazine-2,3-diol-based PSs, **KY-1** and **KY-2** bearing one and two carboxylic acids, respectively, and their sodium salt derivatives **KY-1Na** and **KY-2Na**, were synthesized by a stepwise synthetic protocol (Scheme 1). We prepared compounds **1** and **2**,¹⁵ respectively, for the construction of the phenazine skeleton and the introduction of the formylthiophene unit on the chromophore by the Stille coupling. Phenazine-2,3-diol chromophores **3** and **4** were prepared by the cyclodehydration of 2,5-dibromo-3,6-dihydroxy-*p*-quinone with methyl 3,4-diaminobenzoate or compound **1**, respectively, and then converted into methoxymethyl (MOM)-protected compounds **5** and **6**, respectively. The Stille coupling reaction of **5** or **6** with compound **2** gave compounds **7** and **8**, respectively. Compounds **7** and **8** were hydrolyzed by treatment with a base to generate compounds **9** and **10**, respectively, and then the hydrolysis of **9** and **10** with an acid gave the carboxylic acids **KY-1** and **KY-2**, respectively. Finally, **KY-1Na** and **KY-2Na** were obtained by treatment of **KY-1** and **KY-2**, respectively, with a base. In order to evaluate the hydrophobicity/hydrophilicity of **KY-1Na** and **KY-2Na**, the logarithms ($\log P_{o/w}$)¹⁶ of the 1-octanol/water partition coefficient ($P_{o/w}$) for the PS were measured experimentally. The $\log P_{o/w}$ values of both **KY-1Na** and **KY-2Na** were determined to be -0.9 , indicating that both the PSs are more hydrophilic than **RB** (-0.6)^{10c} and have hydrophilicity equivalent to **MB** (-0.9).^{9d,e} Incidentally, **KO-2** exhibits hydrophobicity with a $\log P_{o/w}$ value of 1.3 . Thus, this fact indicates that **KY-1Na** and **KY-2Na** possess high solubility in water.

Optical properties

The photoabsorption and fluorescence spectra of **KY-1Na** and **KY-2Na** in DMSO and in water (D₂O) are shown in Fig. 2 with those of **KO-2**, **KY-1**, and **KY-2** in DMSO as references for the characterization of the photoabsorption properties of **KY-1Na** and **KY-2Na**, and their optical data are summarized in Table 1. All the five dyes show an intense photoabsorption maximum ($\lambda_{\text{max}}^{\text{abs}}$) at around

400–450 nm with a relatively high molar extinction coefficient ($\epsilon_{\text{max}} = 25\,000\text{--}30\,000\text{ M}^{-1}\text{ cm}^{-1}$), which can be assigned to the $\pi \rightarrow \pi^*$ transition of the phenazine skeleton containing two formylthiophene units.¹⁴ In addition, for **KO-2**, **KY-1**, and **KY-2**, a broad photoabsorption band ($\lambda_{\text{max}}^{\text{abs}} = 520\text{--}535\text{ nm}$) with a moderate ϵ_{max} value (6000–12 000) was also observed in the range of 500 to 650 nm, which is ascribable to the formation of phenoxide ions by the partial deprotonation of the hydroxyl groups.¹⁴ On the other hand, for **KY-1Na** and **KY-2Na** both in DMSO and in water, the photoabsorption spectra in the range of 500 to 600 nm are significantly broadened, and exhibit a hypsochromic shift and become a shoulder band, compared to those of **KO-2**, **KY-1**, and **KY-2** in DMSO. This fact indicates that **KY-1Na** and **KY-2Na** existed as carboxylate anion ($-\text{COO}^-$) species in DMSO as well as in water.¹⁷ In the corresponding fluorescence spectra, all the five dyes show a feeble fluorescence band with a fluorescence maximum wavelength ($\lambda_{\text{max}}^{\text{fl}}$) at 600–635 nm. In fact, their fluorescence quantum yields (Φ_{fl}) were significantly low (≤ 0.03).

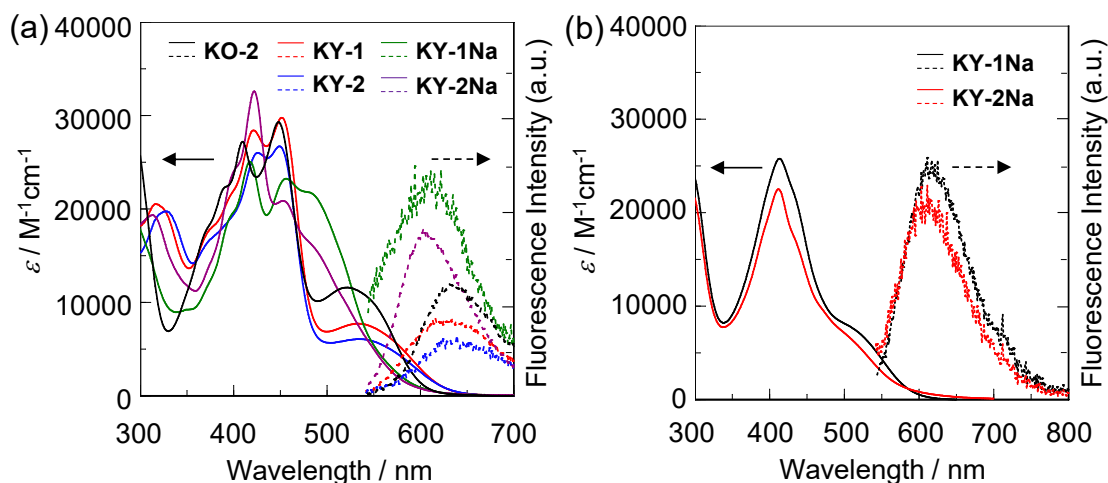


Fig. 2 (a) Photoabsorption and fluorescence spectra ($\lambda^{\text{ex}} = 532$ nm) of **KO-2**, **KY-1**, **KY-2**, **KY-1Na**, and **KY-2Na** (5.0×10^{-5} M) in DMSO. (b) Photoabsorption and fluorescence spectra ($\lambda^{\text{ex}} = 532$ nm) of **KY-1Na** and **KY-2Na** (5.0×10^{-5} M) in D₂O.

Table 1 Optical data and ¹O₂ quantum yields (Φ_{Δ}) of **KO-2**, **KY-1**, **KY-2**, **KY-1Na** and **KY-2Na**

Dye	$\lambda_{\text{max}}^{\text{abs}}/\text{nm}$ ($\epsilon_{\text{max}}/\text{M}^{-1}\text{cm}^{-1}$)	$\epsilon/\text{M}^{-1}\text{cm}^{-1}$ @ $\lambda^{\text{abs}} = 532$ nm	$\lambda_{\text{max}}^{\text{fl}}/\text{nm}$ ($\Phi_{\text{fl}})^c$	Φ_{Δ}
KO-2^a	522 (11 500)	11 300	634 (0.03)	0.17 ^d
KY-1^a	534 (7700)	7700	625 (< 0.02)	0.14 ^d
KY-2^a	534 (6000)	6000	631 (< 0.02)	0.17 ^d
KY-1Na^a	486 ^{shoulder} (21 500)	9600	611 (0.02)	0.13 ^d
KY-2Na^a	486 ^{shoulder} (15 900)	7700	603 (0.02)	0.32 ^d
KY-1Na^b	500 ^{shoulder} (8100)	6100	611 (< 0.02)	0.06 ^e
KY-2Na^b	500 ^{shoulder} (7100)	4500	611 (< 0.02)	0.19 ^e

^a In DMSO. ^b In D₂O. ^c Fluorescence quantum yields (Φ_{fl}) were determined using a calibrated integrating sphere system ($\lambda^{\text{ex}} = 532$ nm). ^d ¹O₂ quantum yields (Φ_{Δ}) based on the relative decomposition rate of DPBF using RB as the standard PS ($\Phi_{\Delta} = 0.76$ in DMSO^{9a}) and DPBF as the ¹O₂ scavenger under irradiation with monochromatic light (532 nm, 300 $\mu\text{W cm}^{-2}$) in DMSO.

^e Φ_{Δ} based on the relative decomposition rate of AMDA using RB as the standard PS ($\Phi_{\Delta} = 0.75$ in water^{9b}) and AMDA as the ¹O₂ scavenger under irradiation with monochromatic light (532 nm, 300 $\mu\text{W cm}^{-2}$) in D₂O/DMSO (99 : 1, v/v).

¹O₂ generation

We evaluated the ¹O₂ generation ability of the phenazine-2,3- diol-based PSs **KO-2**, **KY-1**, **KY-2**, **KY-1Na**, and **KY-2Na** by using an ¹O₂ scavenger. It is well known that 1,3-diphenylisobenzofuran (DPBF) acts as an efficient ¹O₂ scavenger in organic solvents to produce its oxidized product, *o*-dibenzoylbenzene.^{18a,b} Meanwhile, 9,10-anthracenediyl-bis(methylene)dimalonic acid (ABDA), which can react rapidly and irreversibly with ¹O₂ to produce the corresponding endoperoxide (endoperoxideABDA), is widely used as a water-soluble ¹O₂ scavenger.^{18b,c} Therefore, ¹O₂ generation by the five PSs was investigated by monitoring the changes in the photoabsorption spectra of DPBF in the DMSO solution of each PS and ABDA in the aqueous solution (D₂O/DMSO 99 : 1, v/v) of **KY-1Na** and **KY-2Na** under photoirradiation (Fig. 3a–d). DMSO and D₂O/DMSO were bubbled with air for 15 min prior to preparing solutions. Air-saturated DMSO solutions containing DPBF or aqueous solutions containing ABDA and each PS were irradiated with monochromatic light at 532 nm (300 μW cm⁻²) that was obtained by the passage of a xenon light source through a monochromator. In all the DMSO solutions, the photoabsorption of DPBF at around 415 nm decreased with the increase in the photoirradiation time (Fig. 3a and b), which indicates that DPBF reacted with ¹O₂ generated by the photosensitization of the PSs. In order to make clear the difference in ¹O₂ generation ability between the five PSs, the changes in the optical density (ΔOD) at around 415 nm of DPBF are plotted against the photoirradiation time (Fig. 3e), and the slope (*m*_{sam}) is used to estimate the ¹O₂ quantum yield (Φ_Δ): the Φ_Δ values for PSs were determined by the relative method using the slope value (*m*_{ref} = -0.0100) of the plot for **RB** (Φ_Δ = 0.76 in DMSO)^{9a} as a standard (Table 1). Indeed, the correlation coefficient (*R*²) values for the calibration curves of the five PSs are 0.860–0.996, which indicates good linearity, and the *m*_{sam} values become steeper in the following order: **KY-1Na** (-0.0018) < **KY-1** (-0.0033) ≈ **KY-2** (-0.0037) < **KO-2** (-0.0048) < **KY-2Na** (-0.0058). It was found that the Φ_Δ values (0.13–0.17) of **KY-1**, **KY-2**, and **KY-1Na** are equivalent to that of **KO-2** (Φ_Δ = 0.17), and surprisingly **KY-2Na**

exhibited the highest $^1\text{O}_2$ generation ability ($\Phi_{\Delta} = 0.32$). Moreover, for the aqueous solutions of **KY-1Na** and **KY-2Na**, the photoabsorption of ABDA at around 400 nm decreased with the increase in the photoirradiation time (Fig. 3c and d), indicating ABDA reacted with $^1\text{O}_2$ generated by the photosensitization of the PSs. The plots of ΔOD at around 400 nm of ABDA versus the photoirradiation time revealed that the calibration curve for **KY-2Na** shows good linearity with an R^2 value of 0.956, but that for **KY-1Na** has a mediocre R^2 value (0.756) which may be due to a small change in the ΔOD (Fig. 3f). In fact, the msam value (-0.00043) for **KY-2Na** is larger than that (-0.00007) for **KY-1Na**. Thus, the Φ_{Δ} values for PSs were determined by the relative method using the slope value ($m_{\text{ref}} = -0.00084$) of the plot for **RB** ($\Phi_{\Delta} = 0.75$ in water)^{9b} as a standard. It is worth noting here that in water the Φ_{Δ} value (0.19) of **KY-2Na** is much higher than that of **KY-1Na** (0.06), indicating that **KY-2Na** bearing two carboxylic acid sodium salts is superior to **KY-1Na** bearing one carboxylic acid sodium salt for $^1\text{O}_2$ generation. Meanwhile, both the Φ_{fl} and Φ_{Δ} values for phenazine-2,3-diol-based photosensitizers are quite low which indicates a large loss of the excited energy. Thus, we performed time-resolved fluorescence spectroscopy to determine the fluorescence lifetime (τ_{fl}), radiative rate constant ($k_{\text{r}} = \Phi_{\text{fl}}/\tau_{\text{fl}}$), and nonradiative rate constant ($k_{\text{nr}} = (1 - \Phi_{\text{fl}})/\tau_{\text{fl}}$) for **KY-2Na** in DMSO. The τ_{fl} , k_{r} , and k_{nr} values for **KY-2Na** are 2.17 ns, $9.20 \times 10^6 \text{ s}^{-1}$, and $4.51 \times 10^8 \text{ s}^{-1}$, respectively. The ratio of the nonradiative constant to radiative constant ($k_{\text{nr}}/k_{\text{r}}$) is estimated to be 49, indicating that the k_{nr} value is significantly larger than the k_{r} value. Thus, this result suggests that for the phenazine-2,3-diol-based photosensitizers, the accelerated nonradiative decay of the excited state may be the main reason for the large loss of the excited energy. Nevertheless, the photodynamic activities of **KY-1Na** and **KY-2Na** for PDT in murine colon carcinoma cells (Colon26)¹⁹ under visible light irradiation ($>510 \text{ nm}$) were investigated. Colon26 cells were incubated with **KY-1Na** or **KY-2Na** for 24 h. The cells were irradiated for 30 min (9 mW), and cell viability was determined after 24 h of incubation using a WST-8 assay. Both under dark and irradiation conditions, unfortunately, the cell viability

changed little despite the increasing concentration of **KY-1Na** and **KY-2Na** (Fig. 4). In order to investigate the degree of cellular uptake of **KY-2Na** in Colon26 cells, we performed confocal laser scanning microscopy (CLSM) for live cell fluorescence imaging. As is expected, the fluorescence image originating from the photosensitizer **KY-2Na** was not observed. These low photodynamic activities indicate that **KY-1Na** and **KY-2Na** with high solubility in water ($\log P_{o/w} = -0.9$) are impermeable to the cell membrane of Colon26.²⁰ Consequently, these results suggested that the 1O_2 generation ability of phenazine-2,3-diol-based PSs is attributed to the facilitated ISC from the singlet to triplet states by the carbonyl groups based on El-Sayed's rule which allows the change in the molecular orbital type such as transitions of $^1(n\pi^*)$ to $^3(\pi\pi^*)$ and $^1(\pi\pi^*)$ to $^3(n\pi^*)$. Moreover, it was found that **KY-2Na** possesses moderate 1O_2 generation ability not only in DMSO but also in water, which is attributed to the efficient ISC characteristics, as discussed later in the next section.

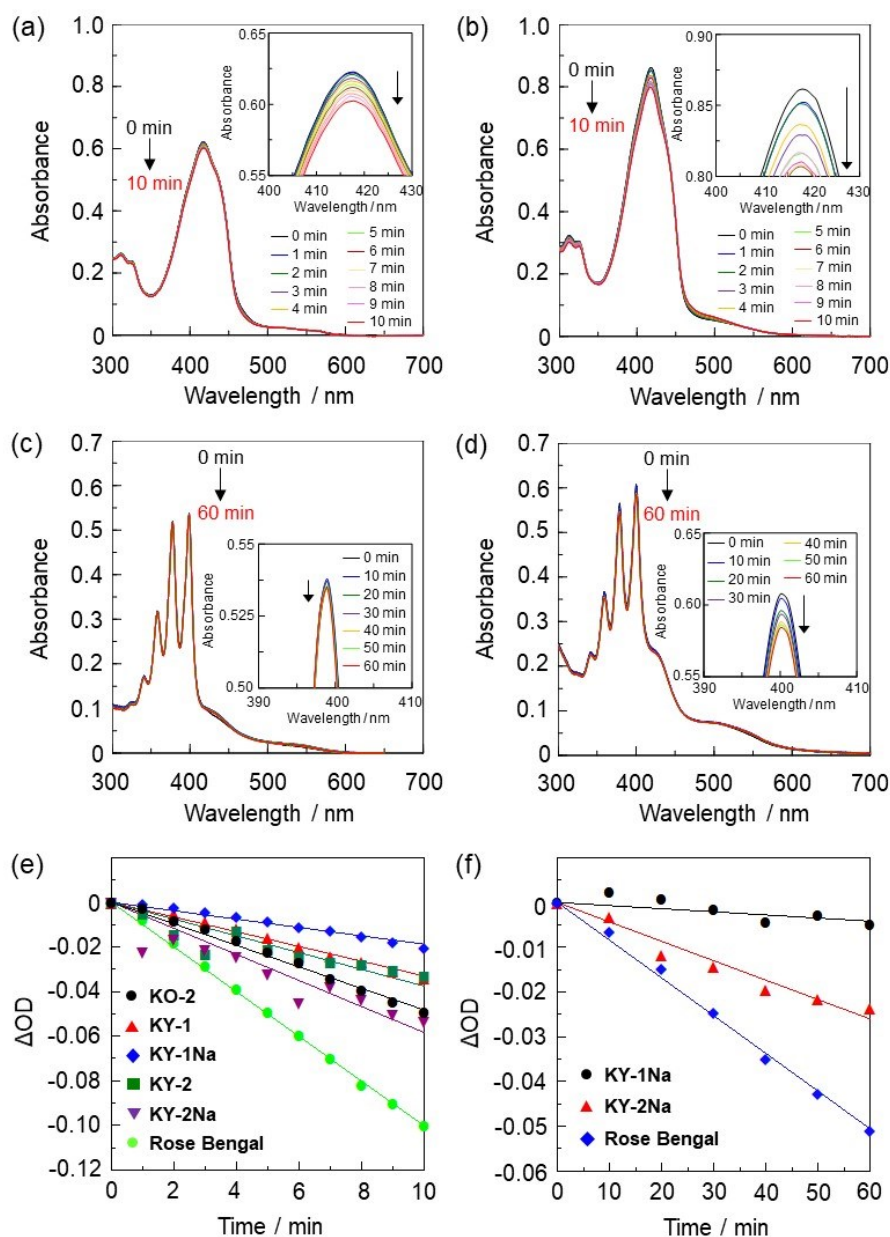


Fig. 3 Photoabsorption spectra for the photooxidation of DPBF (5.0×10^{-5} M) in the presence of (a) **KY-1Na** and (b) **KY-2Na** under photoirradiation with 532 nm ($300 \mu\text{W cm}^{-2}$) in DMSO. Insets are magnifications of maxima in the spectra at around 415 nm. Photoabsorption spectra for the photooxidation of ABDA (5.0×10^{-5} M) in the presence of (c) **KY-1Na** and (d) **KY-2Na** under photoirradiation with 532 nm ($300 \mu\text{W cm}^{-2}$) in D₂O/DMSO (99 : 1, v/v). Insets are magnifications of maxima in the spectra at around 400 nm. (e) Plots of ΔOD at around 415 nm for the photooxidation of DPBF in the presence of **KO-2**, **KY-1**, **KY-2**, **KY-1Na**, **KY-2Na**, and **RB** against the photoirradiation time (532 nm, $300 \mu\text{W cm}^{-2}$) in DMSO. (f) Plots of ΔOD at around 400 nm for the photooxidation of ABDA in the presence of **KY-1Na**, **KY-2Na**, and **RB** against the photoirradiation time (532 nm, $300 \mu\text{W cm}^{-2}$) in D₂O/DMSO (99 : 1, v/v).

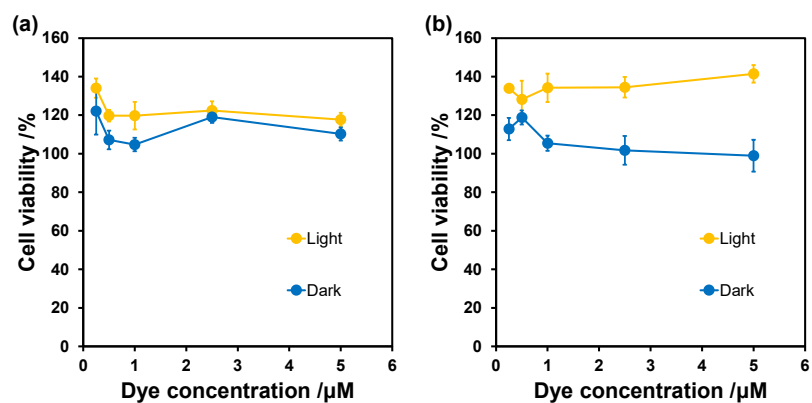


Fig. 4 Photoradiation-induced anticancer effects on Colon26 cells. Colon26 cells were coincubated with (a) **KY-1Na** or (b) **KY-2Na** for 24 h. Subsequently, the cells were photoradiated (> 510 nm, 9 mW/cm^2) for 30 min. After an additional 24 h, the cell viability was measured with the WST-8 assay ($N = 3$). The data were presented as mean \pm SD.

Theoretical calculations

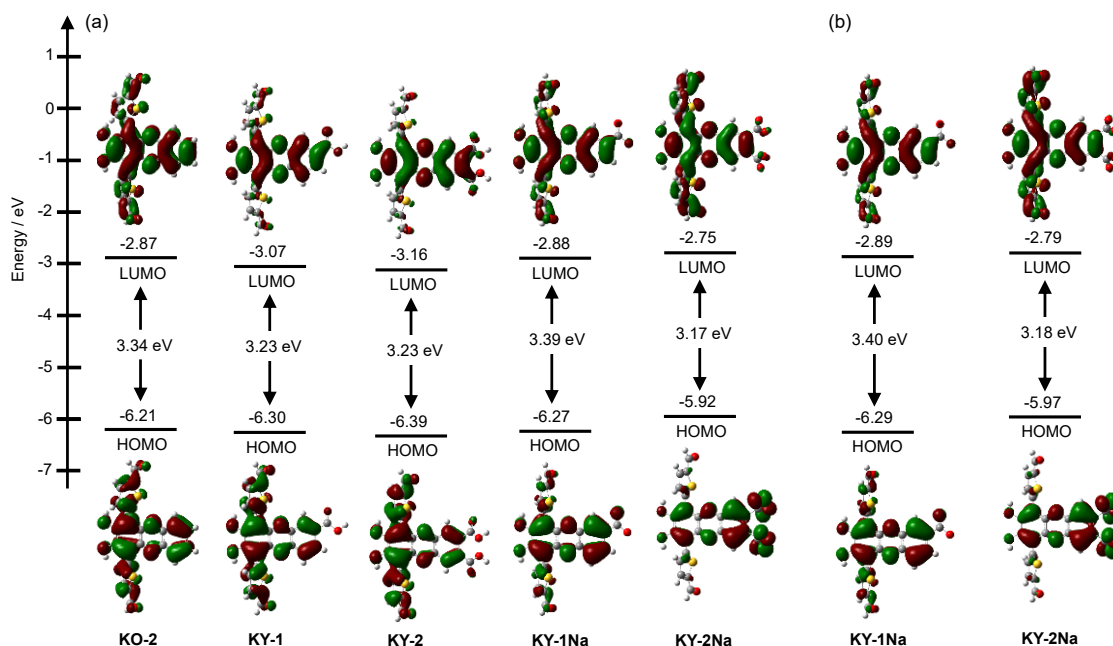


Fig. 5 Energy level diagram, HOMO, and LUMO of (a) **KO-2**, **KY-1**, and **KY-2** at the B3LYP/6-311G(d,p)/DMSO-IEFPCM level, **KY-1Na** and **KY-2Na** as carboxylate anion at the B3LYP/6-311+G(d,p)/DMSO-IEFPCM level, and (b) **KY-1Na** and **KY-2Na** at the B3LYP/6-311+G(d,p)/Water-IEFPCM level by DFT calculations.

Density functional theory (DFT) and time-dependent DFT (TD-DFT) calculations²¹ at the B3LYP/6-311G(d,p)/DMSO-IEFPCM level for **KO-2**, **KY-1**, and **KY-2**, the B3LYP/6-311+G(d,p)/DMSO-IEFPCM level for **KY-1Na** and **KY-2Na** in carboxylate anion forms, and the B3LYP/6-311+G(d,p)/Water-IEFPCM level for **KY-1Na** and **KY-2Na** in carboxylate anion forms were performed to gain insight into the $^1\text{O}_2$ generation properties of these PSs based on the ISC efficiency (Fig. 5). There is little difference in the highest occupied molecular orbital (HOMO) and the lowest unoccupied molecular orbital (LUMO) energy levels among the five PSs. Moreover, the DFT calculations indicate that for **KO-2**, **KY-1**, **KY-2**, and **KY-1Na**, the HOMOs are delocalized over the phenazine-2,3-diol skeleton and formylthiophene units. On the other hand, for **KY-2Na**, the HOMO

is delocalized on the phenazine-2,3-diol skeleton containing the carboxylate anion. Meanwhile, the LUMOs for **KO-2**, **KY-1Na**, and **KY-2Na** are delocalized over the phenazine-2,3-diol skeleton and formylthiophene units, but those for **KY-1** and **KY-2** are delocalized mainly on the phenazine-2,3-diol skeleton and localized partially on formylthiophene units. Thus, DFT calculations suggested that the HOMO and LUMO distributions for the molecular structure of **KY-2Na** are adequately separated, leading to a decrease in the energy gap (ΔE_{ST}) between the S_1 state and the T_1 state that causes efficient ISC,^{22,23} compared to that for the molecular structures of **KO-2**, **KY-1**, **KY-2**, and **KY-1Na**. Indeed, the TD-DFT calculations demonstrated that the ΔE_{ST} (S_1-T_1) values (0.80 eV in DMSO and 0.82 eV in water) of **KY-2Na** are smaller than those (0.96 eV in DMSO and 0.98 eV in water) of **KY-1Na**, that (0.85 eV) of **KY-1** and that of (0.81 eV) of **KY-2** as well as that (0.93 eV) of **KO-2**, resulting in a relatively high Φ_Δ value of **KY-2Na**. Consequently, we demonstrated that phenazine-2,3-diol chromophore-bearing carboxylic acid salts can act as water-soluble halogen-atom-free-heteroanthracene-based PSs for 1O_2 generation.

Conclusions

We have designed and developed phenazine-2,3-diol-based dyes, **KY-1Na** and **KY-2Na** bearing one and two carboxylic acid sodium salts, respectively, as water-soluble halogen-atom-free-heteroanthracene-based photosensitizers (PSs) possessing the ability to generate $^1\text{O}_2$. The logarithms ($\log P_{\text{o/w}}$) of the 1-octanol/water partition coefficient ($P_{\text{o/w}}$) demonstrated that both **KY-1Na** and **KY-2Na** are more hydrophilic than Rose Bengal and have hydrophilicity equivalent to methylene blue. Both the PSs in water show a broad photoabsorption band in the range from 500 to 600 nm. It was found that in water **KY-2Na** exhibits a moderate $^1\text{O}_2$ quantum yield ($\Phi_{\Delta} = 0.19$) value, which is higher than that (0.06) of **KY-1Na**. Density functional theory (DFT) calculations suggested that the HOMO and LUMO distributions for the molecular structure of **KY-2Na** are adequately separated, leading to a decrease in the energy gap (ΔE_{ST}) between the S_1 state and the T_1 state that causes efficient intersystem crossing (ISC), compared to that for the molecular structure of **KY-1Na**. Indeed, time-dependent DFT (TD-DFT) calculations demonstrated that the ΔE_{ST} (S_1-T_1) value (0.82 eV) of **KY-2Na** is smaller than that (0.98 eV) of **KY-1Na**, resulting in a relatively high Φ_{Δ} value of **KY-2Na**. Consequently, we propose that phenazine-2,3-diol chromophore-bearing carboxylic acid salts are one of the promising water-soluble halogen-atom-free-heteroanthracene-based PSs for $^1\text{O}_2$ generation. Further studies on adjustment in the hydrophobicity/hydrophilicity of phenazine-2,3-diol-based PSs suitable for the light-induced cytotoxicity assessment are now in progress to gain insight into the $^1\text{O}_2$ generation under physiological conditions.

Acknowledgements

Chapter 5 is reproduced from “Development of water-soluble phenazine-2,3-diol-based photosensitizers for singlet oxygen generation; K. Yagi, K. Ohira, K. Yamana, K. Imato, R. Kawasaki, A. Ikeda, and Y. Ooyama, *Org. Biomol. Chem.*, **2023**, *21*, 5194–5202.” with permission from The Royal Society of Chemistry.

References

1. I. Pibiri, S. Buscemi, A. P. Piccionello and A. Pace, *ChemPhotoChem*, **2018**, *2*, 535–547.
2. A. A. Ghogare and A. Greer, *Chem. Rev.*, **2016**, *116*, 9994–10034.
3. (a) L.-X. Li, L. Min, T.-B. Yao, S.-X. Ji, C. Qiao, P.-L. Tian, J. Sun and C.-C. Li, *J. Am. Chem. Soc.*, **2022**, *144*, 18823–18828; (b) P. Bayer, J. Schachtner, M. Májek and A. J. von Wangelin, *Org. Chem. Front.*, **2019**, *6*, 2877–2883; (c) M. Prein and W. Adam, *Angew. Chem. Ed. Engl.*, **1996**, *35*, 471–494; (d) W. Adam, S. G. Bosio, N. J. Turro and B. T. Wolff, *J. Org. Chem.*, **2004**, *69*, 1704–1715; (e) A. Greer, *Acc. Chem. Res.*, **2006**, *39*, 797–804; (f) M. N. Alberti, M. Orfanopoulos, *Chem. –Eur. J.*, **2010**, *16*, 9414–9421.
4. (a) L. Burchill and J. H. George, *J. Org. Chem.*, **2020**, *85*, 2260–2265; (b) M. Jaramillo, J. A. Joens and K. E. O’Shea, *Environ. Sci. Technol.*, **2020**, *54*, 6073–6081; (c) W. Adam, S. G. Bosio and N. J. Turro, *J. Am. Chem. Soc.*, **2002**, *124*, 8814–8815; (d) W. Adam, C. R. Saha-Möller and S. B. Schambony, *J. Am. Chem. Soc.*, **1999**, *121*, 1834–1838.
5. (a) M. Gemki, Ö. Taspinar, A. Adler, A. G. Griesbeck, D. Gründemann and H.-G. Schmalz, *Org. Process Res. Dev.*, **2021**, *25*, 2747–2753; (b) M. Klaper and T. Linker, *Chem. –Eur. J.*, **2015**, *21*, 8569–8577; (c) W. Adam and M. Prein, *Acc. Chem. Res.*, **1996**, *29*, 275–283; (d) C. S. Foote, *Acc. Chem. Res.*, **1968**, *1*, 104–110.
6. (a) D. Garcia-Fresnadillo, *ChemPhotoChem*, **2018**, *2*, 512–534; (b) M. L. Marin, L. Santos-Juanes,

- A. Arques, A. M. Amat and M. A. Miranda, *Chem. Rev.*, **2012**, *112*, 1710–1750; (b) E. Díez-Mato, F. C. Cortezón-Tamarit, S. Bogialli, D. García-Fresnadillo and M. D. Marazuela, *Appl. Catal. B*, **2014**, *160–161*, 445–455; (c) H. Kim, W. Kim, Y. Mackeyev, G. S. Lee, H. J. Kim, T. Tachikawa, S. Hong, S. Lee, J. Kim, L. J. Wilson, T. Majima, P. J. Alvarez, W. Choi and J. Lee, *Environ. Sci. Technol.*, **2012**, *46*, 9606–9613.
7. (a) F. Manjón, M. Santana-Magaña, D. García-Fresnadillo and G. Orellana, *Photochem. Photobiol. Sci.*, **2014**, *13*, 397–406; (b) F. Manjón, M. Santana Magaña, D. García-Fresnadillo and G. Orellana, *Photochem. Photobiol. Sci.*, **2010**, *9*, 838–845; (c) F. Manjón, D. García-Fresnadillo and G. Orellana, *Photochem. Photobiol. Sci.*, **2009**, *8*, 926–932; (d) L. Villén, F. Manjón, D. García-Fresnadillo and G. Orellana, *Appl. Catal. B*, **2006**, *69*, 1–9; (e) F. Manjón, L. Villén, D. García-Fresnadillo and G. Orellana, *Environ. Sci. Technol.*, **2008**, *42*, 301–307.
8. (a) L. Benov, *Med. Princ. Pract.*, **2015**, *24*, 14–28; (b) G. Gunaydin, E. M. Gedik and S. Ayan, *Front. Chem.*, **2021**, *9*, 691697; (c) A. Kamkaew, S. H. Lim, H. B. Lee, L. V. Kiew, L. Y. Chung and K. Burgess, *Chem. Soc. Rev.*, **2013**, *42*, 77–88.
9. (a) R. W. Redmond and J. N. Gamlin, *Photochem. Photobiol.*, **1999**, *70*, 391–475; (b) L. V. Lutkus, S. S. Rickenbach and T. M. McCormick, *J. Photochem. Photobiol. A: Chem.*, **2019**, *378*, 131–135; (c) A. Gollmer, A. Felgenträger, W. Bäuml, T. Maisch and A. Späth, *Photochem. Photobiol. Sci.*, **2015**, *14*, 335–351; (d) I. Walker, S. A. Gorman, R. D. Cox, D. I. Vernon, J. Griffiths and S. B. Brown, *Photochem. Photobiol. Sci.*, **2004**, *3*, 653–659; (e) S. A. Gorman, A. L. Bell, J. Griffiths, D. Roberts and S. B. Brown, *Dyes Pigms.*, **2006**, *71*, 153–160; (f) C. Li, Y. Huang, K. Lai, B. A. Rasco and Y. Fan, *Food Control*, **2016**, *65*, 99–105; (g) S. Soltanian, A. Gholamhosseini and M. Banaee, *Aquac. Res.*, **2021**, *52*, 2640–2650.
10. (a) J. Varchola, K. Želonková, D. Chorvat Jr, D. Jancura, P. Miskovsky and G. Bánó, *J. Lumin.*, **2016**, *177*, 17–21; (b) X. T. Zheng, Y. C. Lai and Y. N. Tan, *Nanoscale Adv.*, **2018**, *1*, 2250–2257;

- (c) H.-J. Chen, X.-B. Zhou, A.-L. Wang, B.-Y. Zheng, C.-K. Yeh and J.-D. Huang, *Eur. J. Med. Chem.*, **2018**, *145*, 86–95.
11. (a) R. Bücher, V. V. da Cruz, N. Brover, A. Charisiadis, M. Fondell, R. Haverkamp, M. O. Senge and A. Föhlisch, *Phys. Chem. Chem. Phys.*, **2022**, *24*, 7505–7511; (b) P. G. Mahajan, N. C. Dige, B. D. Vanjare, A. R. Phull, S. J. Kim, S.-K. Hong and K. H. Lee, *J. Fluores.*, **2018**, *28*, 871–882; (c) D. T. Payne, J. Hynek, J. Labuta and J. P. Hill, *Phys. Chem. Chem. Phys.*, **2022**, *24*, 6146–6154; (d) P. M. Antoni, A. Naik, I. Albert, R. Rubbiani, S. Gupta, P. Ruiz-Sanchez, P. Munikorn, J. M. Mateos, V. Luginbuehl, P. Thamyongkit, U. Ziegler, G. Gasser, G. Jeschke and B. Spingler, *Chem. –Eur. J.*, **2015**, *21*, 1179–1183.
12. O. J. Stacey and S. J. A. Pope, *RSC Adv.*, **2013**, *3*, 25550–25564.
13. (a) J. Miao, Y. Huo, G. Yao, Y. Feng, J. Weng, W. Zhao and W. Guo, *Angew. Chem. Int. Ed.*, **2022**, *61*, e202201815; (b) L. A. Ortiz-Rodriguez, S. J. Hoehn, A. Loreda, L. Wang, H. Xiao and C. E. Crespo-Hernández, *J. Am. Chem. Soc.*, **2021**, *143*, 7, 2676–2681.
14. (a) K. Ohira, K. Imato and Y. Ooyama, *Mater. Chem. Front.*, **2021**, *5*, 5298–5304; (b) K. Imato, K. Ohira, M. Yamaguchi, T. Enoki and Y. Ooyama, *Mater. Chem. Front.*, **2020**, *4*, 589–596.
15. S. Tsumura, K. Ohira, K. Hashimoto, K. Imato and Y. Ooyama, *Mater. Chem. Front.*, **2020**, *4*, 2762–2771.
16. M. Li, B. Dyett and X. Zhang, *Anal. Chem.*, **2019**, *91*, 10371–10375.
17. H.-B. Guo, F. He, B. Gu, L. Liang and J. C. Smith, *J. Phys. Chem. A*, **2012**, *116*, 11870–11879.
18. (a) K. Golinick and A. Griesbeck, *Tetrahedron*, **1985**, *41*, 2057–2068; (b) D. Steinebrunner, G. Schnurpfeil, H. H. Doebl, J. A. T. Burgos, D. Wöhrle and A. Wittstock, *Photochem. Photobiol. Sci.*, **2021**, *20*, 547–558; (c) T. Entradas, S. Waldron and M. Volk, *J. Photochem. Photobiol. B: Biol.*, **2020**, *204*, 111787.
19. R. Kawasaki, K. Yamana, R. Shimada, K. Sugikawa and A. Ikeda, *ACS Omega*, **2021**, *6*,

3209–3217.

20. N. J. Yang and M. J. Hinner, *Methods Mol Biol.*, **2015**, 1266, 29–53.
21. M. J. Frisch, G. W. Trucks, H. B. Schlegel, G. E. Scuseria, M. A. Robb, J. R. Cheeseman, G. Scalmani, V. Barone, G. A. Petersson, H. Nakatsuji, X. Li, M. Caricato, A. V. Marenich, J. Bloino, B. G. Janesko, R. Gomperts, B. Mennucci, H. P. Hratchian, J. V. Ortiz, A. F. Izmaylov, J. L. Sonnenberg, D. Williams-Young, F. Ding, F. Lipparini, F. Egidi, J. Goings, B. Peng, A. Petrone, T. Henderson, D. Ranasinghe, V. G. Zakrzewski, J. Gao, N. Rega, G. Zheng, W. Liang, M. Hada, M. Ehara, K. Toyota, R. Fukuda, J. Hasegawa, M. Ishida, T. Nakajima, Y. Honda, O. Kitao, H. Nakai, T. Vreven, K. Throssell, J. A. Montgomery, Jr., J. E. Peralta, F. Ogliaro, M. J. Bearpark, J. J. Heyd, E. N. Brothers, K. N. Kudin, V. N. Staroverov, T. A. Keith, R. Kobayashi, J. Normand, K. Raghavachari, A. P. Rendell, J. C. Burant, S. S. Iyengar, J. Tomasi, M. Cossi, J. M. Millam, M. Klene, C. Adamo, R. Cammi, J. W. Ochterski, R. L. Martin, K. Morokuma, O. Farkas, J. B. Foresman and D. J. Fox, *Gaussian 16, Revision B.01*, Gaussian, Inc., Wallingford CT, 2016.
22. H. Uoyama, K. Goushi, K. Shizu, H. Nomura and C. Adachi, *Nature*, **2012**, 492, 234–238.
23. F. Hu, S. Xu and B. Liu, *Adv. Mater.*, **2018**, 30, 1801350.

Chapter 6

Synthesis and optical properties of phenazinone-based photosensitizers for singlet oxygen generation

Introduction

Photosensitizers (PSs) possessing the singlet oxygen ($^1\text{O}_2$) generation ability have attracted much attention because of their useful applications such as in water purification,¹ antivirals,² and photodynamic therapy (PDT) for cancer treatment.³ These PSs generally produce $^1\text{O}_2$ through the following processes: initially, the photosensitizer (S_0) absorbs light ($h\nu$) to generate the singlet excited state of the photosensitizer (S_n), and then the photoexcited sensitizer (S_n) undergoes intersystem crossing (ISC) to generate the triplet excited state (T_n). After internal conversion (IC) to the lowest excited triplet state (T_1), subsequent energy transfer from the photoexcited PS (T_1) to triplet oxygen ($^3\text{O}_2$) produces $^1\text{O}_2$.⁴ Indeed, phthalocyanine dyes,⁵ phenothiazine dyes,⁶ xanthene dyes,⁷ and boron-dipyrromethene (BODIPY) dyes⁸ are known to show high $^1\text{O}_2$ quantum yield (Φ_Δ) values. For these PSs, halogen atoms such as iodide and bromide atoms are often introduced into the chromophores to promote ISC based on spin-orbit coupling,⁹ but it raises concerns about dark cytotoxicity.¹⁰ To overcome the drawbacks, halogen-atom-free PSs¹¹ such as a family of heteroanthracenes have been extensively studied. Among them, methylene blue (MB) is used as a reference PS for the evaluation of Φ_Δ .¹² Therefore, in order to create a new type of halogen atom-free-heteroanthracene-based PS, we have focused on the phenazine skeleton, because to the best of our knowledge there are few reports on the evaluation of $^1\text{O}_2$ generation ability for phenazine derivatives.¹³ In **Chapter 3**,¹⁴ we have developed phenazine-2,3-diol-based PSs (**KO-0-3**) and demonstrated that the modification of the phenazine-2,3-diol chromophore with formyl groups promotes ISC, leading to efficient $^1\text{O}_2$ generation (Fig. 1a). According to the El-Sayed rule,¹⁵ formyl and carbonyl substituents in a chromophore skeleton allow

ISC by a change in the molecular orbital type, such as $^1(n\pi^*)$ to $^3(\pi\pi^*)$ and $^1(\pi\pi^*)$ to $^3(n\pi^*)$ transitions. Indeed, these PSs exhibited moderate photosensitizing properties for 1O_2 generation ($\Phi_\Delta = 0.41$ for **KO-3**).

Recently, in our continuous work to develop halogen-atom free PSs based on El-Sayed's rule, it was found that 3-hydroxy-10-methylphenazin-2(10*H*)-one (**PZ1**) incorporating a carbonyl group into the chromophore possesses highly efficient photosensitizing capabilities compared to phenazine-2,3-diol-based PSs (Fig. 1b). Indeed, **PZ1** without halogen atoms possesses the superior 1O_2 generation ability to RB ($\Phi_\Delta = 0.68$ in THF) with many halogen atoms as well as MB ($\Phi_\Delta = 0.57$ in dichloromethane)²¹ without halogen atoms. Based on our previous study and El-Sayed's rule, it was assumed that the carbonyl moiety in **PZ1** plays an essential role in the efficient ISC, that is, high Φ_Δ value. In order to confirm the presence of a carbonyl group in **PZ1**, X-ray single crystal structure analyses were required. Therefore, we have designed and synthesized the phenazinone derivative **PZ3** with a 4-chlorobenzoate group. It is well known that the 4-chlorobenzoate group is able to improve crystallizability.¹⁶ Fortunately, we succeeded in performing X-ray single crystal structure analyses for **PZ1** as well as **PZ3**. Furthermore, it was found that the Φ_Δ values are significantly different between **PZ1** and **PZ3**. Therefore, in order to investigate the substituent effects on the optical and 1O_2 generation properties between the phenazinone-based PSs, we prepared **PZ2** with a methoxymethoxy group as a substitute for the hydroxy group. Moreover, the density functional theory (DFT) and time-dependent DFT (TDDFT) calculations were performed to evaluate the ISC efficiency of phenazinone-based PSs. Herein, we report the phenazinone chromophore as a new family of heteroanthracene-based PSs without halogen atoms for efficient 1O_2 generation.

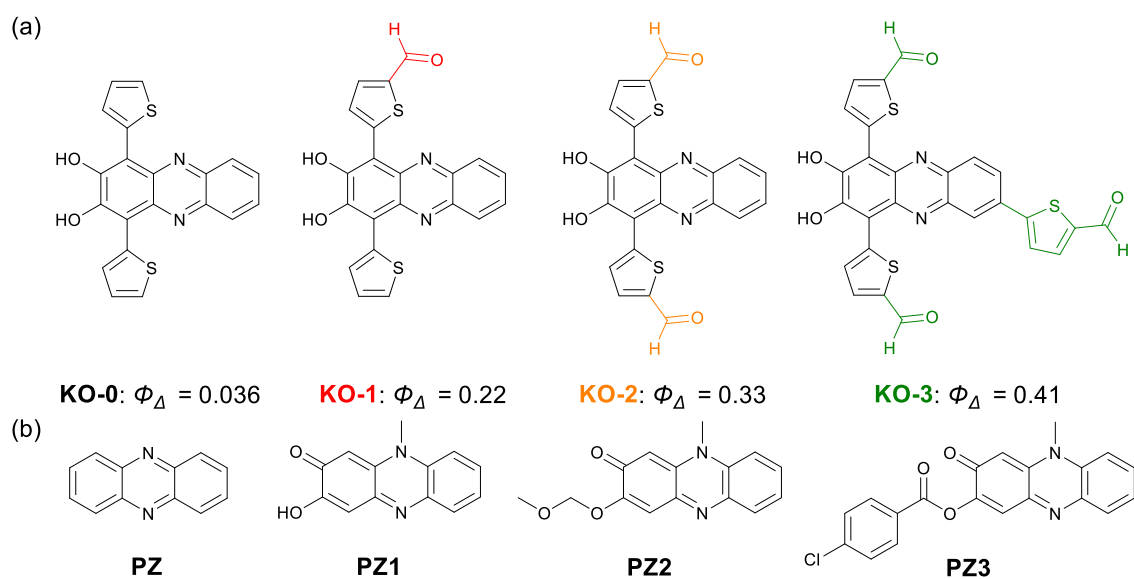


Fig. 1 (a) Chemical structures of phenazine-2,3-diol-based PSs **KO-0–3** and their Φ_{Δ} values employed in **Chapter 3**. (b) Chemical structures of phenazine-2,3-diol (**PZ**) and phenazinone-based PSs **PZ1–3** designed and synthesized in this study.

Experimental

Materials

All solvents and reagents were used as received unless otherwise noted. Rose bengal (RB) was purchased from Sigma Aldrich and recrystallized from methanol twice. 1,3-Diphenylisobenzofuran (DPBF) was purchased from Tokyo Chemical Industry and recrystallized from a mixture of dichloromethane and methanol.

General

^1H NMR and ^{13}C NMR spectra were recorded using Varian-400 (400 MHz) and Varian-500 (500 MHz) FT NMR spectrometers. FT-IR spectra were recorded using a Shimadzu IRTracer-100. High-resolution mass spectral data were acquired using a Thermo Fisher Scientific LTQ Orbitrap XL. Photoabsorption spectra were recorded using Shimadzu UV-3600- plus spectrophotometers. Fluorescence spectra were measured using a Hitachi F-4500 and HORIBA FluoroMax-4 spectrophotometer. The fluorescence quantum yields (Φ_{f}) were determined using a Hamamatsu C9920-01 instrument equipped with CCD by using a calibrated integrating sphere system. Fluorescence decay measurements were performed using a HORIBA DeltaFlex modular fluorescence lifetime system, using a Nano LED pulsed diode excitation source (366 nm and 451 nm). The irradiance of monochromatic light (509 nm) for photosensitizing reactions was adjusted using a Newport 1918-C optical power meter.

X-Ray crystallographic analysis

The reflection data were collected at 100 K on a Bruker AXS SMART APEX II ULTRA diffractometer using monochromated Mo-K α ($\lambda = 0.71073 \text{ \AA}$). The structure was solved by the SHELXT 2014/5 method and refined based on full-matrix least squares on F^2 using SHELXL-2017/1. The non-hydrogen atoms were refined anisotropically. Hydrogen atoms were fixed geometrically and not refined. Crystallographic data have been deposited in the S3 Cambridge Crystallographic Data Centre (CCDC 2194829 for **PZ1**, CCDC 2194831 for **PZ2**, and CCDC 2194832 for **PZ3**).

Crystal of **PZ1**: A suitable crystal of **PZ1** was recrystallized from a mixed solvent of CH₂Cl₂/hexane as a dark red block crystal, air-stable. Crystallographic data: C₁₃H₁₀N₂O₂, $M = 226.23$, monoclinic, $a = 6.7461(17)$, $b = 6.8315(18)$, $c = 21.892(6)$ Å, $\beta = 93.503(3)^\circ$, $V = 1007.0(4)$ Å³, $D_{\text{calcd}} = 1.492$ g cm⁻³, space group P2(1)/n (no.15), $Z = 4$, 4448 reflections measured, 2397 unique ($R_{\text{int}} = 0.0477$), which were used in all calculations. The final $R_1(\text{reflections}) = 0.0434$ (1714) [$I > 2\sigma(I)$], $wR_2(\text{reflections}) = 0.1197$ (2397). GOF = 1.055.

Crystal of **PZ2**: A suitable crystal of **PZ2** was recrystallized from a mixed solvent of CH₂Cl₂/hexane as a dark red block crystal, air-stable. Crystallographic data: C₁₅H₁₄N₂O₃, $M = 270.28$, monoclinic, $a = 10.8605(18)$, $b = 11.1311(18)$, $c = 10.3566(17)$ Å, $\beta = 96.649(2)^\circ$, $V = 1243.6(4)$ Å³, $D_{\text{calcd}} = 1.444$ g cm⁻³, space group P2(1)/c (no.14), $Z = 4$, 6956 reflections measured, 2984 unique ($R_{\text{int}} = 0.0335$), which were used in all calculations. The final $R_1(\text{reflections}) = 0.0389$ (2449) [$I > 2\sigma(I)$], $wR_2(\text{reflections}) = 0.1037$ (2984). GOF = 0.998.

Crystal of **PZ3**: A suitable crystal of **PZ3** was recrystallized from a mixed solvent of CH₂Cl₂/hexane as a red block crystal, air-stable. Crystallographic data: C₂₀H₁₃ClN₂O₃, $M = 364.77$, monoclinic, $a = 12.9125(8)$, $b = 17.0395(10)$, $c = 7.2712(4)$ Å, $\beta = 93.9830(10)^\circ$, $V = 1595.96(16)$ Å³, $D_{\text{calcd}} = 1.518$ g cm⁻³, space group P2(1)/c (no.14), $Z = 4$, 12633 reflections measured, 3827 unique ($R_{\text{int}} = 0.0202$), which were used in all calculations. The final $R_1(\text{reflections}) = 0.0340$ (3316) [$I > 2\sigma(I)$], $wR_2(\text{reflections}) = 0.0818$ (3827). GOF = 0.921.

Evaluation of ¹O₂ quantum yield

Quantum yields (Φ_Δ) for singlet oxygen (¹O₂) generation by **PZ1**, **PZ2**, and **PZ3** were evaluated by monitoring the changes in the photoabsorption spectra of 1,3-diphenylisobenzofuran (DPBF), a ¹O₂ scavenger, in tetrahydrofuran (THF) upon photoirradiation. DPBF traps the generated ¹O₂ to be oxidized. THF was bubbled with air for 10 min, prior to the preparation of the solutions. The concentration of DPBF was 5×10^{-5} M in the air-saturated THF solutions. The concentration of the

photosensitizers (PSs) and rose bengal (**RB**) was adjusted so that the absorbance was ca. 0.03 at the irradiation wavelength (509 nm). The THF solutions containing DPBF and **PZ1**, **PZ2**, or **PZ3** were irradiated with monochromatic light (509 nm, 300 $\mu\text{W cm}^{-2}$) that was obtained by passage of a xenon light source (HAL-320, Asahi Spectra) through a monochromator (CMS-100, Asahi Spectra). Except for the nonirradiated solutions, each spectrum was measured immediately after photoirradiation for 1 min. The procedure was promptly repeated until the total photoirradiation time reached 10 min. The changes in optical density (ΔOD) of DPBF were plotted against photoirradiation time to obtain the slopes (m) and estimate Φ_{Δ} values. W. Wu et. al. reported that **RB** shows a high $^1\text{O}_2$ generation with the $\Phi_{\Delta} = 0.80$ in MeOH.²⁰ To correct the difference of Φ_{Δ} values between MeOH and THF, the Φ_{Δ} values in THF were estimated from the following equation.

$$\Phi_{\Delta\text{RB, THF}} = \Phi_{\Delta\text{RB, MeOH}} \times [(m_{\text{RB, THF}}/m_{\text{RB, MeOH}}) \times (L_{\text{RB, MeOH}}/L_{\text{RB, THF}})]$$

where $m_{\text{RB, MeOH}}$ and $m_{\text{RB, THF}}$ are slopes in the plots of ΔOD at the photoabsorption maximum wavelength of DPBF (413 nm) against photoirradiation time, and $L_{\text{RB, THF}}$ and $L_{\text{RB, MeOH}}$ are light harvesting efficiencies, which are given by $L = 1 - 10^{-A}$ (“ A ” is the absorbance at the photoirradiation wavelength). The $\Phi_{\Delta\text{RB, THF}}$ value was estimated to be 0.68 (Fig. S10). The Φ_{Δ} values of **PZ1**, **PZ2**, and **PZ3** were determined by the relative method using **RB** ($\Phi_{\Delta} = 0.68$ in THF) as a standard according to the following equation:

$$\Phi_{\Delta\text{sam}} = \Phi_{\Delta\text{ref}} \times [(m_{\text{sam}}/m_{\text{ref}}) \times (L_{\text{ref}}/L_{\text{sam}})]$$

where $\Phi_{\Delta\text{sam}}$ and $\Phi_{\Delta\text{ref}}$ are $^1\text{O}_2$ quantum yields of phenazinone-based PSs and **RB**, respectively, m_{sam} and m_{ref} are slopes in the plots of ΔOD at the photoabsorption maximum wavelength of DPBF (413 nm) against photoirradiation time, and L_{sam} and L_{ref} are light harvesting efficiencies, which are given by $L = 1 - 10^{-A}$ (“ A ” is the absorbance at the photoirradiation wavelength).

Theoretical calculations

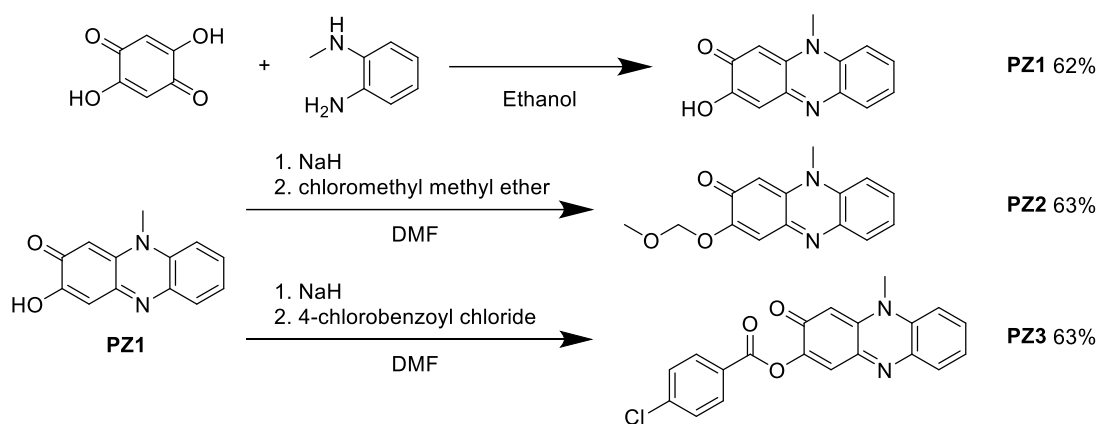
The gaussian 16 program²⁵ was used for density functional theory (DFT) calculations, time-dependent

DFT (TD-DFT) calculations, and natural transitional orbital (NTO) analysis. The S_0 geometries of **PZ** and **PZ1–3** were optimized with frequency calculations at the B3LYP/6-311G(d,p) level. There are no imaginary frequencies for all optimized structures. The TD-DFT calculations of both excited singlet and triplet states were performed using the optimized S_0 geometry at the B3LYP/6-311G(d,p) level. The methoxymethyl group of **PZ2** was replaced with the methyl group for convenience of calculation.

Photodynamic activity experiments

HeLa cells were seeded on 48-well plates (Thermo Fischer Science) and incubated overnight (approximately 18 h). The cells were exposed to **PZ1**, **PZ2**, or **PZ3** at varying concentrations. After 24 h of incubation, the cells were washed with PBS thrice, and photoirradiation (>510 nm) was carried out for 30 min. Afterward, the cells were incubated for 24 h, and the Cell Counting Kit-8 solution was added to the cells. After 30 min of incubation, the absorbance at 450 nm was measured using a microplate reader. The cell viability was measured as the ratio (%) of the number of viable cells in the treated and untreated groups.

Synthesis



Scheme 1 Synthetic routes of **PZ1–3**.

3-Hydroxy-10-methylphenazin-2(10H)-one (PZ1). A solution of 2,5-dihydroxy-1,4-benzoquinone (0.145 g, 1.04 mmol) and *N*-methyl-*o*-phenylenediamine (0.127 g, 1.04 mmol) in ethanol (40 mL) was stirred at 80 °C. After the disappearance of the reactants, the reaction mixture was cooled to room temperature, and the precipitate was filtered and washed with a small amount of ethanol to give **PZ1** as a black solid (0.146 g, 62% yield); m.p. over 300 °C; IR (ATR): $\tilde{\nu}$ = 3179, 1587, 1572, 1545, 1501, 1468 cm^{-1} ; ^1H NMR (400 MHz, $\text{DMSO}-d_6$, ppm): δ = 7.86–8.07 (m, 2H, aromatic), 7.72 (dd, J = 6.7 Hz, 1.5 Hz, 1H, aromatic), 7.51 (dd, J = 7.5 Hz, 0.5 Hz, 1H, aromatic), 6.86 (s, 1H, aromatic), 6.37 (s, 1H, aromatic), 3.94 (s, 3H, CH_3); ^{13}C NMR (125 MHz, $\text{DMSO}-d_6$, ppm): δ = 176.28, 156.64, 147.93, 136.55, 135.53, 130.60, 130.13, 129.45, 124.25, 115.21, 105.89, 97.04, 34.40; HRMS (APCI): m/z found 227.08127 $[\text{M}+\text{H}]^+$, calculated for $\text{C}_{13}\text{H}_{11}\text{N}_2\text{O}_2$ $[\text{M}+\text{H}]^+$: 227.08150.

3-Methoxymethoxy-10-methylphenazin-2(10H)-one (PZ2). A solution of sodium hydride abt. 60 % oil suspension (80.6 mg) and **PZ1** (45.9 mg, 0.203 mmol) in DMF (30 mL) was stirred at 0 °C for 30 min. Then, chloromethyl methyl ether (150 μL , 1.98 mmol) was added to the solution, and the mixture was stirred at 0 °C overnight. The reaction was quenched with water, and then the solution was extracted with CH_2Cl_2 . The organic layer was dried over anhydrous MgSO_4 , filtered, and concentrated. The resulting residue was dissolved in CH_2Cl_2 and subjected to reprecipitation by hexane to afford

PZ2 as a reddish brown solid (35.5 mg, 63.4% yield); m.p. 195–198 °C; IR (ATR): $\tilde{\nu}$ = 2967, 2918, 2828, 1630, 1591, 1572, 1545, 1508 cm^{-1} ; ^1H NMR (500 MHz, acetone- d_6 , ppm): δ = 7.92 (dd, J = 8.1 Hz, 1.5 Hz, 1H, aromatic), 7.86 (d, J = 8.7 Hz, 1H, aromatic), 7.70 (dd, J = 7.0 Hz, 1.5 Hz, 1H, aromatic), 7.46 (dd, J = 7.0 Hz, 1.2 Hz, 1H, aromatic), 7.03 (s, 1H, aromatic), 6.17 (s, 1H, aromatic), 5.39 (s, 2H, CH_2), 3.91 (s, 3H, CH_3), 3.50 (s, 3H, CH_3); ^{13}C NMR (125 MHz, acetone- d_6 , ppm): δ = 177.56, 156.98, 149.54, 136.77, 131.91, 131.14, 124.61, 115.36, 110.68, 99.93, 95.55, 56.90, 34.35; HRMS (APCI): m/z found 271.10785 $[\text{M}+\text{H}]^+$, calculated for $\text{C}_{15}\text{H}_{15}\text{N}_2\text{O}_3$ $[\text{M}+\text{H}]^+$: 271.10772.

3-(*p*-Chlorobenzoyl)-10-methylphenazin-2(10*H*)-one (PZ3). A solution of sodium hydride abt. 60 % oil suspension (39.5 mg) and PZ1 (46.0 mg, 0.203 mmol) in DMF (30 mL) was stirred at 0 °C for 20 min. Then, 4-chlorobenzoyl chloride (128 μL , 1.00 mmol) was added to the solution, and the mixture was stirred at 0 °C overnight. The reaction was quenched with water, and then the solution was extracted with CH_2Cl_2 . The organic layer was dried over anhydrous MgSO_4 , filtered, and concentrated. The crude was dissolved in Toluene, and GPC was performed to give PZ3 as a red solid (47 mg, 63% yield); m.p. 233–236 °C; IR (ATR): $\tilde{\nu}$ = 3067, 3044, 2924, 2853, 1923 cm^{-1} ; ^1H NMR (400 MHz, DMSO- d_6 , ppm): δ = 8.08–8.17 (m, 2H, aromatic), 7.99–8.08 (m, 2H, aromatic), 7.84 (t, J = 7.8 Hz, 8.0 Hz, 1H, aromatic), 7.67–7.77 (m, 3H, aromatic), 7.56 (t, J = 7.8 Hz, 7.6 Hz, 1H, aromatic), 6.40 (s, 1H, aromatic), 3.93 (s, 3H, CH_3); ^{13}C NMR (100 MHz, Acetone- d_6 , ppm): δ = 174.04, 162.62, 151.75, 146.16, 139.08, 137.52, 135.29, 132.85, 131.70, 131.43, 130.39, 129.13, 127.28, 124.38, 121.82, 115.27, 98.81, 34.43; HRMS (ESI): m/z found 365.06900 $[\text{M}+\text{H}]^+$, calculated for $\text{C}_{20}\text{H}_{14}\text{N}_2\text{O}_3\text{Cl}$ $[\text{M}+\text{H}]^+$: 365.06875.

Results and discussion

Synthesis

PZ1 was prepared in one step by the cyclodehydration of *N*-methyl-*o*-phenylenediamine and 2,5-dihydroxy-1,4-benzoquinone (Scheme. 1). In order to perform X-ray single crystal structure analyses, we designed phenazinone derivative **PZ3** with a 4-chlorobenzoate group which is able to improve crystallizability.¹⁶ In addition, in order to investigate the substituent effects on the optical and ¹O₂ generation properties, we devised **PZ2** with a methoxymethoxy group as a substitute for the hydroxy group. The reactions of **PZ1** with chloromethyl methyl ether or 4-chlorobenzoyl chloride gave **PZ2** and **PZ3**, respectively. These PSs were obtained in moderate yields (62–63%) and successfully characterized by ¹H NMR, ¹³C NMR, FTIR, and high-resolution mass spectrometric analysis. Furthermore, X-ray single crystal analysis was performed on the PSs.

X-Ray crystal structures

As shown in Fig. 2, for all the three PSs, the bond lengths of C2–O1 and C3–O2 are *ca.* 1.25 Å and *ca.* 1.36 Å, respectively. Therefore, C2–O1 and C3–O2 have typical C=O double bond and C–O single bond lengths, respectively, indicating undoubtedly that the three PSs have a phenazinone skeleton. Interestingly, **PZ1**, **PZ2**, and **PZ3** have high planarity with small root-mean-square deviations of 0.0487, 0.0717, and 0.1033 Å, respectively, despite the presence of an sp³ nitrogen atom.

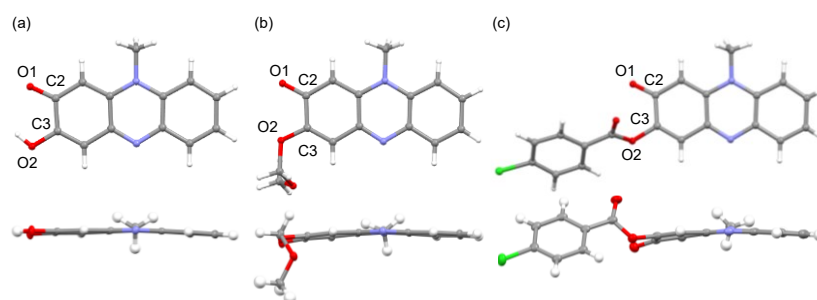


Fig. 2 X-ray crystal structures of (a) **PZ1**, (b) **PZ2**, and (c) **PZ3**. Selected bond lengths (Å): C2–O1 1.2566(18), 1.2418(16), and 1.2422(15), C3–O2 1.3436(18), 1.3582(15), and 1.3906(15) for **PZ1**, **PZ2**, and **PZ3**, respectively.

Optical properties

The photoabsorption and fluorescence spectra of **PZ1–3** in THF are shown in Fig. 3 with comparison to those of phenazine-2,3-diol (**PZ**), and their optical data are summarized in Table 1. **PZ** showed two photoabsorption maximums ($\lambda_{\text{max}}^{\text{abs}}$): a narrow band at around 390 nm is attributed to the $\pi \rightarrow \pi^*$ transition of the phenazine skeleton which is supported by DFT calculation, and the other weak band at around 480 nm (molar extinction coefficient (ε) = 1700 M⁻¹ cm⁻¹) is ascribable to the formation of phenoxide ions by the partial deprotonation of the hydroxyl groups.¹³ On the other hand, **PZ1** exhibited an intense photoabsorption band with a $\lambda_{\text{max}}^{\text{abs}}$ (ε = 10900 M⁻¹ cm⁻¹) at 478 nm¹⁷ compared to **PZ**. It was found that the introduction of the methoxymethoxy group or 4-chlorobenzoate group into the phenazinone chromophore leads to a further bathochromic shift of the photoabsorption band ($\lambda_{\text{max}}^{\text{abs}}$ = 487 nm for **PZ2** and 510 nm for **PZ3**). TDDFT calculations demonstrated that the values of excitation energy from the S₀ state to the S₁ state are 2.86 eV for **PZ1**, 2.87 eV for **PZ2**, and 2.73 eV for **PZ3** (Fig. 5 and Table S6). Moreover, the DFT calculations revealed that the highest occupied molecular orbital (HOMO) and the lowest unoccupied molecular orbital (LUMO) energy levels of **PZ3** are lower than those of **PZ1**, but the lowering in the LUMO energy level is larger than that in the HOMO energy level (Fig. S15, HOMO = -5.78 eV, LUMO = -2.64 eV for **PZ1** and HOMO = -6.00 eV, LUMO = -2.94 eV for **PZ3**). Thus, the bathochromic shift of the photoabsorption bands from **PZ1** to **PZ3** is mainly attributed to the stabilization of the LUMO energy level through the introduction of the electron-withdrawing 4-chlorobenzoyl group into the phenazinone skeleton, resulting in a decrease in the HOMO–LUMO band gap ($\Delta E_{\text{H-L}}$ = 3.14 eV and 3.06 eV for **PZ1** and **PZ3**, respectively). Consequently, the bathochromic shift of the calculated photoabsorption bands from **PZ1** to **PZ3** was in good agreement with the experimental results (Fig. 3a and Table 1). In addition, **PZ2** with a methoxymethoxy group also exhibited a photoabsorption band in a longer wavelength region by 9 nm, compared to **PZ1**. However, the DFT and TDDFT calculations showed almost the same values of

ΔE_{H-L} (3.14 eV for **PZ1** and 3.16 eV for **PZ2**) and excitation energy (2.86 eV for **PZ1** and 2.87 eV for **PZ2**) between **PZ1** and **PZ2**, in which the HOMO and the LUMO energy levels of **PZ2** (HOMO = -5.72 eV and LUMO = -2.56 eV) are slightly higher than those of **PZ1** (HOMO = -5.78 eV and LUMO = -2.64 eV). Meanwhile, the bathochromic shift of the photoabsorption bands from **PZ1** to **PZ2** would be explained based on the extended Hammett equation.¹⁸ Thus, it is suggested that the substitution of a methoxymethoxy group for a hydroxy group reduces the electron-donating effect on the phenazinone chromophore because the substituent constants of hydroxy and methoxy groups are -0.37 and -0.268, respectively, leading to the bathochromic shift of the photoabsorption bands from **PZ1** to **PZ2**. In the corresponding fluorescence spectra, **PZ** showed two fluorescence bands with a fluorescence maximum wavelength ($\lambda_{\max}^{\text{fl}}$) at 440 nm and 555 nm, which would originate from the phenazine skeleton and its phenoxide ion, respectively. On the other hand, **PZ1**, **PZ2**, and **PZ3** showed a fluorescence band with a $\lambda_{\max}^{\text{fl}}$ of 554 nm, 579 nm, and 597 nm, respectively, originating from phenazinone skeleton. The fluorescence quantum yields (Φ_{f}) of **PZ1**, **PZ2**, and **PZ3** were significantly low (0.03 for **PZ1**, 0.04 for **PZ2**, and 0.05 for **PZ3**), which is attributed to ISC and IC as discussed later.

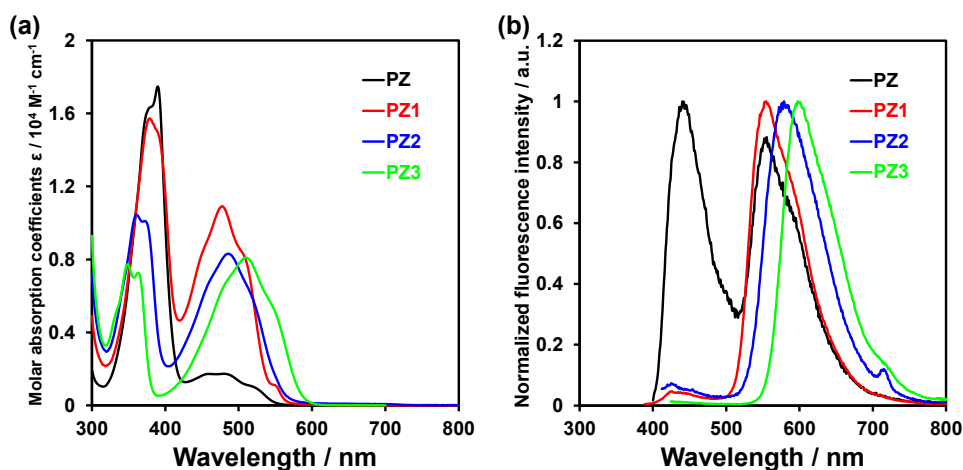


Fig. 3 (a) Photoabsorption and (b) fluorescence ($\lambda_{\text{ex}} = 361\text{--}390$ nm) spectra of **PZ** and **PZ1–3** (1.0×10^{-4} M) in THF.

Table 1. Optical data and $^1\text{O}_2$ quantum yields (Φ_{Δ}) of **PZ** and **PZ1–3** in THF

Dye	$\lambda_{\text{max}}^{\text{abs}} / \text{nm}$ ($\epsilon / \text{M}^{-1}\text{cm}^{-1}$)	$\lambda_{\text{max}}^{\text{fl}} / \text{nm}$ (Φ_{fl}^a)	$\tau_{\text{fl}} / \text{ns}^b$	Φ_{Δ}^c
PZ	390 (17500)	440, 555 (< 0.02)	2.13, 3.54 ^d	0.28
	480 (1700)	558 (0.09)	2.89 ^e	
PZ1	378 (15700)	554 (0.03)	3.40 ^e	0.86
	478 (10900)			
PZ2	361 (10500)	579 (0.04)	3.26 ^e	0.54
	487 (8300)			
PZ3	349 (7700)	597 (0.05)	1.14 ^e	0.069
	510 (8100)			

^a Fluorescence quantum yields ($\lambda_{\text{ex}} = \lambda_{\text{max}}^{\text{abs}}$) were determined by using a calibrated integrating sphere system. ^b Fluorescence lifetimes. ^c $^1\text{O}_2$ quantum yields (relative decomposition rate of DPBF (1,3-diphenylisobenzofuran)) using RB as a standard ($\Phi_{\Delta} = 0.68$ in THF) and DPBF as a $^1\text{O}_2$ scavenger. The Φ_{Δ} values were estimated under assumption that the reactivity of $^1\text{O}_2$ was independent of the kind of solvents. ^d Photoexcited at 366 nm. ^e Photoexcited at 451 nm.

¹O₂ generation

Thus, we evaluated the ¹O₂ generation ability of the phenazinone PSs **PZ1–3**. It is well-known that 1,3-diphenylisobenzofuran (DPBF) acts as an efficient ¹O₂ scavenger to produce its oxidized product, *o*-dibenzoylbenzene.¹⁹ Thus, ¹O₂ generation by **PZ1–3** in THF was investigated by monitoring the photoabsorption spectral changes of DPBF accompanied by the reaction of DPBF with the generated ¹O₂ (Fig. 4a–c). THF was bubbled with air for 10 min prior to preparing solutions. Air-saturated THF solutions containing DPBF and each PS were irradiated with monochromatic light at 509 nm (300 μW cm⁻²) that was obtained by passage of a xenon light source through a monochromator. In all the solutions, the photoabsorption of DPBF at around 413 nm decreased with photoirradiation time, which indicates that DPBF reacted with ¹O₂ generated by the photoexcitation of the PSs. However, the decrements in absorbance at 413 nm were significantly different between the PSs. Thus, the changes in optical density (ΔOD) of DPBF at 413 nm were plotted against photoirradiation time to estimate Φ_Δ values of these PSs (Fig. 4d): the Φ_Δ values were estimated from the slopes (*m*_{sam}) of the plots using rose bengal (**RB**, Φ_Δ = 0.68 in THF) as a standard sample (Table 1). The correlation coefficient (*R*²) values for the calibration curves of **PZ1–3** and **RB** were 0.992–0.999, which indicates good linearity, and the *m*_{sam} values increased in the order of **PZ3** (0.0010) < **PZ2** (0.0070) < **RB** (0.0083) < **PZ1** (0.010). As the result, the Φ_Δ values were estimated to be 0.54, and 0.069 for **PZ2** and **PZ3**, respectively. It is worth noting here that **PZ1** exhibited the highest ¹O₂ generation ability (Φ_Δ = 0.86). Indeed, the Φ_Δ values of **PZ1** and **PZ2** are higher than those of **KO-0–3** as well as **PZ** (Φ_Δ = 0.036–0.41 for **KO-0–3** and 0.33 for **PZ**). Thus, it was found that the phenazinone-based PS **PZ1** without halogen atoms possesses the superior ¹O₂ generation ability to **RB** (Φ_Δ = 0.68 in THF) with many halogen atoms as well as **MB** (Φ_Δ = 0.57 in dichloromethane)²¹ without halogen atoms.

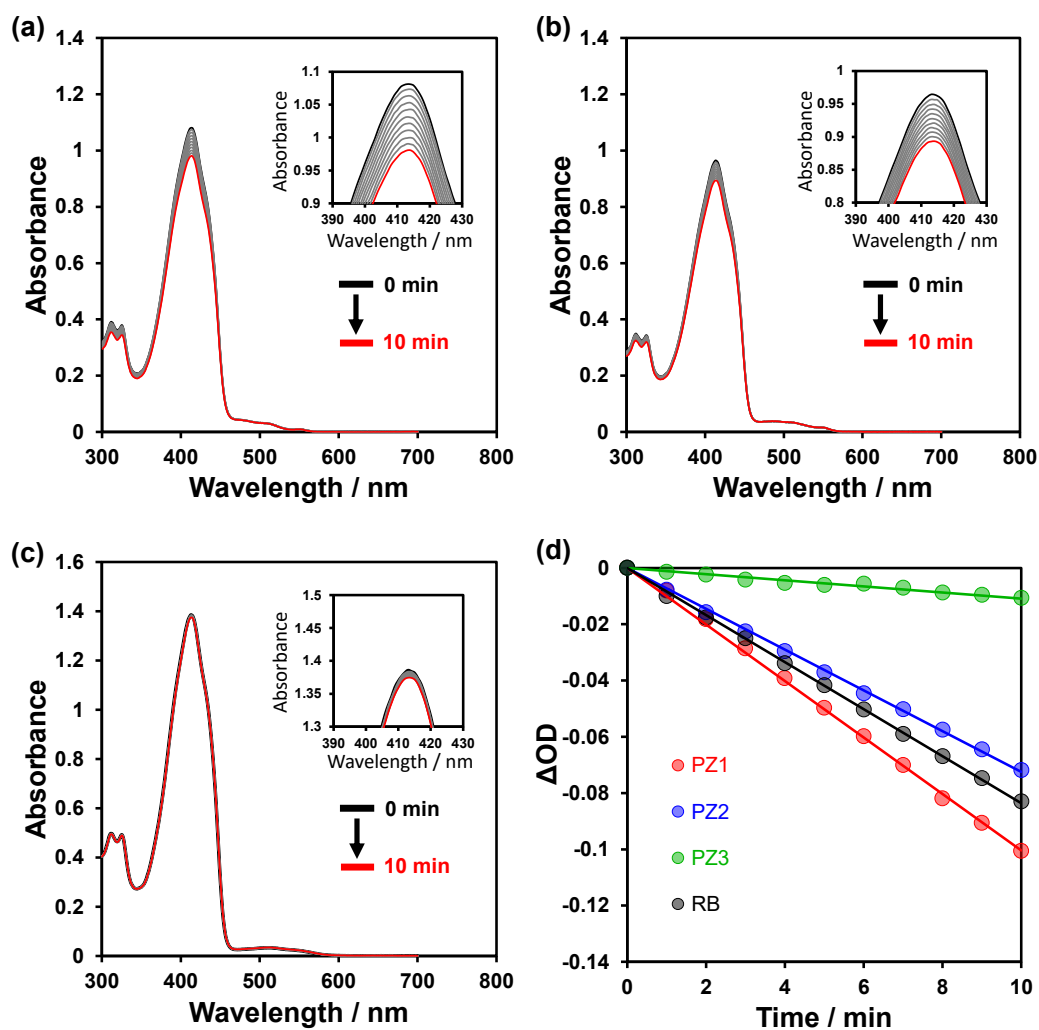


Fig. 4 Photoabsorption spectra of DPBF (5×10^{-5} M) in the presence of (a) **PZ1**, (b) **PZ2**, and (c) **PZ3** (abs. @509 nm = ca. 0.03) upon irradiation with monochromatic light (509 nm, $300 \mu W cm^{-2}$) in THF. Insets are magnifications of peak tops in the spectra around 410 nm. (d) Plots of ΔOD of DPBF at 413 nm against photoirradiation time (509 nm, $300 \mu W cm^{-2}$) in the presence of **PZ1**, **PZ2**, **PZ3**, and **RB**.

Photophysical processes

Table 2. Rate constants in photophysical processes for **PZ1–3**

Dye	$k_r / 10^7 \text{s}^{-1}$	$k_{nr} / 10^7 \text{s}^{-1}$	$k_{ISC} / 10^7 \text{s}^{-1}$	$k_{IC} / 10^7 \text{s}^{-1}$
PZ1	1.3	28.1	25.4	2.8
PZ2	0.86	29.8	16.7	13.1
PZ3	2.5	85.3	6.1	79.2

In order to clarify the optical factors affecting the Φ_Δ values, we investigated the photophysical processes of the phenazine-based PSs **PZ1–3** for $^1\text{O}_2$ generation. In this context, the radiative (k_r) and nonradiative (k_{nr}) decay rate constants were evaluated from the Φ_{fl} and fluorescence lifetime (τ_{fl}) values (Table 1) according to equation (1) and (2):²²

$$k_r = \Phi_{fl} / \tau_{fl} \quad (1)$$

$$k_{nr} = (1 - \Phi_{fl}) / \tau_{fl} \quad (2)$$

In addition, the ISC (k_{ISC}) and IC (k_{IC}) rate constants were also evaluated according to equation (3) and (4):

$$k_{ISC} = \Phi_T / \tau_{fl} \quad (3)$$

$$k_{nr} = k_{IC} + k_{ISC} \quad (4)$$

where the triplet generation quantum yield (Φ_T) was approximated by Φ_Δ .²³ Table 2 summarizes the values of k_r , k_{nr} , k_{ISC} , and k_{IC} for **PZ1–3**. The k_r values of all these PSs were low ($0.86\text{--}2.5 \times 10^7 \text{s}^{-1}$) due to the low Φ_{fl} values (≤ 0.05). **PZ3** showed a significantly low k_{ISC} value relative to the k_{nr} value, resulting in a high k_{IC}/k_{nr} value ($= 0.93$). This high k_{IC}/k_{nr} value is ascribable to the vibrational relaxation to the lowest excited state caused by a flexible 4-chlorobenzoate group. On the other hand, **PZ1** without a flexible substituent showed a significantly low k_{IC}/k_{nr} value ($= 0.10$), and thus the k_{ISC} value accounts for much of the k_{nr} value. **PZ2** showed a relatively small k_{IC}/k_{nr} value ($= 0.44$) due to the methoxymethoxy group with moderate flexibility, resulting in the moderate k_{ISC} .²⁴ Consequently,

these evaluations suggested that Φ_{Δ} values of **PZ1–3** depend on k_{ISC} , and thus **PZ1** with high k_{ISC} shows a high Φ_{Δ} value.

Theoretical calculations

To further understand the photophysical processes, spin-orbit coupling (SOC) matrix elements were analyzed for **PZ** and **PZ1–3** using TDDFT calculation at B3LYP/6-31G(d,p)/THF-CPCM level,²⁵ in which the methoxymethyl group of **PZ2** was replaced with the methyl group for convenience of calculation. The SOC constants and the vertical excitation energies from the S_0 state to the S_n and T_n states for these PSs were calculated using their S_0 state geometries (Fig. 5 and Table 3). The optimized structures of **PZ1–3** showed high planarity despite the presence of an sp^3 nitrogen atom and are in good agreement with those obtained from the X-ray single crystal analysis. The oscillator strengths (f) for the S_0 to the S_1 state of **PZ1–3** were higher than that of **PZ** (0.035 for **PZ**, 0.204 for **PZ1**, 0.220 for **PZ2**, and 0.258 for **PZ3**), indicating that the phenazinone PSs show the stronger photoabsorption as observed in the photoabsorption spectra (Fig. 3a). As shown in Fig. 5, the HOMO–2 of **PZ** and **PZ1–3** are the frontier n-orbitals that consist of the lone pair electrons on the nitrogen atoms for **PZ** and on the carbonyl oxygen atom for **PZ1–3**, and it was found that the HOMO–2→LUMO transitions significantly contribute to their T_3 states (92–96 %). In addition, the S_1 states of these PSs are $^1(\pi\pi^*)$. Therefore, it was revealed that these PSs have ISC pathways ($S_1 (\pi, \pi^*) \rightarrow T_3 (n, \pi^*)$) which meet the El-Sayed rule.¹⁵ Indeed, in these major ISC pathways, these PSs exhibited relatively large SOC matrix elements (8.82 cm^{-1} for **PZ**, 17.45 cm^{-1} for **PZ1**, 17.58 cm^{-1} for **PZ2**, and 18.15 cm^{-1} for **PZ3**). Except for **PZ3**, the result that the SOC matrix elements of **PZ1–3** were larger than that of **PZ** was, consistent with the differences in their 1O_2 generation abilities ($\Phi_{\Delta} = 0.28$ for **PZ**, 0.86 for **PZ1**, 0.54 for **PZ2**, and 0.069 for **PZ3**). Thus, these calculations demonstrated that the n orbitals on the carbonyl oxygen in the **PZ1–3** play an essential role in 1O_2 generation. Moreover, the S_1 – T_3 energy gaps (ΔE_{ST}) of

PZ1–3 (0.03–0.10 eV) were smaller than that of **PZ** (0.30 eV), which are thermodynamically beneficial for efficient ISC. Consequently, this work revealed that the phenazinone chromophores possess thermodynamically feasible ISC characteristics from S_1 to T_3 state ($\Delta E_{ST} = 0.03\text{--}0.10$ eV) based on the El-Sayed rule, and thus the Φ_{Δ} values of **PZ1–3** are dominated by the k_{ISC} , which is decreased by the flexible substituent.

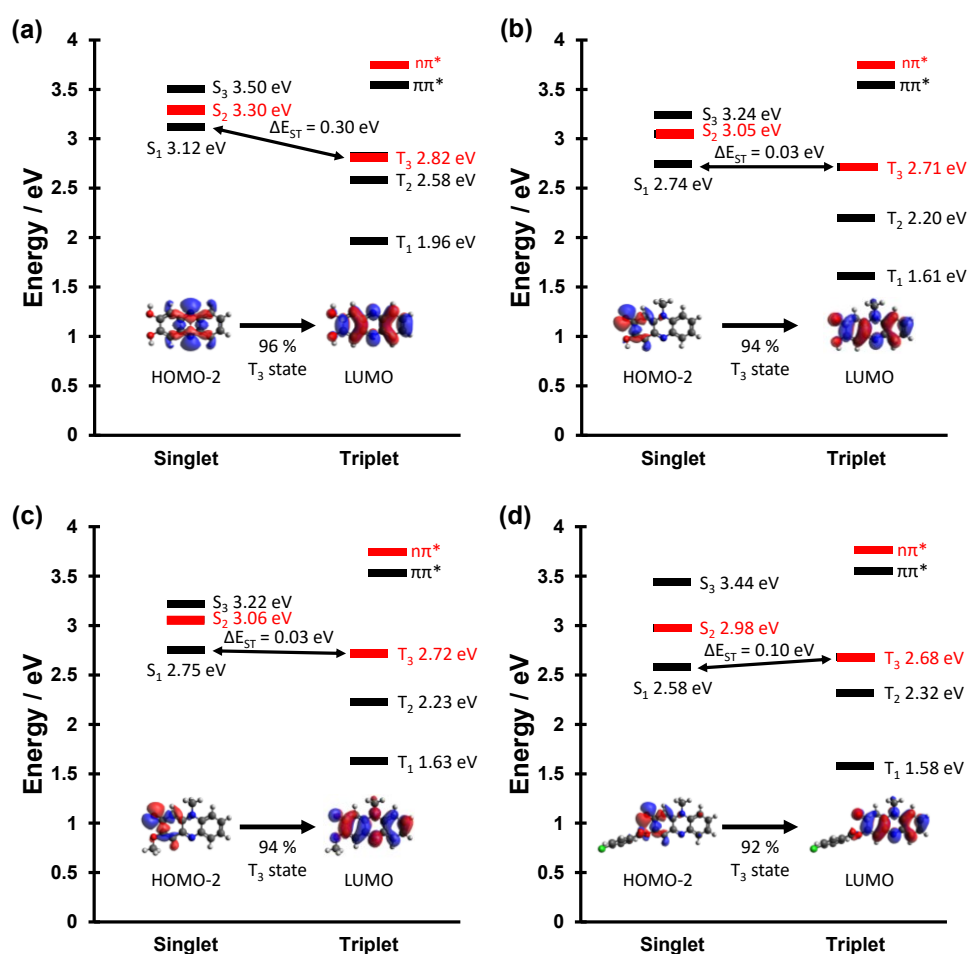


Fig. 5 Schematic diagrams showing vertical excitation energies of (a) **PZ**, (b) **PZ1**, (c) **PZ2**, and (d) **PZ3** for singlet and triplet excited states. The insets represent the frontier n-orbitals that contribute to the (n, π^*) triplet states. The methoxymethyl group of **PZ2** was replaced with the methyl group for convenience of calculation.

Table 3 Spin–orbit coupling (SOC) constants and the energy gaps (ΔE_{ST}) between the lowest excited singlet states (S_1) and the triplet states (T_n).

Dye	Triplet states	SOC / cm^{-1}	ΔE_{ST} / eV
PZ	T ₁	0	-1.16
	T ₂	0.02	-0.54
	T ₃	8.82	-0.30
	T ₄	0	0.10
	T ₅	0	1.00
PZ1	T ₁	1.01	-1.13
	T ₂	0.16	-0.54
	T ₃	17.45	-0.03
	T ₄	0.44	0.59
	T ₅	0.66	0.64
PZ2	T ₁	1.03	-1.12
	T ₂	0.17	-0.52
	T ₃	17.58	-0.03
	T ₄	0.39	0.59
	T ₅	0.73	0.64
PZ3	T ₁	0.48	-1.00
	T ₂	0.20	-0.26
	T ₃	18.15	-0.10
	T ₄	0.72	0.68
	T ₅	0.98	0.78

Photodynamic activity toward HeLa cells

The photodynamic activity of **PZ1–3** toward human cervical cancer (HeLa) cell lines were determined.²⁶ Cell viability was determined as the ratio (%) of the number of viable cells treated and not treated with **PZ1–3** using the WST-8 method. As shown in Fig. 6, the dark toxicity of **PZ1–3** toward the cells was observed.

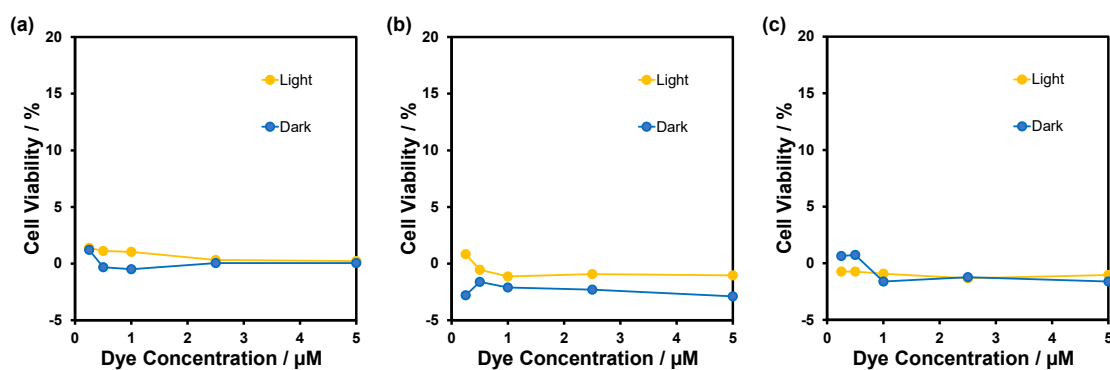


Fig. 6 Viability of cells treated with (a) **PZ1**, (b) **PZ2**, or (c) **PZ3** toward HeLa cells in the dark and after photoirradiation. The cells were treated with various concentrations of PSs and kept in the dark or subjected to irradiation. Cell viability was evaluated 24 h after treatment. Cell viability was confirmed using the WST-8 method.

Conclusions

In conclusion, we have designed and developed the phenazinone derivatives **PZ1**, **PZ2**, and **PZ3** with a hydroxy, a methoxymethoxy, and a 4-chlorobenzoate substituent, respectively, as halogen-free-heteroanthracene-based PSs. It was found that the phenazinone incorporating a carbonyl group into the skeleton allows an efficient ISC based on the El-Sayed rule. Indeed, **PZ1** exhibited the high $^1\text{O}_2$ generation ability ($\Phi_{\Delta} = 0.86$), which is a superior photosensitizing ability to **PZ2** ($\Phi_{\Delta} = 0.54$) and **PZ3** ($\Phi_{\Delta} = 0.069$) with a flexible substituent. Consequently, we propose that the phenazinone skeleton is one of the halogen-atom-free-heteroanthracene-based chromophores as PSs.

Acknowledgements

Chapter 6 is reproduced from “Synthesis and optical properties of phenazinone-based photosensitizers for singlet oxygen generation; K Ohira, M. Yamamoto, K. Imato, and Y. Ooyama, *New J. Chem.*, **2023**, 47, 2711–2718.” with permission from The Royal Society of Chemistry.

References

1. D. G. Fresnadillo, *ChemPhotoChem*, **2018**, 2, 512–534.
2. K. A. Mariewskaya, A. P. Tyurin, A. A. Chistov, V. A. Korshun, V. A. Alferova and A. V. Ustinov, *Molecules*, **2021**, 26(13), 3971.
3. A. Kamkaew, S. H. Lim, H. B. Lee, L. V. Kiew, L. Y. Chung and K. Burgess, *Chem. Soc. Rev.*, **2013**, 42, 77–88.
4. M. C. Derosa and R. J. Crutchley, *Coor. Chem. Rev.*, **2002**, 233–234, 351–371.
5. B. Barut, C. Ö. Yalçın and Ü. Demirbaş, *J. Photochem. Photobiol. A Chem.*, **2021**, 405, 112946.
6. (a) K. Piwowar, A. Blacha-Grzechnik and J. Zak, *J. Electrochem. Soc.*, **2019**, 166, G163–G169; (b) F. Ronzani, A. Trivella, E. Arzoumanian, S. Blanc, M. Sarakha, C. Richard, E. Oliveros and S. Lacombe, *Photochem. Photobiol. Sci.*, **2013**, 12, 2160–2169.
7. T. M. Ebaston, F. Nakonechny, E. Talalai, G. Gellerman and L. Patsenker, *Dyes Pigm.*, **2021**, 184, 108854.
8. (a) L. Wang, J. Bai, and Y. Qian, *New J. Chem.*, **2019**, 43, 16829–16834; (b) H. Wang, C. Li, Q. Wu, H. Wen, T. Sun, and Z. Xie, *J. Mater. Chem. B*, **2022**, 10, 4967–4973; (c) M. Liu, C. Wang, and Y. Qian, *New J. Chem.*, **2021**, 45, 18082–18089; (d) J. Chen, Y. Cui, K. Song, T. Liu, L. Zhou, B. Bao, R. Wang, and L. Wang, *Biomater. Sci.*, **2021**, 9, 2115–2123; (e) I. J. Gomez, M. Russo, O. A. Arcidiacono, E. M. Sanchez-Carnerero, P. Klan, and L. Zajickova, *Mater. Chem. Front.*, **2022**, 6, 1719–1726.

9. (a) Y. Ooyama, T. Enoki and J. Ohshita, *RSC Adv.*, **2016**, 6, 5428–5435; (b) A. Mohan, E. Sebastian, M. Gudem and M. Hariharan, *J. Phys. Chem. B*, **2020**, 124, 6867–6874.
10. O. J. Stacey and S. J. A. Pope, *RSC Adv.*, **2013**, 3, 25550–25564.
11. (a) J. Miao, Y. Huo, G. Yao, Y. Feng, J. Weng, W. Zhao and W. Guo, *Angew. Chem. Int. Ed.*, **2022**, 61, e202201815; (b) L. A. Ortiz-Rodriguez, S. J. Hoehn, A. Loreda, L. Wang, H. Xiao and C. E. Crespo-Hernández, *J. Am. Chem. Soc.*, **2021**, 143(7), 2676–2681.
12. R. W. Redmond and J. N. Gamlin, *Photochem. Photobiol.*, **1999**, 70, 391–475.
13. (a) Y. Hirata and I. Tanaka, *Chem. Phys. Lett.*, **1976**, 43, 568–570; (b) K. Imato, K. Ohira, M. Yamaguchi, T. Enoki and Y. Ooyama, *Mater. Chem. Front.*, **2020**, 4, 589–596.
14. K. Ohira, K. Imato and Y. Ooyama, *Mater. Chem. Front.*, **2021**, 5, 5298–5304.
15. (a) M. A. El-Sayed, *Acc. Chem. Res.*, **1968**, 1, 8; (b) M. Baba, *J. Phys. Chem. A*, **2011**, 115, 9514–9519; (c) S. Tsumura, K. Ohira, K. Hashimoto, K. Imato and Y. Ooyama, *Mater. Chem. Front.*, **2020**, 4, 2762–2771; (d) H. Shu, H. Li, J. Rao, L. Chen, X. Wang, X. Wu, H. Tian, H. Tong and L. Wang, *J. Mater. Chem. C*, **2020**, 8, 14360–14364.
16. M. Jäger, H. Görls, W. Günther, and U. S. Schubert, *Chem. Eur. J.*, **2013**, 19, 2150–2157.
17. K. Ogawa, M. Miura, T. Nakayama and J. Harada, *Chem. Lett.*, **2003**, 32(9), 840–841.
18. D. H. McDaniel and H. C. Brown, *J. Org. Chem.*, **1958**, 23(3), 420–427.
19. J. Zou, Z. Yin, P. Wang, D. Chen, J. Shao, Q. Zhang, L. Sun, W. Huang and X. Dong, *Chem. Sci.*, **2018**, 9, 2188–2194.
20. W. Wu, J. Sun, X. Cui and J. Zhao, *J. Mater. Chem. C*, **2013**, 1, 4577–4589.
21. L. Huang, X. Cui, B. Therrien and J. Zhao, *Chem. Eur. J.*, **2013**, 19, 17472–17482.
22. Y. Hayashi, A. Morimoto, T. Maeda, T. Enoki, Y. Ooyama, Y. Matsui, H. Ikeda and S. Yagi, *New J. Chem.*, **2021**, 45, 2264–2275.
23. (a) S. Cekli, R. W. Winkel, E. Alarousu, O. F. Mohammed and K. S. Schanze, *Chem. Sci.*, **2016**,

- 7, 3621–3631; (b) R. D. Pensack, Y. Song, T. M. McCormick, A. A. Jahnke, J. Hollinger, D. S. Seferos and G. D. Scholes, *J. Phys. Chem. B*, **2014**, *118*, 2589–2597.
24. P. F. Heelis, *Chem. Soc. Rev.*, **1982**, *11*, 15–39.
25. (a) M. J. Frisch, G. W. Trucks, H. B. Schlegel, G. E. Scuseria, M. A. Robb, J. R. Cheeseman, G. Scalmani, V. Barone, G. A. Petersson, H. Nakatsuji, X. Li, M. Caricato, A. V. Marenich, J. Bloino, B. G. Janesko, R. Gomperts, B. Mennucci, H. P. Hratchian, J. V. Ortiz, A. F. Izmaylov, J. L. Sonnenberg, D. Williams-Young, F. Ding, F. Lipparini, F. Egidi, J. Goings, B. Peng, A. Petrone, T. Henderson, D. Ranasinghe, V. G. Zakrzewski, J. Gao, N. Rega, G. Zheng, W. Liang, M. Hada, M. Ehara, K. Toyota, R. Fukuda, J. Hasegawa, M. Ishida, T. Nakajima, Y. Honda, O. Kitao, H. Nakai, T. Vreven, K. Throssell, J. A. Montgomery, Jr., J. E. Peralta, F. Ogliaro, M. J. Bearpark, J. J. Heyd, E. N. Brothers, K. N. Kudin, V. N. Staroverov, T. A. Keith, R. Kobayashi, J. Normand, K. Raghavachari, A. P. Rendell, J. C. Burant, S. S. Iyengar, J. Tomasi, M. Cossi, J. M. Millam, M. Klene, C. Adamo, R. Cammi, J. W. Ochterski, R. L. Martin, K. Morokuma, O. Farkas, J. B. Foresman and D. J. Fox, *Gaussian 16, Revision B.01*, Gaussian, Inc., Wallingford CT, 2016; (b) F. Neese, *Wiley Interdiscip. Rev.: Comput. Mol. Sci.*, **2022**, *12*, e1606.
26. R. Kawasaki, K. Yamana, R. Shimada, K. Sugikawa and A. Ikeda, *ACS Omega*, **2021**, *6*, 3209–3217.

Summary

In this thesis, the author conducted research on the development of phenazine- and phenazinone-based PSs for $^1\text{O}_2$ generation.

In **Chapter 1**, a brief historical introduction to photosensitization, the mechanisms of $^1\text{O}_2$ generation, and methods of its detection were outlined.

In **Chapter 2**, the phenazine-based PSs possessing several substituents (**KI-1–5**) have been developed and it was found that the introduction of an electron-withdrawing nitro group into the phenazine chromophore (**KI-5**) extended the photoabsorption edge up to the NIR region (700–800 nm) but inhibited the photosensitized $^1\text{O}_2$ generation due to the fast nonradiative decay of $^1\text{PS}^*$. Furthermore, **KI-2** substituted by formyl groups exhibited a superior photosensitizing ability ($\Phi_{\Delta} = 0.48$) according to El-Sayed's rule.

In **Chapter 3**, building on **Chapter 2**, the effect of formyl groups on $^1\text{O}_2$ generation was investigated. The Φ_{Δ} values of Phenazine-based PSs **KO-0–3**, which have zero to three formyl groups, respectively, increased in the order of **KO-0** (0.036) < **KO-1** (0.22) < **KO-2** (0.33) < **KO-3** (0.41) with increasing number of formyl groups. Furthermore, TD-DFT calculations demonstrated that the SOC constants of ISC pathways, which meet El-Sayed's rule, were relatively large (7.66–7.77 cm^{-1}). Therefore, it was indicated that formyl groups facilitate the ISC from the lowest singlet excited states of the PSs (S_1) to the triplet excited states (T_n), leading to the efficient $^1\text{O}_2$ generation.

In **Chapter 4**, the author investigated the effect of substitution of cyano group for nitro group on $^1\text{O}_2$ generation, drawing inspiration from the photophysical properties of **KI-5** in **Chapter 2**. Compared to **KI-5**, **YC-2** with the cyano group in place of the nitro group exhibited the improved Φ_{Δ} value (0.02 for **KI-5** and 0.29 for **YC-2**). Furthermore, TD-DFT calculations revealed that the substitution of the cyano group for the nitro group in phenazine-based chromophore reduces the ΔE_{ST} value of the ISC pathway (0.40 eV for **KI-5** and 0.06 eV for **YC-2**), leading to the efficient ISC for $^1\text{O}_2$ generation.

In **Chapter 5**, for further application toward the water purification systems and PDT, water-soluble phenazine-based PSs **KY-1Na** and **KY-2Na** bearing one and two carboxylic acid sodium salts, respectively, have been developed. **KY-1Na** and **KY-2Na** exhibited the ability for $^1\text{O}_2$ generation in water. Moreover, **KY-2Na** had a higher efficiency in $^1\text{O}_2$ generation compared to **KY-1Na**, with Φ_{Δ} values of 0.19 for **KY-2Na** and 0.06 for **KY-1Na**. However, the Colon26 viability changed little despite the increasing concentration of **KY-1Na** and **KY-2Na** due to the low permeability to the cell membrane of Colon26.

In **Chapter 6**, Phenazinone derivatives **PZ1–3** where a carbonyl group is incorporated into the chromophore are designed and developed as halogen-atom-free-heteroanthracene-based PSs possessing the ability to generate $^1\text{O}_2$. It was found that **PZ1** exhibited a higher Φ_{Δ} value than rose bengal (**RB**) known as a reference PS to generate $^1\text{O}_2$ (0.86 for **PZ1**, 0.54 for **PZ2**, 0.069 for **PZ3**, and 0.68 for **RB**). Moreover, the rate constants (k_r , k_{nr} , k_{ISC} , and k_{IC}) of **PZ1–3** indicated that the reason for the low Φ_{Δ} of **PZ2** and **PZ3** comes from the vibrational relaxation caused by a flexible methoxymethoxy and 4-chlorobenzoate group, respectively. In contrast, TD-DFT calculations indicated that the SOC constants for **PZ1–3** were significantly large (17.45 cm^{-1} for **PZ1**, 17.58 cm^{-1} for **PZ2**, and 18.15 cm^{-1} for **PZ3**), leading to efficient ISC. While **PZ1–3** showed notably different $^1\text{O}_2$ generation abilities, all of these PSs exhibited dark toxicity toward HeLa cells.

As described in this thesis, the author established the synthetic guidelines for new phenazine- and phenazinone-based PSs with the superior ability to produce $^1\text{O}_2$. These findings will contribute to the development of new halogen-atom-free-heteroanthracene-based PSs.

List of publications

- Chapter 2.** Phenazine-based Photosensitizers for Singlet Oxygen Generation
K. Imato, K. Ohira, M. Yamaguchi, T. Enoki, and Y. Ooyama, *Mater. Chem. Front.*, **2020**, 4, 589–596.
- Chapter 3.** Development of phenazine-2,3-diol-based photosensitizers: effect of formyl groups on singlet oxygen generation
K. Ohira, K. Imato, and Y. Ooyama, *Mater. Chem. Front.*, **2021**, 5, 5298–5304.
- Chapter 4.** Development of phenazine-2,3-diol-based photosensitizers: effect of substitution of the cyano group for the nitro group on singlet oxygen generation
K. Ohira, C.-H. Yu, K. Imato, and Y. Ooyama, *New J. Chem.*, **2023**, 47, 16799–16808.
- Chapter 5.** Development of water-soluble phenazine-2,3-diol-based photosensitizers for singlet oxygen generation
K. Yagi, K. Ohira, K. Yamana, K. Imato, R. Kawasaki, A. Ikeda, and Y. Ooyama, *Org. Biomol. Chem.*, **2023**, 21, 5194–5202.
- Chapter 6.** Synthesis and optical properties of phenazinone-based photosensitizers for singlet oxygen generation
K. Ohira, M. Yamamoto, K. Imato, and Y. Ooyama, *New J. Chem.*, **2023**, 47, 2711–2718.

Other publications not included in this thesis

1. Sterically Hindered Stiff-Stilbene Photoswitch Offers Large Motions, 90% Two-Way Photoisomerization, and High Thermal Stability
K. Imato, A. Sasaki, A. Ishii, T. Hino, N. Kaneda, K. Ohira, I. Imae, and Y. Ooyama, *J. Org. Chem.*, **2022**, *87*, 15762–15770.
2. Synthesis, optical and electrochemical properties of (D- π)₂-type and (D- π)₂Ph-type fluorescent dyes
K. Takemura, K. Ohira, T. Higashino, K. Imato, and Y. Ooyama, *Beilstein J. Org. Chem.*, **2022**, *18*, 1047–1054.
3. Synthesis, Optical and Electrochemical Properties of Benzofuro[2,3-c]carbazoloquinol Fluorescent Dyes
Y. Ooyama, K. Ohira, Y. Kagawa, and K. Imato, *Electrochemistry*, **2021**, *89*, 562–566.
4. Development of optical sensor for water in acetonitrile based on propeller-structured BODIPY-type pyridine-boron trifluoride complex
S. Tsumura, K. Ohira, K. Imato, and Y. Ooyama, *RSC Adv.*, **2020**, *10*, 33836–33843.
5. Synthesis, optical and electrochemical properties of propeller-type 3,5,8-trithienyl-BODIPY dyes
S. Tsumura, K. Ohira, K. Hashimoto, K. Imato, and Y. Ooyama, *Mater. Chem. Front.*, **2020**, *4*, 2762–2771.
6. Development of Fluorescent Sensors Based on a Combination of PET (Photo-induced Electron Transfer) and FRET (Förster Resonance Energy Transfer) for Detection of Water
D. Jinbo, K. Ohira, K. Imato, and Y. Ooyama, *Mater. Adv.*, **2020**, *1*, 354–362.

Acknowledgements

This thesis is a summary of my studies from 2019 to 2024 under the direction of Professor Yousuke Ooyama at Hiroshima University.

I would like to express the deepest appreciation to Professor Yousuke Ooyama for his enthusiastic direction and valuable suggestion. Furthermore, I am also grateful to Professor Atsushi Ikeda who provide the great research environment and give the helpful and careful advises. Also, I would like to say thank you to Assoc. prof. Keiichi Imato, Assoc. prof., Ichiro Imae, Assoc. prof. Kenji Komaguchi, Asst. prof. Riku Kawasaki, and Mr. Keita Yamana for their helpful discussion.

I would like to extend my sincere thanks to Ms. Tomoko Amimoto and Ms. Naomi Kawata (Natural Science Center for Basic Research and Development; N-BARD) for their technical support and inputs. I am grateful to Dr. Toshiaki Enoki, Mr. Tsuyoshi Wakita, Mr. Shuhei Tsumura, Mr. Toru Takaki, Mr. Daisuke Jinbo, Mr. Yuta Mise, Ms. Ayane Sasaki, Mr. Kotaro Obayashi, Mr. Nao Ueki, Ms. Chih-Hsin Yu, Mr. Ayumu Yamane, Mr. Koki Momota, Ms. Saori Miho, Mr. Kosuke Takemura, Mr. Hiroki Uehara, Mr. Kazunori Yagi, Ms. Miki Morimoto, Mr. Takuma Fumoto, Mr. Taiki Higashino, Mr. Taichi Hino, Mr. Akira Ishii, Mr. Masahiro Yamamoto, Ms. Emiko Nishimoto, Mr. Yuta Tsujii, Mr. Naoki Kaneda, Mr. Kunpei Kodzuka, Mr. Yasuto Hara, Ms. Yujie Ma, Mr. Kazuki Tao, Mr. Taichi Hidaka, Mr. Satoru Maekawa, Ms. Misaki Majima, Mr. Yuto Ida, Mr. Kosuke Okutani, Mr. Soseki Kurokawa, Mr. Hiroto Tsuyama, Mr. Sora Nihonmatsu, Mr. Soma Hodono, and Mr. Shogo Amimoto for their kindness and collaborations.

Hiroshima University Graduate School Research Fellowship and Osimo Foundation are acknowledged for the financial support of my research at Hiroshima University.

Finally, I would like to express my sincere appreciation to my parents (Toshiaki Ohira and Chieko Ohira), to my brother (Fumiya Ohira), and to my grandparents (the late Isamu Ohira, Kayoko Ohira, Koichi Atsumi, and Yaeko Atsumi) for their consistent support and encouragement for my life.

March 2024

Kazuki Ohira